UNIVERSITY OF
LIVERPOOL

INVESTIGATIONS ON THE CREDIBILITY OF CFD SIMULATIONS OF BUOYANT TURBULENT JETS

Thesis submitted in accordance with the requirements of the

University of Liverpool for the degree of Doctor in Philosophy

by

Maria Diamanti

December 2009

ACKNOWLEDGEMENTS

I would like to take this opportunity to express my gratitude to my supervisor Dr. K.H.M. Ali for his invaluable advice, guidance and patience throughout this study.

I gratefully acknowledge the financial support from the Greek State Scholarships Institute (I.K.Y.) and the Engineering and Physical Sciences Research Council (EPSRC UK) for the giving me the opportunity to carry out the present study. The assistance of Mr. M.I. Jones, Mr. R. Downward from the hydraulic laboratory with the experimental set ups and Mr. J. Wilkinson with the experimental measurements is also deeply acknowledged.

ABSTRACT

Analysing and predicting mixing in natural water bodies is of vital importance. Computational Fluid Dynamics (CFD) is a promising way of making it easier and faster to predict mixing in natural water bodies, yet there is still concern over the reliability of the results produced. Investigating the applicability of commercial CFD models for predicting mixing due to buoyant turbulent jets and the potential for misleading results is investigated.

Experiments were performed on the buoyant surface jet and the heavy wall jet and the data obtained were used to validate CFD simulations of the experimental set-ups. Generally CFD managed to predict the pattern of the flow and the computed results compared well with the experimental data in most cases. There were however several possible risks identified that could lead to misleading results.

NOTATION

B	*Buoyancy Flux*
b	*Jet half width*
b_o	*Jet width*
C	*Chézy coefficient*
F	*Force*
f	*Friction factor*
Fr	*Froude number*
Fs	*Safety Factor*
g	*Acceleration due to gravity*
g'	*Buoyancy acceleration*
h	*Water (flow) depth*
$h1, h2, h3$	*Grid sizes*
k	*Turbulence kinetic energy*
L	*Characteristic length*
p	*static pressure*
Q	*Discharge rate*
r	*Grid refinement factor*
Re	*Reynolds number*
Ri	*Richardson number*
S	*Salinity*
Ss	*Specific gravity*
T	*Temperature*
t	*Time*
U	*Velocity*
u, v, w	*Velocities in the x, y, z direction*
u_m	*Maximum velocity*
U_o	*Initial velocity*
$\Delta\rho$	*Density Difference*
ε	*Turbulence dissipation rate*
μ	*Molecular viscosity*
ν	*Kinematic viscosity coefficient*

ρ	*Fluid density*
ρ_a	*Ambient fluid density*
τ	*Shear stress*

ABBREVIATIONS

AIAA	American Institute for Aeronautics and Astronautics
BC	Boundary Conditions
BSJ	Buoyant Surface Jet
CFD	Computational Fluid Dynamics
CSO	Combined Sewer Overflow
GCI	Grid Convergence Index
HSJ	Homogeneous Surface Jet
HWJ	Heavy Wall Jet
RANS	Reynolds Averaged Navier-Stokes
RNG	Renormalisation Group
RSM	Reynolds Stress Model
TKE	Turbulent Kinetic Energy
VOF	Volume Of Fluid
ZEF	Zone of Established Flow
ZFE	Zone of Flow Establishment

TABLE OF CONTENTS

LIST OF FIGURES

LIST OF TABLES

LIST OF PHOTOS

Chapter 1. Introduction and Background

Buoyant jets play an important role at the initial mixing phase for pollutant discharges. Buoyant surface discharges into ambient water bodies can exhibit multiple complex flow processes, which cover the spatial range from the near field, with initial jet mixing, to the far field, with passive ambient diffusion. Efficient and reliable predictive techniques covering the whole range of these processes are needed for the design of discharges and the prediction of natural mixing processes.

1.1. Mixing in Natural Water Bodies

Water is the most important natural resource and is vital for life. Many essential nutrients for life are also transported and dispersed by the motion of water. Unfortunately, over many years, many natural water bodies have been treated like a convenient way of disposing of waste, and, in the process, inadvertently polluting inland and coastal waters. Pollutants get transported and mixed by the motion of water in a similar way to nutrients. The ever increasing human interference with the natural environment demands a far better ability to analyse and predict mixing in natural bodies of water, and to control pollution in the various forms it can take, from thermal pollution to heavy metals and pesticides. The need to ensure water quality has become absolutely imperative.

Mixing occurs naturally in water bodies through the motion of the water which can be initiated through the action of wind and waves and by temperature and density differences. Mixing, and the resultant dilution of pollutants, has been considered nature's ability for self purification. Different mixing mechanisms are prevalent in different types of water bodies and mixing occurs at different rates. The increased pollutant loads generated by human activities have, however, undermined nature's

ability for self purification. For this reason, discharges into natural water bodies have to be carefully considered and should aim to aid natural mixing.

Natural Mixing in Estuaries

A classic, oft-quoted scientific definition of an estuary by oceanographer Donald Pritchard in 1967 states that an estuary is:

> 'A *semi enclosed coastal body of water which has a free connection with the open sea and, within which, seawater mixes and usually is measurably diluted with freshwater from land runoff.*'[1]

One of the main features of an estuary is the mixing of fresh and salt water as the predominant mixing mechanism. Mixing in estuaries is influenced by many factors, such as tides, bed topography, inflows, temperature currents, winds, and water chemistry. The defining parameter for mixing in estuaries is, however, the density difference between fresh and salt water, which is affected by two main factors: temperature and salinity.

Generally, freshwater runoff flows into the head of an estuary and moves, as an upper layer of low-density water, toward the mouth of the estuary near the open ocean. Beneath this upper layer, an opposing inflow of denser, salty seawater occurs. Mixing takes place at the contact between these water masses. This is the classical pattern of estuarine circulation. Often, no single mixing pattern applies as topography plays a significant role along with numerous other parameters that determine the specific mixing pattern in each case.

Characteristic patterns of salt and freshwater mixing and circulation are used to classify estuaries. Mixing and circulation types include stratified, partially mixed,

[1] Pritchard, D.W. 1967. What is an estuary: physical viewpoint, pp.52-63. In: G.H. Lauff (ed.) Estuaries. American Association for the Advancement of Science, Washington, D.C.

and well mixed. Stratified or 'salt-wedge' conditions occur when both river flow and tides are strong. Seawater intrudes into the estuary along the bottom as it is slightly heavier than the freshwater coming downstream. At the boundary between the fresh water and saltwater layers, high shear forces only allow limited mixing between the two. In cross-section, the salt water is like an intruding wedge along the bottom. Well-mixed estuarine conditions occur when river flows are low and tides are weak. Partially mixed conditions occur when both river flow and tides are moderate to high or strong. These conditions are more typical during winter. At different times of the year, any given estuary may fall into any of these classifications. Generally, however, estuaries that drain large river basins more frequently exhibit stratified or partially mixed conditions than do estuaries with smaller drainages. A schematic of mixing processes in estuaries is shown in Figure 1.1.

Mixing and circulation characteristics are important because they strongly influence an estuary's ecological functioning. Mixing and circulation patterns also determine how pollution concentrates, or disperses, and how long it takes to flush the system of wastes. Located as they are at the 'bottom' of watersheds, estuaries collect a variety of pollutants, introduced nutrients and organic matter, toxic metals, pesticides, herbicides, pathogenic bacteria and viruses, oil and other hydrocarbons, sediment, radioactive waste, plastic debris and other trash.

In brief the coastal environment can be highly diverse and density differences are one of the main determining factors influencing the mixing processes in estuaries and other coastal areas.

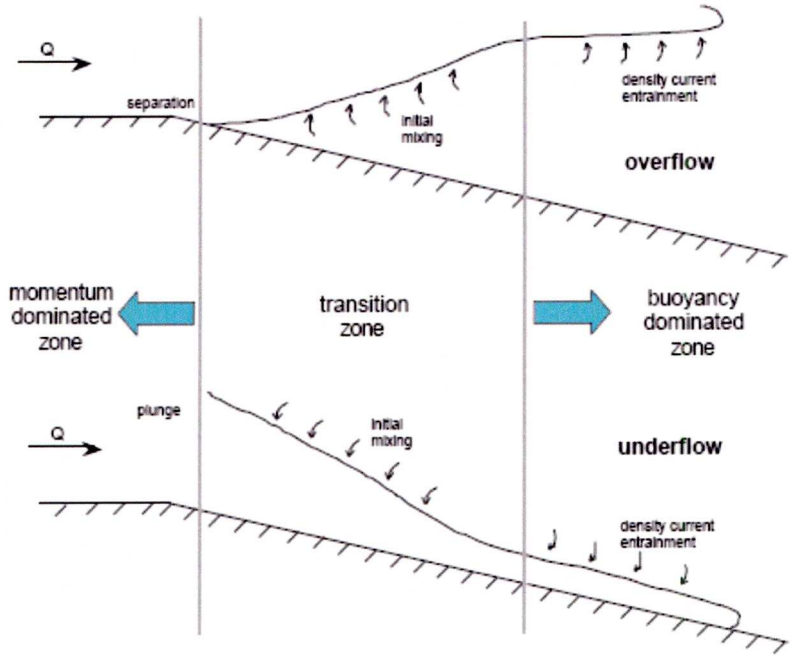

Figure 1.1: Diagram of Mixing Processes in Coastal Regions

1.2. Pollution of Natural Water Bodies

Pollutants are transported and mixed by the motion of water, and can be classified in many ways, for example, according to their properties or the danger they pose to life. The most meaningful classification for hydrodynamics and mixing processes, however, is the classification based on how the pollutants enter the water body.

Pollution of natural water bodies can be broadly classified into two main categories depending on how the pollutants enter the water body, namely:

(a) diffuse or 'non-point' source pollution that emanates from diffuse sources, such as run-off from agricultural land, and which cannot be traced to a specific outlet, and

(b) 'point' source pollution that includes discharges from specific locations that can be traced back.

1.2.1 Types of Pollution

1.2.1.1 Diffuse (non-point) Sources of Pollution

Diffuse water pollution is mainly determined by the way land and soil are managed. Non-point or diffuse sources are the sources of pollutants carried off the land by urban or agricultural run-off. Pollutants from such sources may be discharged directly into the water body or into rivers that carry the contaminants to the water body. Diffuse sources usually do not contain clearly distinct mixing processes and are difficult to understand and, consequently, to predict.

Diffuse water pollution can have significant effects on wildlife and on water quality. These effects include groundwater and surface water contamination and the subsequent loss, or need for treatment, of drinking water resources. Other effects include microbiological contamination of water supplies; nutrient enrichment and eutrophication; oxygen depletion, and consequent toxicity to plant and animal life.

1.2.1.2 Point Sources of Pollution

Point sources are normally discharges from specific outlets that can be traced to a single point or source and emit fluids of varying quality directly into water bodies. Point sources can be used for many purposes and can be found in different settings, varying from pipes discharging directly into the water body (Photo 1.1) to submerged offshore sea outfalls for discharges of sewage flows from municipal sewage treatment plants, cooling water discharges from thermal–electric plants or brine effluents from desalination installations.

Photo 1.1: Water Pollution from Point Source[2]

Another significant, and sometimes disregarded, point source of pollution for water bodies is Combined Sewer Overflows (CSO). Combined Sewer Overflows are apparatuses installed in combined sewerage systems that, under certain flow conditions, allow a certain amount of untreated flow to be discharged directly into a water body to prevent the sewerage system from being surcharged. Combined sewerage systems carry both raw sewage that can carry bacteria and pathogens and urban runoff that can carry toxic chemicals and pollutants. CSOs are considered point sources of pollution, and can cause severe damage to both human health and the environment.

The hydrodynamics of an effluent discharging into a receiving body of water from a point source can be conceptualised as a mixing process occurring in two separate regions. In the first region, the initial jet characteristics of momentum flux, buoyancy

[2] Photo from: http://www.waterencyclopedia.com/images/wsci_03_img0431.jpg. Last retrieved November 2009

flux due to density differences and outfall geometry influence the degree of mixing. This region, also known as near-field, encompasses the buoyant jet flow and any surface bottom or layer interaction. The jet characteristics are the discharge flow rate, its momentum flux and its buoyancy flux, which represents the effect of the relative density difference between the discharge and the ambient conditions in combination with the gravitational acceleration. As the effluent travels away from the source, the jet characteristics become less important and the second stage of mixing, known as far-field is attained. In this region mixing is controlled by passive diffusion due to ambient turbulence and advection by the ambient velocity field.

Both vertical and lateral mixing can be influenced by active mixing processes in the near field of the discharge. Active mixing by momentum jets and buoyancy effects due to density differences can lead to a reduction of the length and the time needed for complete mixing. However, the accurate prediction of such mixing processes is appreciably complex.

1.2.2 Pollution in Estuaries

Of the 32 largest cities in the world, 22 are located on estuaries according to Ross (1995).[3] Intense human activities in the vicinity of estuaries and coastal waters make them even more prone to pollution as a result of these activities.

Although estuaries are as susceptible to diffuse pollution as any other natural water body, the pressure from point sources is even more significant in estuaries when compared to other natural water bodies. The two main sources of pollutants discharged into estuaries are industrial waste and sewage. The former may be toxic, while heavy discharges of sewage contain pathogenic micro-organisms.

[3] Ross, D.A. 1995. *Introduction to Oceanography.* New York: Harper Collins College Publishers.

1.3. The Role of Density in Water Mixing

The density of water plays an important role in natural mixing in water bodies. Water density has unique physical properties and does not monotonically increase with increasing temperatures. Instead water reaches its maximum density when the temperature is 4°C. Density is also significantly influenced by salinity and sediment concentrations.

Water density (ρ) is a significant parameter in hydrodynamics and water quality studies and is largely determined by three parameters: temperature T, salinity S and the concentration of total suspended sediments. Density variations are the driving force in many cases of mixing in nature. For buoyant discharges it is the buoyancy differences that control the flow pattern and consequently the mixing.

Density variations also create conditions that restrict vertical mixing and because of this restriction natural water bodies tend to stratify, that is they separate into distinct vertical layers. Stratification is a complicated phenomenon that presents great difficulty in developing an analytical model that accurately represents the processes, both on spatial and temporal scale. The main processes involved in stratification are molecular diffusion, interfacial shear erosion and turbulence. Turbulence plays a much more significant role in the improvement of mixing than molecular diffusion as its influence is on a much larger scale.

1.4. Scope of Present Research

Mixing is very important in nature, and many studies have investigated mixing with many attempts made to create models that can reasonably accurately predict mixing. Predictive methodologies for examining mixing from point sources are also important. However, hydraulic model studies that can replicate the mixing process, scaled down with reasonable accuracy, are too costly to perform and insufficient for examining a range of possible ambient/discharge conditions.

Computational Fluid Dynamics (CFD) appears to be a promising and cost effective solution to the problem. CFD codes promise to enable the user to accurately predict the physical aspects of hydrodynamic mixing processes that determine the fate and distribution of discharges for a variety of parameters. However, CFD is still in an early stage of development, especially when it comes to turbulent flows, and predicted results are not always realistic and reliable.

The scope of this research project is to investigate the applicability and credibility, along with the degree of simplicity, of employing commercial CFD codes to investigate mixing processes resulting from buoyant jets.

Comparisons of the computational results with experimental results both from experiments performed as part of the present project and from data published by previous research were made to assess the performance of CFD. The lack of benchmarking cases for buoyant jet mixing in water bodies meant that experiments had to be undertaken to obtain the data to validate the models.

1.5. Thesis Structure

Chapter 1. Introduction and Background introduces some background as to why mixing in nature is so important and why studying and predicting mixing in natural water bodies is beneficial, if not essential, in the present time. Predicting mixing accurately is becoming imperative with the increasing interference with natural water bodies and increasing number of discharges, such as discharges from thermal plants and desalination plants.

Chapter 2. Theoretical Considerations on Turbulent Jets focuses on the theoretical background of water mixing from turbulent jets. This chapter presents the basic principles of turbulent jet mixing and explains the differences of the various jets studied. The jet characteristics are discussed and results from previous research are also included. The chapter contains a review of the literature on turbulent jets thought to be relevant to the present study. The cases presented are those most similar to the present study. Although some of the research presented is old, the cases were included as they are extensively used and are widely accepted as accurate.

Chapter 3. CFD Literature Review and Theory presents an overview of the concepts and theory involved in the computational modelling of fluid dynamics phenomena. As there are several commercial CFD codes, the focus has been on the models used in the *FLUENT* package. The main equations solved are presented along with procedures required to set up a CFD simulation. Turbulence modelling and multiphase modelling are discussed. Finally, there is extensive discussion on the possible errors and uncertainties in a computational fluid dynamics simulation. A classification of possible errors is presented along with methods for checking for errors and uncertainties.

The experiments conducted as part of the study on turbulent jets are presented in ***Chapter 4. Experiments on Turbulent Jets*** which compares experimental work, done previously by other researchers, and aims to provide assurance that results obtained can be used for the validation of the simulations.

Modelling procedures and results are presented in ***Chapter 5. CDF Modelling of Buoyant Turbulent Jets***. Simulations were performed for a homogeneous surface jet, buoyant surface jets and heavy wall jets. The results are compared with the experimental data and comments made on the observations.

Discussions of the results and a review of the conclusions from the study are presented in ***Chapter 6. Discussion and Conclusions***. Possible directions of future research are also suggested.

Chapter 2. Theoretical Considerations on Turbulent Jets

As the main characteristics of jets of particular interest to this study are turbulent mixing and entrainment, some significant definitions and concepts are presented prior to the presentation of the study. Previous studies on these aspects of turbulent jets are also outlined.

2.1. Turbulent Jets

2.1.1 Definition of a Turbulent Jet

It is a common occurrence in the environment for one fluid to intrude into another. Everyday examples include rivers flowing into the sea, waste water discharges from pipes into rivers or lakes and plumes exiting from industrial smokestacks. In every case, a fluid with some momentum and/or buoyancy exits from a relatively narrow nozzle and intrudes into a larger body of fluid with different characteristics, such as different speeds, temperatures or contamination levels. Such fluid streams, resulting from the intrusion of one fluid into another, are described as jets.

As there are different arrangements of stream flows which can be encountered, it is helpful to categorize the various types of jets. A useful way to categorise turbulent jets is whether they inject momentum, buoyancy or both into the ambient fluid. In this classification a turbulent jet can be described as a:

- ***Pure Jet*** – A pure jet is a discharge that carries momentum but has no buoyancy difference to the ambient receiving fluid.
- ***Buoyancy only Jet (or Plume)*** – A plume is a discharge that has different buoyancy levels to the receiving fluid but no initial momentum.
- ***Buoyant Jet*** – When both momentum and buoyancy are discharged into the ambient receiving fluid the jet is described as a buoyant jet.

Buoyant jets can be further divided into:

- ***Positively Buoyant Jets***, where the buoyancy force acts vertically upwards against gravity; and
- ***Negatively Buoyant Jets*** where the buoyancy force acts downwards in the direction of the gravity force.

2.1.2 Applications of Turbulent Jets

Jets are a basic flow configuration that has many practical applications. The practical applications of turbulent jets are many and these jets are used and studied in many different fields of engineering. Aerospace, automotive, mechanical, chemical and process engineering all use different aspects of jet flows. There are also many practical applications of turbulent jets in civil and environmental engineering.

In environmental engineering turbulent jets are one of the many techniques used to achieve the faster dilution of pollutants. Turbulent jets are capable of entraining large volumes of ambient fluid and mixing this with the discharge fluid. To optimise these techniques and achieve better results, it is important to understand the structure of the jet because mixing and transport of scalars, such as temperature, oxygen and chemicals, are governed by jet turbulence characteristics.

2.1.3 Basic Characteristics of Turbulent Jets

Richard French in his book 'OPEN CHANNEL HYDRAULICS' (1985), states the behaviour of a turbulent jet depends on three classes of parameters:

i. **Jet Parameters** include variables such as the jet discharge rate, the initial jet velocity distribution and turbulence level, the jet momentum flux, the density of the jet fluid and the tracer concentration.

ii. **Environmental Parameters** refer more to the receiving fluid rather than the jet itself. Parameters here include the turbulence levels in the ambient fluid, currents that might be present as well as existing density stratifications.

iii. **Geometric Factors** include the nozzle shape and dimensions, the position of the jet and its orientation and the presence of boundaries that could interfere with the development of the jet flow.

Considering the parameters that influence the behaviour of a jet, almost every situation is a separate problem requiring specific investigation. Certain characteristics are, however, shared by all types of turbulent jets.

A jet is formed by the flow issuing from a nozzle into an ambient fluid. From the velocity (and sometimes also buoyancy) difference between the jet and the ambient fluid, a thin shear layer is created. This shear layer is highly unstable and is subjected to flow instabilities that eventually lead to the formation of large-scale vortical structures (as shown in Figure 2.1). The interaction of these structures produces strong flow fluctuations, entraining the ambient fluid into the jet flow and enhancing the mixing. The shear layer, and consequently the jet, spreads along the direction perpendicular to the main jet flow.

The central portion of the jet, called the potential core, is a region with almost uniform mean velocity. Because of the spread of the shear layer, the potential core eventually disappears at a distance of about four to six diameters downstream from the nozzle. This region of the jet is called Zone of Flow Establishment (ZFE). The entrainment process continues further beyond the end of the potential core region and the velocity distribution of the jet eventually relaxes to an asymptotic bell-shaped

Gaussian velocity profile. This part of the jet is referred to as the Zone of Established Flow (ZEF).

Another characteristic of jets is the jet half-width, b. The half width is defined as the distance between the axis of the jet and the location where the local velocity u equals half of the local maximum or centre line velocity, u_m. The increase in the jet half-width with downstream distance provides a measure of the spread rate of the jet. Due to the spread, the jet centre line velocity, u_m, decreases downstream beyond the potential core region in the ZEF.

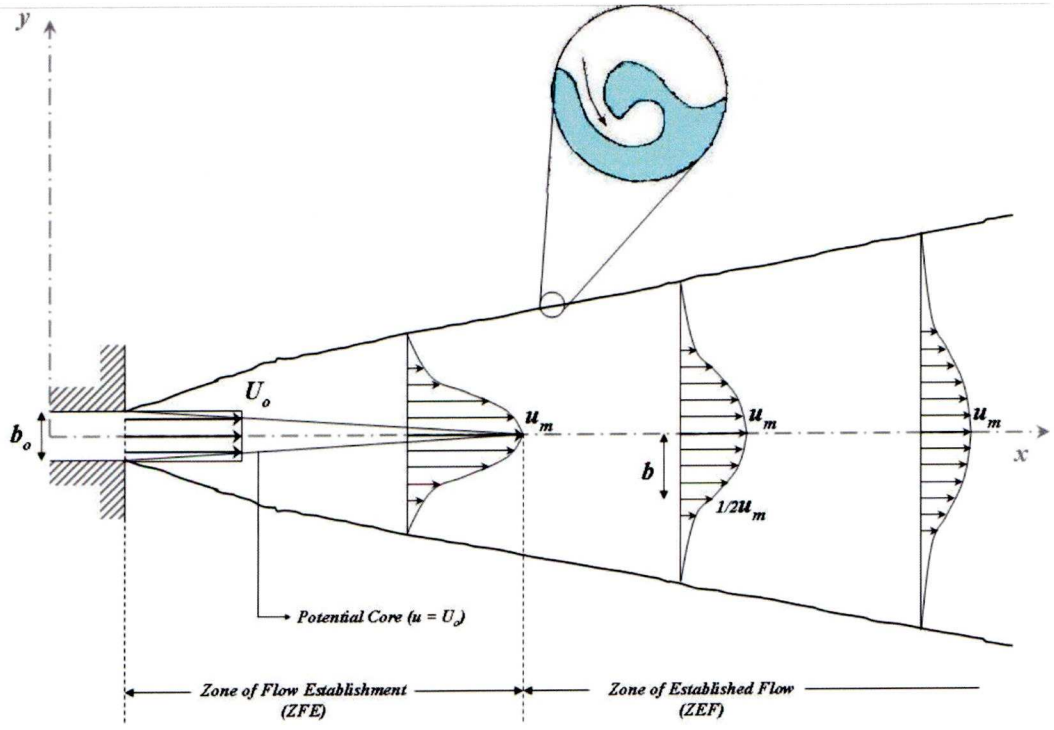

Figure 2.1: Schematic of a Turbulent Jet and its Downstream Development

2.2. Turbulence

2.2.1 Definition of Turbulence

Turbulence is a phenomenon that commonly occurs in nature but is not yet sufficiently understood. This lack of understanding of exactly what turbulence is and why it occurs makes it difficult to give turbulence a universal definition. An early definition given by Taylor and von Karman (1937)[4]:

> *'Turbulence is an irregular motion which in general makes its appearance in fluids, gaseous or liquid, when they flow past solid surfaces or even when neighbouring streams of the same fluid flow past or even on another'.*

Turbulence is generally three dimensional and time dependent. For a complete description of turbulent flows an enormous volume of information is required.

2.2.2 The Reynolds Number

The Reynolds number is a dimensionless quantity that is generally used to describe whether a fluid flow is turbulent. Effectively the Reynolds number gives a measure of the ratio of inertial forces to viscous forces acting on the fluid and quantifies the relative importance of these two types of forces for given flow conditions. The Reynolds number (Re) is given by:

$$\mathrm{Re} = \frac{uL}{\nu} \qquad \textit{(Eq. 2-1)}$$

Where u is the mean flow velocity in m/s, L is the characteristic length in m and ν is the kinematic fluid viscosity in m^2/s.

A general rule is that turbulent flows occur when the velocity is high and viscosity is low, whereas laminar flows occur when the viscosity is high and the velocity low. The interim stage, when neither of these types of forces is prevalent, is called

4 As given in: Wilcox, D. C., 2002, 'Turbulence Modelling for CFD', DCW Industries, 2nd Edition

transitional flow. Although the Reynolds number is a measure of the ratio between these two types of forces there is no specific value of the Reynolds number above which a flow is turbulent. According to the Encyclopaedia Britannica transition between laminar and turbulent flow does not occur at a specific value of the Reynolds number but in a range, usually beginning between 1,000 to 2,000 and extending upward to between 3,000 and 5,000.

2.2.3 The Navier-Stokes Equations

The Navier-Stokes equations are the fundamental equations that describe the flow of fluids. They are an expression of Newton's second law and describe the conservation of momentum. It is assumed, although not proven, that they also describe turbulence, but the numerical solution of the Navier–Stokes equations for turbulent flow is extremely difficult and has only been achieved for simple flows, and after certain assumptions.

The Navier-Stokes equations are non-linear partial differential equations. The equations dictate velocity and not position and a solution of the Navier–Stokes equations is called a velocity field or flow field. The solution describes the velocity of the fluid at a given point in space and time. Once the velocity field is found, other aspects, such as flow rate or drag force, may be solved.

The general form of the Navier-Stokes equations for fluid motion is given as:

$$\frac{\partial}{\partial t}(\rho\vec{u}) + \nabla\cdot(\rho\vec{u}\vec{u}) = -\nabla p + \nabla\cdot(\overline{\overline{\tau}}) + \rho\vec{g} + \vec{F} \qquad \textit{(Eq. 2-2)}$$

Where: p is the static pressure, $\rho\vec{g}$ is the gravitational body force, $\vec{F}$ the external body forces and $\overline{\overline{\tau}}$ the shear tensor, given by:

$$\overline{\overline{\tau}} = \mu\left[\left(\nabla\vec{u} + \nabla\vec{u}^{T}\right) - \frac{2}{3}\nabla\cdot\vec{u}I\right] \qquad \textit{(Eq. 2-3)}$$

Where: μ is the molecular viscosity and I the unit tensor.

2.2.4 Solutions for Turbulent Flows

In most practical applications the entire velocity field is not, however, required and only the mean flow properties are needed to describe turbulent flows. Numerical or even analytical solutions of turbulent flows can be accomplished using approximations that provide a more or less detailed description of the state of the flow. One simple method is the use of semi-empirical correlations. Another method involves application of Reynolds averaging to the equations of motion.

The Reynolds-averaged Navier-Stokes equations (RANS) approach, describes the evaluation of mean flow quantities. In the RANS approach the Reynolds stress term, $\overline{u_i' u_j'}$, appears as an effect of turbulent fluctuations, and needs to be modelled to close the system of equations. The principal disadvantage of this approach is that the model represents the mean turbulence using averaged scales. While the small scales tend to depend only on viscosity, and may be somewhat universal, the larger scales are very strongly affected by the boundary conditions. Thus, there is no universal RANS model to accurately different turbulent flows.

For incompressible flow the RANS equations are written as:

$$\rho \frac{\partial \vec{u}_j \vec{u}_i}{\partial x_j} = \rho \vec{f}_i + \frac{\partial}{\partial x_j}\left[-\bar{p}\delta_{ij} + \mu\left(\frac{\partial \vec{u}_i}{\partial x_j} + \frac{\partial \vec{u}_j}{\partial x_i} \right) \right] - \rho \overline{u_i' u_j'} \qquad \textit{(Eq. 2-4)}$$

Where: p is the static pressure, μ the molecular viscosity, and ρ the fluid density.

2.3. Buoyant Mixing

If a discharge is lighter or heavier than the receiving water the initial mixing can be strongly influenced by differences in densities. The parameter most likely to determine the density effects is the buoyancy flux given as:

$$B = Qg\frac{\Delta\rho}{\rho_a} \qquad \textit{(Eq. 2-5)}$$

Where: Q is the discharge rate, g the acceleration due to gravity, $\Delta\rho$ difference in density between the discharge and the receiving water and ρ_a the density of the receiving water.

A buoyancy-affected flow is referred to as a positively buoyant or a negatively buoyant flow, depending on whether the buoyancy force is acting to aid, or to oppose, the forced convection flow.

2.3.1 The Richardson Number

A method to determine whether buoyancy is the dominant force in a flow is the Richardson number *Ri*. The Richardson number is a dimensionless number that expresses the ratio of potential to kinetic energy and is given by the equation:

$$Ri = \frac{gh}{u^2} \qquad \textit{(Eq. 2-6)}$$

Where g is the acceleration due to gravity, h is the length scale and u the velocity.

Where the density differences are small it is common to use the reduced gravity g', also called buoyant acceleration, to calculate the Richardson number.

In such flows the parameter is called the densimetric Richardson number and is written as:

$$Ri = \frac{g'h}{u^2} \qquad \textit{(Eq. 2-7)}$$

where :

$$g' = g\frac{\rho_\alpha - \rho_o}{\rho_\alpha} \qquad \textit{(Eq. 2-8)}$$

2.3.2 The Densimetric Froude Number

The Froude number is a dimensionless number, closely related to the densimetric Richardson number, used to compare inertia with gravitational forces. The relationship between the densimetric Froude number and the densimetric Richardson number is:

$$Fr = \frac{1}{Ri} \qquad \textit{(Eq. 2-9)}$$

The densimetric Froude number is normally written as:

$$Fr = \frac{u}{\sqrt{g'h}} \qquad \textit{(Eq.2-10)}$$

A high Froude number signifies the inertia forces are dominant over the gravitational forces so it is more likely there is a turbulent mixing zone whereas a low densimetric Froude number is a sign of stratified flow.

2.4. Types of Jets Studied

Basic characteristics of three different types of jets are described in this section, namely the plane surface jet, the buoyant surface jet and the heavy wall jet.

2.4.1 The Plane Surface Jet and the Buoyant Surface Jet

A jet is classified as a surface jet when it is discharged horizontally at the surface over a stagnant mass of ambient receiving water. The intense shear at the surface of velocity discontinuity induces turbulence and the stagnant fluid is accelerated, while a portion of the jet loses some momentum. The thickness of the fluid layer affected by this exchange is known as the mixing layer. The width of this mixing layer increases continuously with distance from the point of discharge. Velocity distributions at different locations downstream of the point of discharge have the

same shape. For fully submerged jets the velocity distributions are symmetrical with respect to the x axis. A schematic of a plane surface jet is in *Figure 2.2.*

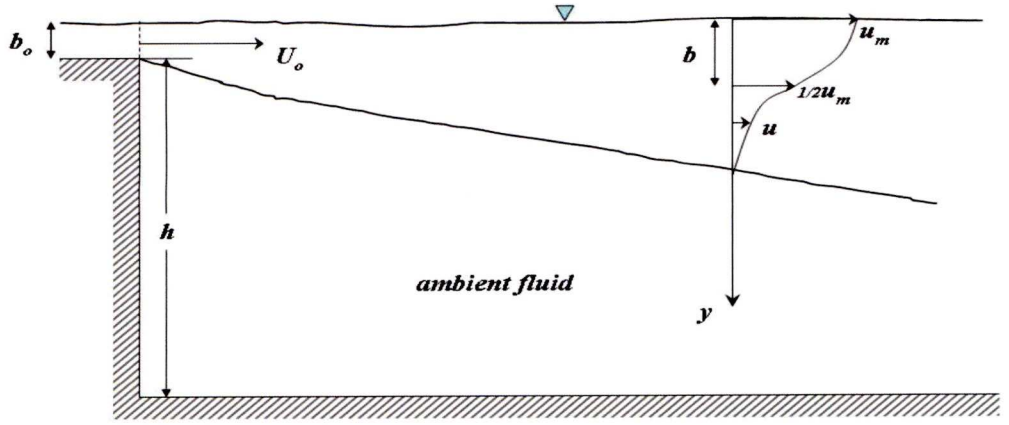

Figure 2.2: Characteristics of a Plane Surface Jet

A buoyant jet is the fluid motion caused by the sustained injection of fluid momentum and buoyancy through an orifice into an ambient receiving fluid body and gradually evolving along a trajectory within the receiving fluid. Although, when mixing in nature the relative density differences between the effluent and the receiving water are normally very small, the density differences can have a significant effect on the behaviour of a buoyant surface jet in comparison with a plane surface jet.

Buoyant jet motions are prevalent in the natural environment and in many engineering applications. Many discharges into the environment, derived from sources of both momentum and buoyancy, are classed as buoyant jets. The initial flow is often driven mostly by the momentum of the fluid leaving the nozzle. However, because of a possible different density of the effluent and its surroundings, the jet is, as a result, acted on by buoyancy forces. Far enough from the nozzle, all buoyant jets act like plumes where their flow is driven by the density gradient.

Physical Processes of Buoyant Surface Jets

Depending on the source and ambient flow interaction many complexities and a rich variety of flow phenomena can take place in buoyant jet flows. The discharge can be steady or time variable, the buoyancy of the discharge relative to the ambient may be caused by a variety of reasons, like temperature or salinity differences, and the nozzle can be of various shapes and dimensions. The receiving fluid body is characterised by its density field, its velocity field and its overall geometry. The ambient may be of uniform density; may contain stable density stratification or may exhibit internally unstable stratification conditions. The ambient velocity field can vary from stagnant conditions to laminar flow or turbulent flow.

The buoyant surface jet is a specific case of a plane surface jet. Similarly to the surface jet, a jet is classified as a surface buoyant jet, when it is discharged horizontally at the surface of stagnant ambient receiving fluid of slightly higher density. Although the flow patterns of the buoyant surface jet and the neutral (homogeneous) jet display striking similarities with the flow pattern, the basic physical mechanisms are very different due to the effects of gravity on the flow. A schematic of the characteristics of a surface buoyant jet is given in *Figure 2.3.*

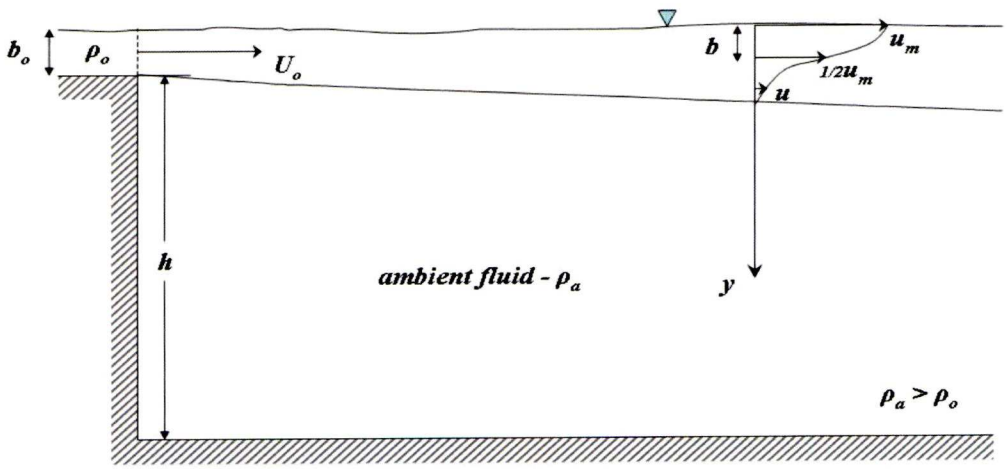

Figure 2.3: Characteristics of a Buoyant Surface Jet

A horizontal jet that comes out of a nozzle with uniform velocity U_o and density ρ_o, mixes with ambient fluid of uniform density ρ_a. The initial jet parameters are the specific mass and the horizontal momentum and buoyancy fluxes. The initial density difference between the jet and ambient fluid may be due to the temperature or salinity of the two fluids. In a heated jet, the temperature difference produces the density deficiency that is responsible for the initial jet specific buoyancy flux.

2.4.2 The Wall Jet and Heavy Wall Jets

A wall jet is created when a fluid is discharged tangentially to a wall boundary. This type of flow presents interesting instabilities as it combines both a mixing and a boundary layer. The dissimilar parameter in the case of wall jets, in comparison with other types of jets, is the presence of the boundary which greatly influences the flow pattern. Wall jets can often also be created as a result of flow impinging on a wall and separating. Velocity distributions along the wall boundary present similarities.

A heavy wall jet is the fluid motion caused by the sustained injection tangentially along a wall of a fluid of higher density into the ambient receiving fluid body and gradually evolving along the wall within that receiving fluid. Heavy wall jet motions are often encountered in the natural environment. Tides, flows of seawater under baffles and above weirs can all result in the development of heavy wall jets. Depending on the situation the flow can be driven by the momentum of the discharging fluid or the gravitational forces.

Physical Processes of Heavy wall Jets

For a heavy wall jet to be created fluid of a higher density is discharged tangentially along a wall bounding the ambient receiving fluid with a lower density. A schematic of the characteristics of a heavy wall jet is in Figure 2.4.

The velocity profiles are very similar to those for the non-buoyant wall jet, with the maximum velocity occurring near the wall boundary. The maximum velocity is observed at a distance δ from the wall and from that point it decays following a Gaussian distribution shape.

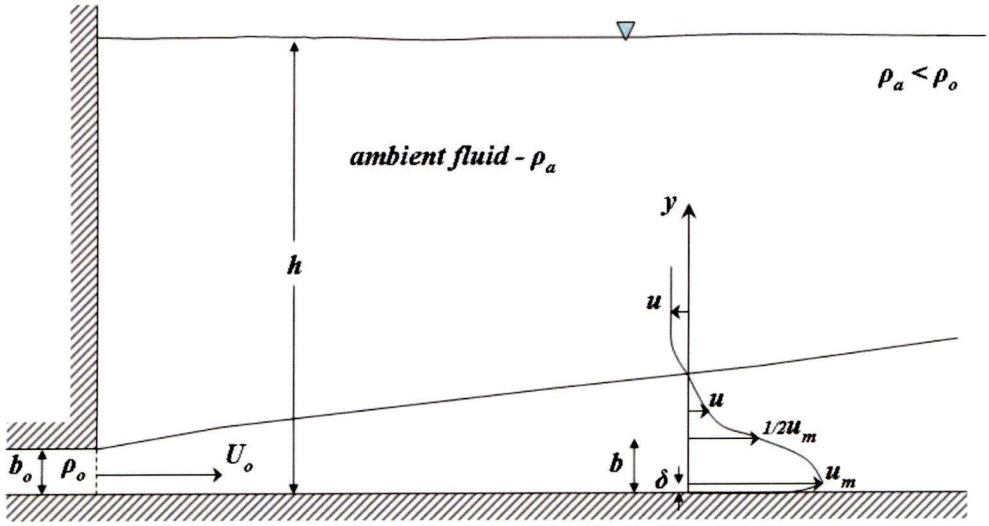

Figure 2.4: Characteristics of a Heavy Wall Jet

A horizontal jet that comes out of a nozzle tangentially along a wall with uniform velocity U_o and density ρ_o, mixes with ambient fluid of uniform density ρ_a. The initial jet parameters are the specific mass, the horizontal momentum, the buoyancy fluxes and the presence of the wall that is introducing boundary effects to the jet flow field. The initial density difference between the jet and ambient fluid may be due to the temperature or salinity of the two fluids.

Often a wall jet can be unforced and develop only by momentum induced by gravitational forces. In the present study the development of a heavy wall jet from a surface discharge is investigated (see Figure 2.5). Due to the effect of gravity, difference in density and the presence of a wall boundary the jet develops to a heavy jet, resulting in completely different flow behaviour. The flow patterns resulting from

a positively or negatively buoyant surface discharge are completely different as the density difference is the parameter that determines the heavy jet flow.

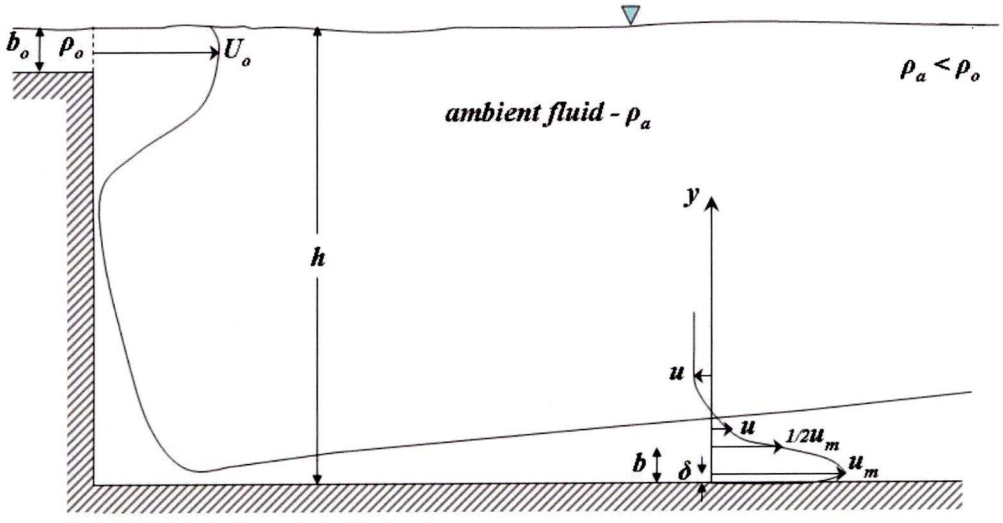

Figure 2.5: Characteristics of a Gravity Driven Heavy Wall Jet

2.5. Review of Previous Studies

The wide range of uses for turbulent jets means jet behaviour has been extensively studied experimentally and there is confidence that certain assumptions made are valid. Some notable studies on surface buoyant jets and wall jet flows conducted over the years are listed below. This is not a complete list of previous studies, but the list contains the experimental studies that are the most similar or of interest in the current study.

Studies on turbulent jets were conducted as early as 1915. Trüpel gave the first velocity profile of a submerged turbulent jet, as stated by Rajaratnam (1976) in his book 'TURBULENT JETS'. G. Abramovich (1963) in his book 'THE THEORY OF TURBULENT JETS' extensively describes the main characteristics of the development of turbulent jets giving several examples of experimental data from various researchers. One of the main findings of these early studies was that for a turbulent

jet issuing from a slot, there will be a Zone of Flow Establishment (ZFE) of length L_o in which the centre line velocity U_o remains constant and for distances greater than L_o there will be a Zone of Established Flow (ZEF) where the jet is fully developed and the velocity profiles follow a Gaussian pattern with maximum centre line velocity less than the inlet velocity U_o.

Further studies that focused on different set ups of turbulent jets all confirming the above. Specific studies of interest focusing on the water surface buoyant jet and the water heavy or denser wall jet are outlined below.

2.5.1 Buoyant Surface Jet Experimental Study Overview

As buoyant jets are common in nature several researchers have undertaken experiments on different aspects and for different fluids. Koh (1971) and Wiuff (1978) specifically performed experiments on turbulent buoyant surface water jets. The most noteworthy and extensively verified experimental observations are described below.

Chu and Vanvari (1976) undertook experiments investigating buoyant surface jets and confirmed that normalised velocity profiles were closely approximated by a Gaussian distribution. However, the growth of the jet was found to be restricted by the free surface. Chu and Vanvari assumed the presence of the free surface was reducing turbulent fluctuation and therefore reducing the growth of the width of the jet. On density profiles they observed that maximum buoyancy was found at the free surface and that buoyancy decayed almost linearly to zero at the jet boundary, but they failed to provide an explanation for this phenomenon.

Lal and Rajaratnam (1977) also undertook experiments on turbulent buoyant surface jets. From experimental observations they concluded that the normalised velocity profiles for all the experiments, and regardless of the flow's Richardson number, were described by the following exponential equation:

$$\frac{u}{u_m} = e^{-0.693(y/b)^2} \qquad \textit{(Eq. 2-11)}$$

Rajaratnam and Subramanya (1985) further investigated buoyant surface jets and confirmed Equation 2-11 also described in Chu and Vanvari's observations. Their results on the normalised velocity profiles are given in Figure 2.6.

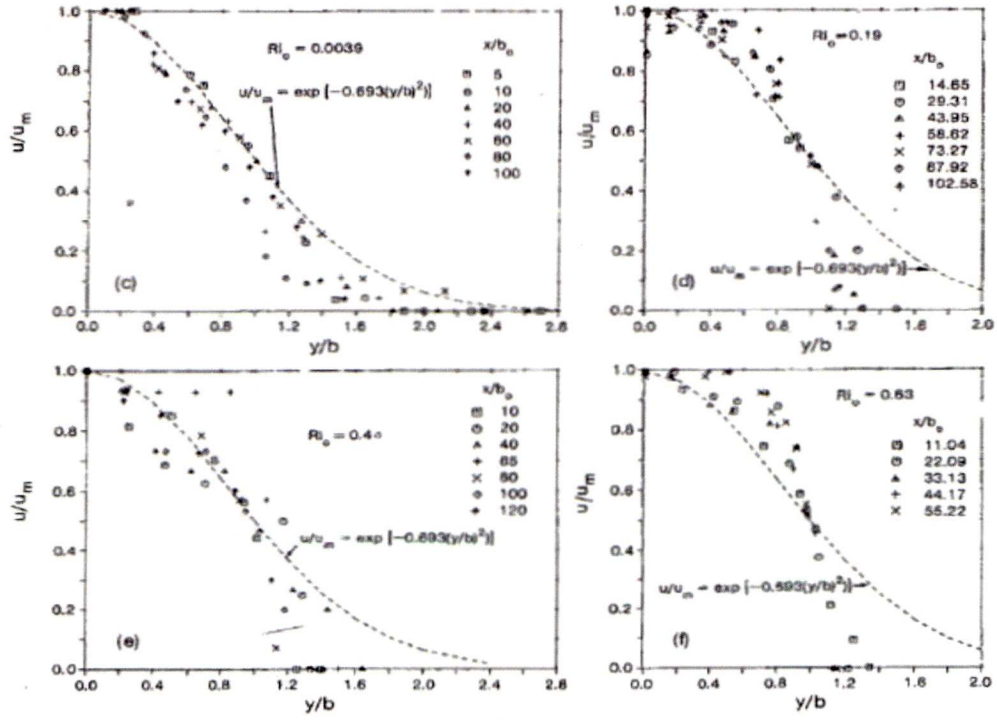

Figure 2.6: Normalised Velocity Profiles of Buoyant Surface Jet

(after Rajaratnam and Subramanya, 1985)

Rajaratnam and Subramanya (1985) compared their observations with observations on non-buoyant surface jets made by Rajaratnam and Humphreys (1984). The comparisons indicated the jet width of a buoyant jet was consistently smaller than that of a non-buoyant surface jet but velocities consistently decayed at a lesser rate

for a buoyant than for a non-buoyant surface jet. These comparisons are shown in Figure 2.7.

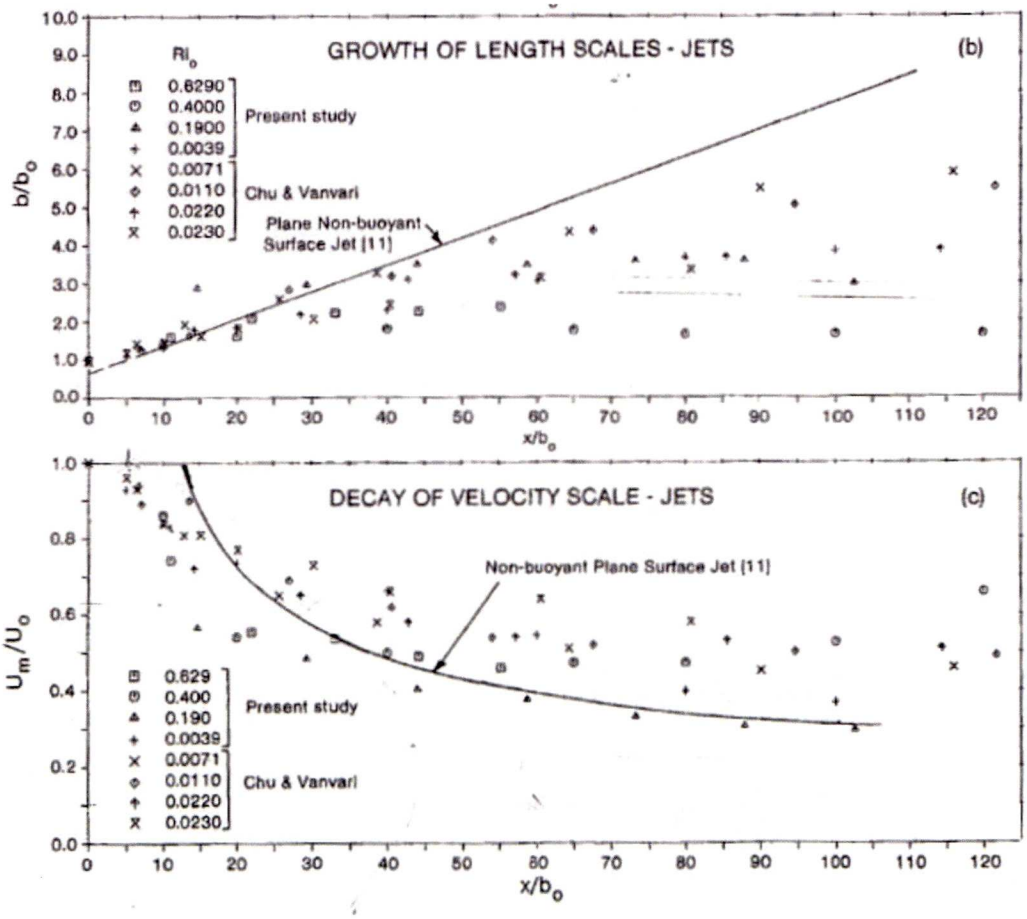

Figure 2.7: Experimental Observations of Buoyant Surface Jet

(after Rajaratnam and Subramanya, 1985)

2.5.2 Heavy Wall Jet Experimental Study Overview

Wall jet flow is not as well studied or documented as other types of jet flows particularly as it relates to surface pressure fluctuations or to the presence of surface roughness.

Rajaratnam undertook a number of experimental studies on turbulent wall jets in co-operation with various researchers. Wu and Rajaratnam (1995) and later Ead and Rajaratnam (2002) undertook experimental studies on plane turbulent wall jets.

Rajaratnam and Subramanya (1986) however, performed an experimental study specifically on denser (or heavy) wall jets.

All these studies considered the velocity distribution along the axis of the jet and concluded that the maximum velocity is observed at distance δ from the wall boundary, essentially dividing the jet into two layers.

The region from the point where the maximum velocity occurs and further away from the wall boundary is called the outer layer and it was observed that the velocity decay followed a Gaussian distribution. In the region between the wall boundary and the maximum velocity, or the lower layer, the flow is assumed to be laminar. Experimental velocity profiles of turbulent wall jets as provided by Ead and Rajaratnam (2002) are shown in Figure 2.8 overleaf.

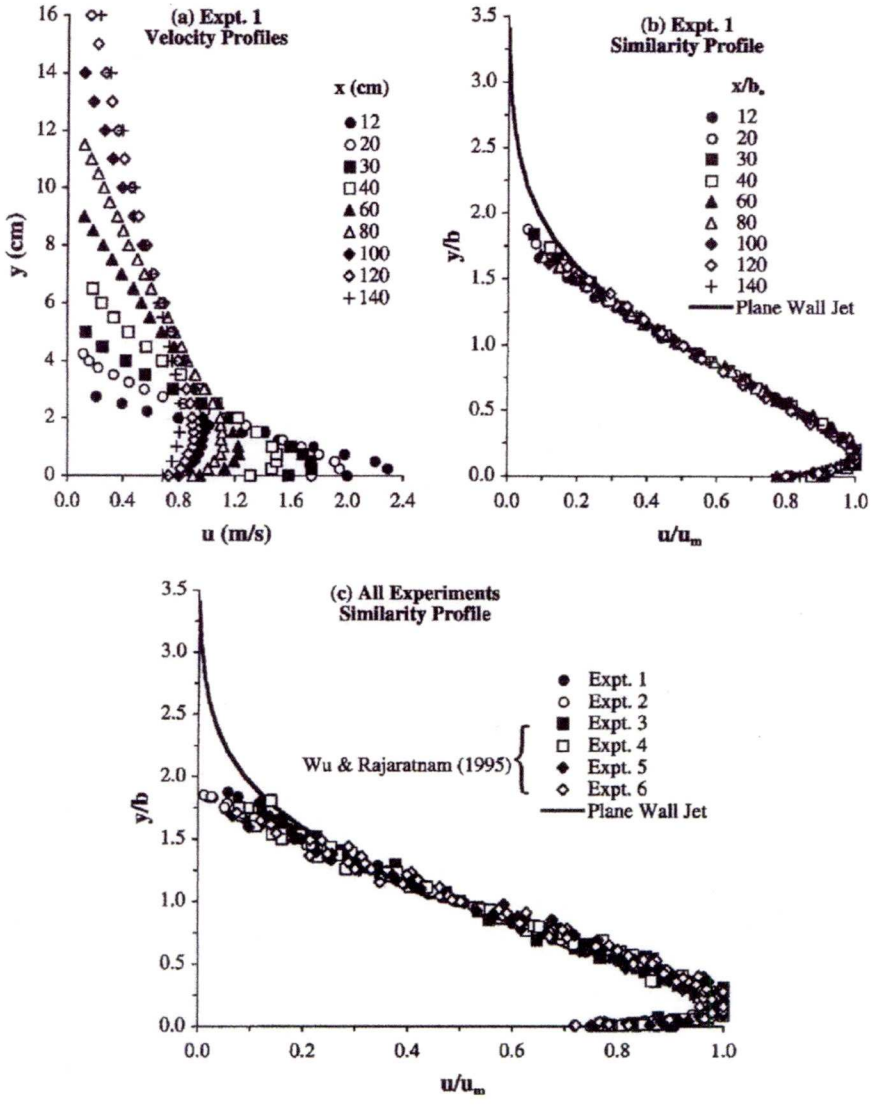

Figure 2.8: Velocity Profiles for Plane Wall Jets
(after Ead and Rajaratnam, 2002)

Rajaratnam and Subramanya (1986) in their study of heavy wall jets observed that the width of a heavy wall jet was smaller than that of a non-buoyant wall jet. They also provide dimensionless temperature defect profiles for a range of initial Richardson numbers Ri_o. The temperature defect profiles are in Figure 2.9 overleaf.

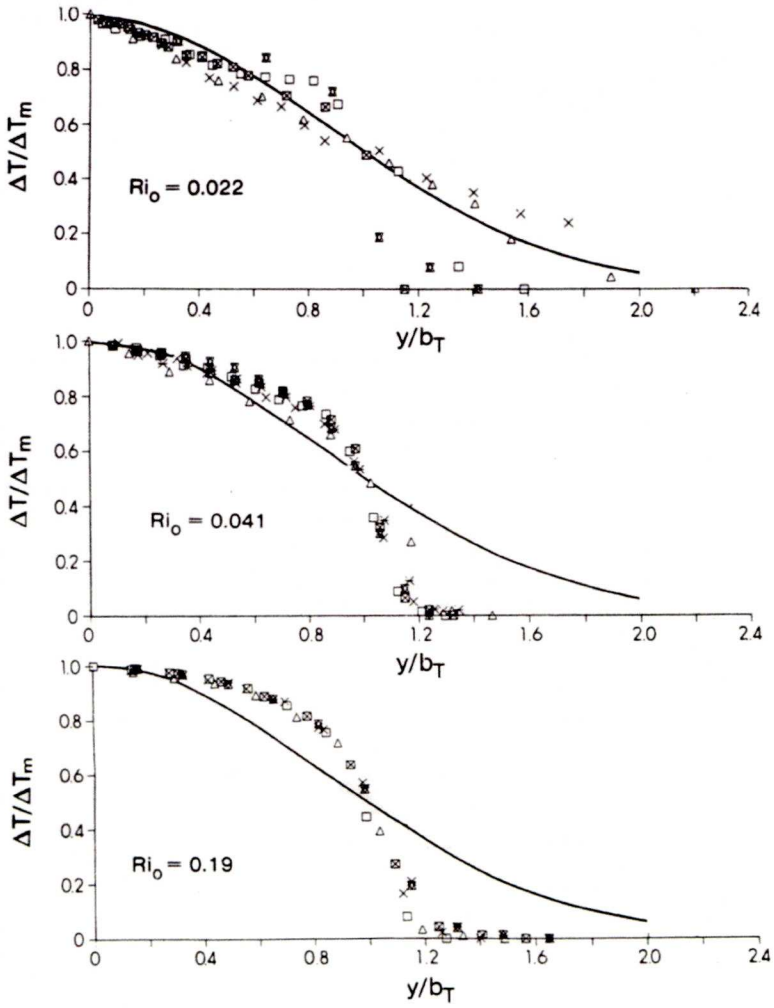

Figure 2.9: Dimensionless Temperature Defect Profiles for Plane Denser Wall Jets

(after Rajaratnam and Subramanya, 1986)

From Figure 2.9, however, it is observed that the temperature does not defect on a Gaussian distribution in the outer layer of the jet in keeping with the velocity decay. It is commonly assumed that buoyancy decay follows the pattern of the velocity decay, this nevertheless, is an assumption and no detailed studies have been undertaken to further scrutinize this assumption.

Chapter 3. CFD Literature Review and Theory

Computational Fluid Dynamics (CFD) is the analysis of fluid flow and associated phenomena by means of computer based simulation. The spatial domain is discretized into small cells to form a volume grid (mesh) and then a suitable numerical algorithm is applied to solve the equations of motion. There are several commercial CFD packages available; for this study the code used is *FLUENT* and particular equations refer to this code.

3.1. Introduction to Computational Fluid Dynamics

Computational Fluid Dynamics, or CFD, provides a useful tool that allows computational investigations of complex fluid flows by solving the equations of motion within a given geometry and physical context. Such solutions are normally unattainable in other ways, as the Navier-Stokes equations have few simple and analytical solutions which generally do not apply in practical cases.

3.1.1 Applications of CFD

The technique is powerful and has a wide range of applications, both industrial and non-industrial, which include:

- aerodynamics of aircrafts and vehicles
- hydrodynamics of ships
- turbo machinery
- electrical and electronic engineering
- chemical process engineering
- marine engineering
- environmental engineering
- hydrology and oceanography
- external and internal environments of building
- biomedical engineering

The main reason CFD has lagged behind other computer-aided engineering tools is the tremendous complexity of the underlying behaviour which precludes a general description of fluid flows that is both economical and sufficiently complete.

3.1.2 CFD Elements

CFD codes developed for solving flow problems are structured around numerical algorithms that tackle the fluid flow problem. All CFD codes are comprised of three elements: a pre-processor, a solver and a post processor. A diagram of the three CFD process stages is displayed in Figure 3.1.

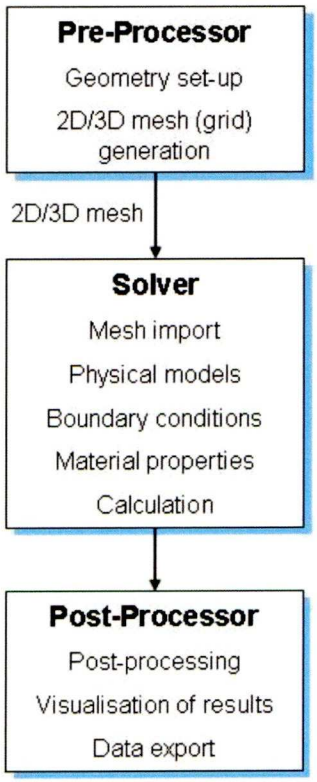

Figure 3.1: CFD Simulation Process Stages

(a) Pre-processor

Pre-processing consists of the input of a flow problem into a CFD program. At the pre-processing stage the user has to accurately define the flow domain. A volume mesh, or grid, that describes the flow domain has to be generated and the appropriate mesh type and size has to be chosen. Any simplifications made when defining the

domain also need to be carefully considered, as they could greatly influence the flow and consequently the results obtained. This stage is usually the most time consuming when performing a CFD analysis and particularly prone to user errors.

(b) Solver

The solver stage is the stage in the analysis where the physical and chemical, if applicable, phenomena to be modelled are defined and the numerical algorithm computes the solution to the specified flow problem. The fluid properties are also defined at this stage along with the appropriate boundary conditions. The choices made by the user at this stage greatly influence the outcome of the analysis and have to be carefully considered. This stage is crucial when performing a CFD analysis and is also prone to user errors.

Generally, the algorithm for the finite volume method consists of three steps:

- Formal integration of the governing equations of fluid flow over all the control volumes of the solution domain.
- Discretization. This stage involves the substitution of a variety of finite difference type approximations for the terms in the integrated equation representing flow processes such as convection, diffusion and sources.
- Solution of the algebraic equations by an iterative method.

The solver stage of a CFD analysis, depending on the computational capacity of the computer used for the analysis, the nature and complexity of the flow and the size of the domain, can take anything from minutes to days to obtain a solution.

(c) Post-processor

The post-processing stage only has to do with the presentation and, more specifically, the visualisation of the obtained results. Several tools, such as domain

geometry and grid display, vector plots, contour plots, line and surface plots and particle tracking are available in all CFD commercial packages. Although CFD packages offer post-processing options, quite often, for more impressive results, external post-processing packages are used. A relatively recent development in the visualisation of the results of CFD analyses is animation for dynamic results display; a particularly useful tool in time dependent flows. Finally, data export facilities for further external manipulation of the results obtained is available.

3.1.3 Advantages of CFD Compared to Experimental Approaches

There are several unique advantages of CFD over experiment-based approaches to fluid systems design. Some major advantages are the substantial reduction in lead times, costs of new designs and the ability to study systems where controlled experiments are difficult, or even impossible, to perform, such as with very large systems. Finally, the ability to study systems under hazardous conditions at and beyond their normal performance limits, such as safety studies and accident scenarios, and the practically unlimited level of detail of results obtained gives CFD a real lead compared to experimental approaches.

3.2. Grids

One of the main concepts behind CFD is dividing the fluid geometry into small cells and, for each cell, solving equations for property variables such as velocity, pressure and turbulence. The cells are obtained by dividing the fluid body into a grid. The composition and quality of the grid is important for the accuracy and the stability of the solution of the equations. Grids can be classified according to several characteristics such as shape, orthogonality, structure and position of variables. Grids

can be structured or unstructured, depending on the characteristics of the flow domain (see Figure 3.2).

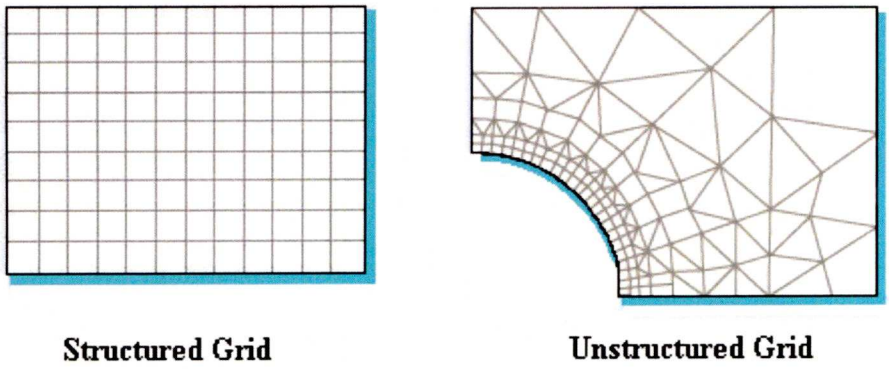

Figure 3.2: Grid Types

3.3. The Finite Volume Method

The finite volume method is one of the premiere numerical methods used in the simulation of fluid flows. The basic characteristic of the method, making it suitable for this type of application, is that it is fully conservative, meaning that, at any mesh density level, transported quantities are fully conserved. This basic property is due to the method discretizing an integral form of the governing equation, yielding a semi-discrete balance equation.

Discretization is the transformation of the partial differential equation into a new equation, where the variable in one cell is a function of the variable in the neighbouring cells. The new function can be thought of as the weighted average of the concentration in the neighbouring cells. Finite Volume Discretization is a two step process that first involves the transformation of the governing equations into a set of semi-discrete balance equations, followed by the transformation of these equations into a set of algebraic equations. Each of these steps requires some

assumptions with regard to the accuracy of the method and with regard to the type of profile assumed between control volumes. A schematic demonstration of the discretization process is given in Figure 3.3 with the directions described according to geographic position, i.e. north, south, east and west.

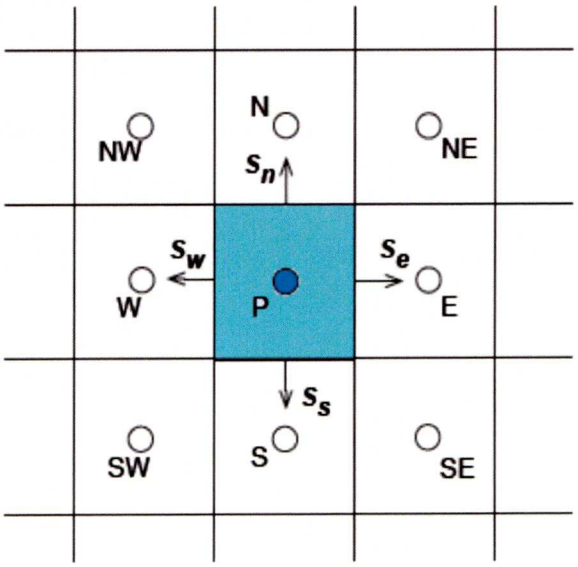

Figure 3.3: Schematic of Discretization

3.4. Basic Equations

When performing a CFD simulation for any given flow regime the code solves conservation equations for mass and momentum for every cell of the domain. For turbulent flows additional transport equations are solved to represent the fluctuating velocity fields.

3.4.1 The Continuity Equation

The continuity equation is a mathematical statement to ensure the rate at which mass enters the domain is equal to the rate at which mass leaves the domain. The continuity equation is written as:

$$\frac{\partial \rho}{\partial t} + \nabla \cdot (\rho \vec{u}) = 0 \qquad \textit{(Eq. 3-1)}$$

Where: ρ is the fluid density, $\vec{u}$ the velocity vector and t the time.

3.4.2 The Momentum Conservation Equation

The conservation of momentum equation is an expression of Newton's second law of motion to a continuum. In fluid dynamics the Navier-Stokes equations form a vector continuity equation describing the conservation of linear momentum which is written as:

$$\frac{\partial}{\partial t}(\rho \vec{u}) + \nabla \cdot (\rho \vec{u} \vec{u}) = -\nabla p + \nabla \cdot (\overline{\overline{\tau}}) + \rho \vec{g} + \vec{F} \qquad \textit{(Eq. 3-2)}$$

Where: p is the static pressure, $\rho \vec{g}$ is the gravitational body force, $\vec{F}$ the external body forces and $\overline{\overline{\tau}}$ the shear tensor, given by

$$\overline{\overline{\tau}} = \mu \left[\left(\nabla \vec{u} + \nabla \vec{u}^T \right) - \frac{2}{3} \nabla \cdot \vec{u} I \right] \qquad \textit{(Eq. 3-3)}$$

Where: μ is the molecular viscosity and I the unit tensor.

3.5. Boundary and Initial Conditions

In CFD to model a flow problem, the domain of interest is regarded as finite (isolated). However, in reality, there is no such thing as a finite domain as every fluid flow case is influenced by its surrounding environment. To represent the effect of the surrounding environment, the appropriate initial and boundary conditions have to be implemented at the edges of the domain. These are composed of a mathematical model and, when required, numerical values.

The fact that the boundary conditions have an impact on the solution within the computational domain makes their correct selection a matter of great importance. If

the boundary condition is located too close to the flow area of interest there is the possibility that it will force the solution, leading to a numerical simulation that does not represent reality. As each boundary condition represents a mathematical model, the wrong choice can lead to unrealistic results. Therefore boundary conditions are a critical component of the simulation and great care is required when locating and implementing them in the CFD model.

The most common boundary conditions in the discretized equations of the finite volume used by the *FLUENT* package are:

- Inlet boundary
- Outlet boundary
- Wall boundary
- Pressure boundary
- Symmetry (or axis) boundary, and
- Periodic boundary

3.5.1 Inlet Boundary Conditions

Inlet boundaries are the boundaries where the distributions of all flow variables are specified and are typical for incoming flows. In the *FLUENT* package one can find the following inlet boundary conditions:

i. Velocity inlet: the velocity at the inlet is specified via the setting of a velocity field, which can be a constant value, a profile or individual nodal values.

ii. Mass flow inlet: the mass flow is specified.

The inlet boundary specification is very important where the inlet is far enough from the area of interest so the flow has the chance to develop fully. The inlet velocity can be approximately specified and still not influence the results at the area of interest.

The disadvantage to this is that the greater the domain, the longer the time required for the computation.

3.5.2 Outlet Boundary Conditions

Outlet boundary conditions are usually used in conjunction with the inlet boundary. Boundary conditions are essentially conditions imposed on the derivatives of the flow variables that set the mass flow rate at the outlet equal to the mass which enters the domain at the inlet. With the exception of velocity, all other transported quantities, for example, the turbulence kinetic energy, k, and the turbulence dissipation rate , ε, are given a zero normal gradient.

$$\frac{\partial k}{\partial n} = 0 \text{ and } \frac{\partial \varepsilon}{\partial n} = 0 \qquad \textit{(Eq. 3-4)} \text{ and } \textit{(Eq. 3-5)}$$

The procedure for the velocity field is different to ensure the essential for the finite volume mass conservation. As the flow into the domain must at all times equal the mass flow out for an incompressible flow, the normal velocity field gradient is initially set to zero, the mass conservation discrepancy is calculated and corrected by setting the normal velocity gradient to a constant. The main assumption behind this is that of a fully developed flow. The equation describing this is:

$$\frac{\partial u}{\partial n} = const. \qquad \textit{(Eq. 3-6)}$$

Because of the assumption behind the imposed derivative conditions, it is important that the location of the outlet boundary is selected far away from geometrical disturbances so that the flow reaches a fully developed state where no change occurs in the flow direction. It is normally possible to make reasonably accurate predictions of the flow direction some distance from obstacles, giving the opportunity to locate the outlet boundary perpendicular to the flow direction. Outlet boundaries close to

regions of the flow where there are large changes in the flow variables can force the solution, giving incorrect results.

3.5.3 Wall Boundary Conditions

The wall boundary condition is the most frequently encountered in cases of confined fluid flows. At solid walls for viscous flows the no-slip condition is applied for the velocity components. The no-slip condition indicates that the fluid sticks to the wall, or moves with the same velocity as the wall if a moving wall condition is specified.

In turbulent flows however, in particular for flows over rough surfaces, the friction with the wall can play a significant role in flow development. For this reason, when modelling a turbulent wall-bounded flow in which the wall roughness effects are considered significant, the wall roughness is specified and the 'law of the wall' equation is solved to calculate the velocity at the grid cells directly adjacent to the wall. In terms of the 'law of the wall' the average velocity of a turbulent flow at a certain point is proportional to the logarithm of the distance from that point to the wall.

3.5.4 Constant Pressure Boundaries

The constant pressure boundary condition is used in situations where exact details of the flow distribution are unknown. Values for pressure are set at the boundary, which can either be an inlet or an outlet depending on the available information.

3.5.5 Symmetrical (or Axis) Boundaries

Symmetrical boundaries are used where there is a known axis in the domain and the flow pattern is essentially mirrored. They provide a useful tool in saving computational time as only half the domain is required. However, they should not be assumed unless there is great confidence that there is indeed such an axis to the flow.

They should be avoided altogether in turbulent flows as the nature of turbulence is chaotic and non-symmetrical. Conditions set at a symmetry boundary are:

i. there is no flow across the boundary, and

ii. there is no scalar flux across the boundary.

In implementation, normal velocities are set to zero at a symmetry boundary and all other properties just outside the domain are equated to the values at the nearest node just inside the domain.

3.5.6 Periodic Boundaries

Periodic boundaries arise from a different type of symmetry in a flow. To set a periodic boundary the flux of all flow variables leaving the outlet periodic boundary are set equal to the flux entering the inlet periodic boundary. This is achieved by equating the values of each variable at the nodes just upstream and downstream of the inlet to the nodal values just upstream and downstream of the outlet.

3.6. Turbulence Models

Turbulence is the unsteady aperiodic motion in which all three velocity components fluctuate causing mixing of matter, momentum and energy. Turbulence modelling is one of the three key issues in CFD.

A flow regime is characterised turbulent when there are random fluctuations of local velocities that mix transported quantities, such as momentum, energy or even pollutants, causing them to also fluctuate. In CFD there are several assumptions for turbulence modelling approaches, called turbulence models. A turbulent model is a computational procedure that uses a set of modified (time-averaged) equations that

convert the instantaneous governing equations into computationally less expensive to solve equations by introducing unknown variables that have to be determined.

The *FLUENT* package provides the following turbulence models options:

- Spalart-Allmaras (One equation)
- k-ε (Two equations)
    - Standard k-ε model
    - Renormalisation group (RNG) k-ε model
    - Realizable k-ε model
- k-ω (Two equations)
    - standard k-ω model
    - Shear Stress Transport (SST) k-ω model
- Reynolds Stress Model (RSM) (Five equations)
- Large Eddy Simulation (LES) model

The choice of the turbulent model depends on the physics of the flow, the accuracy required and certain other factors. There are no rules for which model is appropriate for a specific flow and trials should be performed for the selection of the turbulence model. However, it has been ascertained through trials that certain models perform poorly with certain flows.

A brief description of the turbulence models available in the *FLUENT* v.6.0 code follows.

3.6.1 Spalart-Allmaras

The Spalart-Allmaras (1992) is a simple one equation model, based on Boussinesq's approach that solves a transport equation for a modified form of the kinematic

turbulent viscosity. The Spalart-Allmaras model was specifically designed for aerospace applications involving wall-bounded flows and its application is not recommended for other types of flows.

3.6.2 The k-ε Models

All k-ε models are two equation models that solve transport equations for turbulent kinetic energy, k, and for its dissipation rate, ε. Although the overall approach of all k-ε models is the same, the different models have certain differences, such as methods used for the calculation of the turbulent viscosity, the constants (Prandtl numbers) governing the turbulent diffusion of k and ε and the generation and destruction terms in the ε equation.

(a) The Standard k-ε Model

The standard k-ε model (Launder and Spalding, 1974) is a semi-empirical model. In its derivation it is assumed that the flow is fully turbulent and any effects of molecular viscosity are negligible, making it only valid for fully turbulent flows. This compels the use of wall functions for the viscous sub-layer near wall boundaries. Since the model does not calculate the individual Reynolds stresses and assumes that the three main components of velocity are equal, turbulence is considered to be isotropic.

(b) The Renormalisation Group (RNG) k-ε Model

The RNG k-ε model (Yakhot and Orszag, 1986) is similar to the standard k-ε but includes some refinements. It has an additional term in its ε equation and includes the effect of swirl in turbulence. Furthermore, it provides an analytical formula for turbulent Prandtl numbers and accounts for low Reynolds numbers, in contrast to the standard k-ε model. One further difference from the standard k-ε model is the modified constants used in the RNG k-ε model.

(c) The Realizable k-ε Model

This realizable k-ε model (Shih *et al.* 1995) differs significantly from the two other k-ε models as it contains a different formulation for the turbulent viscosity and a completely different transport equation for the dissipation rate, ε.

3.6.3 The k-ω Models

(a) The Standard k-ω Model

The standard k-ω model (Wilcox, 1998) is another two equation turbulence model. The equation for the turbulent kinetic energy dissipation, ε, is replaced by an equation for the dissipation of unit turbulent kinetic energy, ω, which is easier to integrate.

(b) The Shear Stress Transport (SST) k-ω Model

The SST k-ω model (Menter, 1994) is a combination of the k-ε and standard k-ω models. It contains a blending function which activates the standard k-ω model in the near wall region and the k-ε model in the free stream. The constants in the SST k-ω model have been modified from those used in the standard k-ω model.

3.6.4 The Reynolds Stress Model (RSM)

The Reynolds Stress Model (RSM) solves transport equations for the Reynolds stresses as well as the equation for the dissipation rate. This means four equations for two-dimensional problems and seven equations for three-dimensional ones. Because of the number of equations solved the RSM is much more demanding computationally and requires longer periods to reach a solution.

3.6.5 The Large Eddy Simulation (LES) Model

The Large Eddy Simulation (LES) model is the only model that is a combination of RANS and Direct Numerical Simulation (DNS). This technique directly solves the large eddies in turbulent flows and models the smaller scale eddies that are

impractical to solve directly. LES is a more recent method that seems very promising; however it is still not widely applicable because of the large computational resources required.

3.6.6 Turbulence Models' Comparison

As there is no single turbulence model that can resolve the physics at all flow conditions different turbulence models are usually suggested by CFD software vendors to suit the demands of individual classes of problems. The choice of the turbulence model depends on the type of flow, the required level of accuracy and the available computational resources. Key features of the commonly used turbulence models available in *FLUENT* are described in the Table 3.1.

The recommendations supplied by the vendors are a useful tool to identify and eliminate turbulence models that are not suitable for the type of flow to be studied. These recommendations, however, are not suggestions but rather highlight the weaknesses of certain models in capturing the characteristics of certain types of flow. Hence, they are usually used as a guide to eliminate certain turbulence model options. The remaining models may then be used to undertake sensitivity tests to determine which model is the most suitable for the type of flow to be studied.

Table 3.1: Comparison of Turbulence Models[5]

Model	Description	Applications
Spalart-Allmaras Model	▪ One-equation model	Designed specially for aerospace applications involving wall-bounded high speed flows.
Standard k-ε Model	▪ Simplest of two-equation models	Robust. Suitable for initial iterations.
RNG k-ε Model	▪ Variant of standard k-ε ▪ Has an additional term in ε equation.	Accurate for rapidly strained and swirling flows.
Realizable k-ε Model	▪ Variant of standard k-ε ▪ New formulation for turbulent viscosity ▪ New transport equation for ε	Accurate for spreading of both planar and rounded jets. Recommended for flows with separation and recirculation.
Standard k-ω Model	▪ Solves for k-ω ▪ ω = Specific dissipation rate (ε/k)	Recommended for low-Re flows, wall bounded boundary layer, and for transitional flows.
SST k-ω Model	▪ Variant of Standard k-ω model ▪ Behaves like k-ω in near wall region ▪ Behaves like standard k-ε in the free stream	More accurate and reliable for a wider class of flows like airfoils, transonic shock waves, etc.
Reynolds Stress Model	▪ Five-equation model ▪ Avoids isotropic formulation of turbulent viscosity	Suitable for complex 3D flows with strong swirl/rotation. Run time and memory intensive.

3.7. Multiphase Models

Multiphase flow refers to situations where more than one fluid or more than one phase of the same fluid are present. In multiphase flow, a phase can be defined as an identifiable class of material that has a particular inertial response to, and interaction with, the flow.

The *FLUENT* code models several different fluids in a single domain using the Euler-Euler approach where the different phases are treated mathematically as interpenetrating continua and conservation equations are solved for each phase. The

[5] Table taken from the document: "MODELLING TURBULENT FLOWS IN FLUENT" obtained from http://www.fluent.com

multiphase models available in *FLUENT* are the Volume of Fluid (VOF) model, the mixture model and the eulerian model.

3.7.1 The Volume of Fluid (VOF) Model

The VOF model can model two or more immiscible fluids by solving a single set of equations and tracking the volume fraction of each fluid throughout the domain.

The VOF formulation relies on the fact that two or more phases are not really interpenetrating. For each additional phase added to the model, a variable called the 'volume fraction' is introduced. The sum of all volume fractions for each cell is equal to one. All variables in the cell represent volume-averaged values consistent with the volume fraction of each phase in the cell. One limitation of the shared-fields approximation is that where large velocity differences exist between the phases, the accuracy of the velocities computed near the interface can be adversely affected.

3.7.2 The Mixture Model

The mixture model is a multiphase model that can be used to model multiphase flows where the phases move at different velocities, but assume local equilibrium over short spatial length scales. It differs from the VOF as it allows the phases to interpenetrate and move at different velocities. The mixture model solves the continuity equation for the mixture, the momentum equation for the mixture, the energy equation for the mixture, and the volume fraction equation for the secondary phases, as well as algebraic expressions for the relative velocities if the phases are moving at different velocities.

3.7.3 The Eulerian Model

The eulerian model is the most complicated of the three multiphase models available in *FLUENT* as it does not solve a single set of equations like the earlier two models but different sets of equations, with additional sets of conservation equations introduced for each phase. The eulerian model because of the additional equations is computationally much more demanding than the other two models.

3.8. CFD Analysis Process

Performing a CFD analysis can be a complicated task with a variety of issues that need to be considered and a number of steps that need to be undertaken. As a result it is useful to identify the various stages of the analysis in advance and consider the various aspects of each stage separately.

Stages involved in the process of planning and performing a CFD analysis are:

a) Analysis Assessment of Requirements

The first step of the CFD analysis process is determining the objective of the analysis. There are several aspects of the analysis that need to be considered as part of the determination of the objective. Such aspects are the operating conditions, the dimensionality of the spatial model (1D/2D/3D), the temporal model (steady or unsteady) and the nature of the flow (inviscid / laminar or turbulent).

b) Analysis Specification

The next step is to determine the geometry and the extent of the finite flow domain in which the flow is to be simulated. Simplifications of the geometry need to be considered as they may be required to allow an analysis with reasonable effort. Initial and boundary conditions also need to be established.

c) Geometry Creation

The geometry and flow domain need to be created in such a manner as to provide input for the grid generation. For this reason, the modelling of the geometry has to take into account the structure and topology of the grid generation.

d) Grid Generation

At this stage of the analysis the flow domain is discretized into a grid, which should exhibit at least some minimal grid quality as defined by certain measures. These measures include orthogonality (especially at the boundaries), relative grid spacing (15 % to 20 % stretching is considered a maximum value) and grid skewness. In addition the maximum spacing should be consistent with the desired resolution of important features.

e) Model Set Up

As a finite flow domain is specified, physical conditions are required on the boundaries of the flow domain. The simulation generally starts from an initial solution and uses an iterative method to reach a final flow field solution. The strategy for performing the simulation involves determining such things as the use of space-marching or time-marching, the choice of turbulence or chemistry model, and the choice of algorithms for the iterations.

f) Solution Process and Monitoring

As the simulation proceeds, the solution is monitored to determine if an iterative converged solution has been obtained.

g) Post-processing

Post-processing involves extracting the desired flow properties from the computed flow field.

h) Sensitivities Examination

The sensitivity of the computed results must be examined to understand the possible differences in the accuracy of results and/or performance of the computation for such things as flow conditions and turbulence model time step.

i) Solution Verification and Validation

To verify the solution, the findings from the different simulations should be compared with findings from analytic, computational or experimental studies to establish the validity of the computed results.

3.9. Uncertainty and Error in CFD Simulations

There are many and diverse potential sources of uncertainty and error that cause CFD simulation results to differ from their true or exact values, or even from realistic values in many cases. The American Institute of Aeronautics and Astronautics (AIAA) in 1998 published a guideline for the verification and validation of CFD simulations,[6] in which the given definitions for uncertainty and error differ from what is usually defined as uncertainty and error in experimental investigations. The classical definitions are inadequate for computational simulations because the exact value is usually not known. Furthermore, these definitions link error with uncertainty, whilst the AIAA definitions differentiate error and uncertainty according to what is known. The definitions for error and uncertainty in CFD simulations, as given by the AIAA, are discussed in the following sections.

3.9.1 Definition of Uncertainty

Uncertainty is defined as *'A potential deficiency in any phase or activity of the modelling process that is due to the lack of knowledge.'* (AIAA G-077-1998e)

[6] American Institute of Aeronautics and Astronautics: Guide for the Verification and Validation of Computational Fluid Dynamics Simulations (G-077-1998e)

Potential is the key word in the above definition of uncertainty, which indicates that deficiencies may, or may not, exist. Uncertainty refers to lack of knowledge about the physical processes that go into building the model and also applies to describing deficiencies in turbulence modelling.

3.9.2 Definition of Error

Error is defined as *'A recognizable deficiency in any phase or activity of modelling and simulation that is not due to lack of knowledge'*. (AIAA G-077-1998e)

In contrast with the definition of uncertainty, the definition of error implies the deficiency is identifiable upon examination and is not a result of lack of knowledge.

As errors are identifiable, they can also be more easily classified. A basic classification of errors in CFD simulations is normally in two broad categories, as acknowledged or unacknowledged errors.

Acknowledged Errors

Examples of acknowledged errors include rounding-off errors and discretization errors. There are procedures for identifying these and possibly removing them, otherwise they can remain in the code with their magnitude estimated and listed.

Unacknowledged Errors

Unacknowledged errors are mainly programming errors or defects in the code. There are no set procedures for finding these and they may continue to exist within the code or simulation. These types of errors are discovered by systematically performing verification studies of sub-routines in the code and, in the entire code, reviewing the lines of code and performing validation studies.

Errors and deficiencies in the code lie within the programmers' responsibility and any analyses undertaken with commercial CFD packages are assumed to be free of errors and, if any exist, they are unknown to the user.

3.9.3 Classification of Errors

Although errors are broadly classified under two main categories: acknowledged and unacknowledged errors, there are many identifiable types of errors. These types of errors are discussed below, with specific mention made of user errors.

3.9.3.1 Physical Approximation Error and Physical Modelling Error

Physical approximation and modelling errors can either occur due to uncertainty in the formulation of the model or when the model is deliberately simplified by the user. These errors deal with the continuum model only and are concerned with the choice of the governing equations which are solved and models that are chosen for the fluid or solid properties.

Mehta (1998) outlines the sources of physical errors as:

1. the phenomenon is not thoroughly understood;
2. parameters used in the model are known but with some degree of uncertainty;
3. appropriate models are simplified, thus introducing uncertainty; and
4. an experimental confirmation of the models is not possible or is incomplete.

Even when a physical process is known to a high level of accuracy, a simplified model may be used within the CFD code for the convenience of a more efficient computation. Physical modelling errors are examined by performing validation studies that focus on certain models.

3.9.3.2 Computer Round-off Error

Computer round-off errors develop with the representation of floating point numbers on the computer and the accuracy at which numbers are stored. Round-off errors are acknowledged but, generally, they are not considered significant when compared with other types of errors.

3.9.3.3 Iterative Convergence Error

The iterative convergence error exists because iterative methods used in the computation of the solution must ultimately have a stopping point. Convergence is a major issue with the use of CFD software and can lead to significant errors. CFD problems in general are non-linear, and the solution techniques use an iterative process to successively improve a solution until convergence is reached.

In mathematics, convergence describes approaching a limit of an infinite sequence or series. Asserting convergence is to claim the existence of a limit, which may itself be unknown. So, as this definition indicates, the exact solution to the iterative problem is unknown, but the objective is to be sufficiently close to the solution for a particular required level of accuracy. Convergence therefore needs to be associated with a requirement for a particular level of accuracy which depends on the purpose to which the solution is to be applied.

Convergence is also often measured by the level of residuals. Residuals are the measure to which discretized equations are not satisfied. The user should therefore be aware of this, as it is up to the user to decide what convergence criterion should be used to assess a solution.

3.9.3.4 Discretization Error

Discretization errors, also known as numerical errors, are those errors that occur from the representation of the governing flow equations and other physical models as algebraic expressions in a discrete domain of space and time.

Discretization error is divided into two types:

- Spatial discretization error, and
- Temporal discretization error

A consistent numerical method will approach the continuum representation of the equations and therefore zero discretization error as the number of grid points or time steps increases and the size of the grid spacing or time step length approaches zero.

With the refinement of the grid, the solution becomes less sensitive to the grid spacing and approaches the continuum solution. This is known as grid convergence and the grid convergence study is a useful procedure for determining the level of discretization error existing in a CFD solution. The errors addressed by a grid convergence study are ordered discretization errors that are dependent on the grid size and vanish as the grid size approaches zero.

The discretization errors are the main source of concern to a CFD code user during an application. The reason is that discretization errors are dependent on the quality of the grid and the time step; however, it is difficult to precisely indicate the relationship between a quality grid or time step and an accurate solution prior to beginning the simulation.

3.9.3.5 User Errors

A user can obviously be a significant source of error in CFD simulations. User errors can be difficult to identify as they may show up as modelling or discretization errors.

In the case of a user introduced error, such as wrongly identifying whether a flow is turbulent or laminar, a converged solution may be obtained; however, the conclusions drawn from the simulation may be incorrect. User errors may not always be evident. Such an example is the proper choice of turbulence model for certain turbulent flows. The potential for usage errors increases with an increased number of options available in a CFD code.

It is possible the user may intentionally introduce modelling and discretization error in an attempt to expedite the simulation at the expense of accuracy. This may be appropriate as, for example, there may not be adequate computational resources to simulate at the suitable grid density or if the objective of the simulation is to get more general information at less accuracy as is the case in the conceptual stage of a design study. User errors can exist in any stage of the CFD analysis, from the geometry set up to post processing.

3.10. Verification and Validation

As already discussed, there are many potential sources of error and uncertainty in CFD simulations. The tasks of verification and validation are attempts to quantify the extent to which error and uncertainty affect the performance of a model when its results are compared against reality. For results obtained from a CFD analysis to be reliable, a careful numerical verification and validation of predictions is necessary.

The two processes are fundamental in ensuring the mathematical model is correct, the chosen numerical schemes are adequate and the numerical techniques implemented do not significantly influence the numerical solution. Finally, performing verification and validation assessment is the method to ensure the results compare, to some degree, with reality.

Roache (1998) gives the following definitions for verification and validation:

> *'Verification is the process of determining that a model implementation accurately represents the developer's conceptual description of a model and the solution to the model'.* (AIAA G-077-1998)

> *'Validation is the process of determining the degree to which the model is accurate in its representation of the real world from the perspective of the intended uses of the model'.* (AIAA G-077-1998)

Credibility of a CFD simulation is obtained by demonstrating acceptable levels of uncertainty and error as determined through verification and validation assessment.

There is disagreement among CFD experts on exact procedures for verification and validation of CFD simulations. CFD is maturing, but is still an emerging technology of a complex nature, involving strongly coupled non-linear partial differential equations which attempt to computationally model theoretical and experimental models in a discrete domain of often quite complex geometric shape. A detailed assessment of errors and uncertainties has to concern itself with the three roots of CFD: theory, experiment and computation.

3.10.1 Verification Assessment

Verification assessment examines if the programming and computational implementation of the conceptual model is correct. It is also used to examine the mathematics in the models through comparison to exact analytical results.

The approach used for the verification of CFD simulations is to identify and quantify the errors in the model implementation and the solution. There are two aspects of verification: verification of a code and verification of a calculation. The objective of verifying a code is error evaluation by finding and removing errors in the code. The

objective of verifying a calculation is error estimation by determining the accuracy of a calculation.

3.10.2 Validation Assessment

Whilst verification has been described as solving the equations right, validation has been described as solving the right equations. In essence, the validation assessment determines if the computational simulation agrees with physical reality by examining the science in the models through comparison to real world observations. For this reason validation has no meaning for the entire CFD code. It is only possible to validate the code for a specific experiment or range of applications for which there is experimental data. Applying the code to flows beyond the region of validity is termed prediction.

It is accepted that the experimental data sets themselves will contain bias errors and random errors which must be properly considered before any conclusions are drawn. The accuracy required in the validation activities is dependent on the application, and the validation should be flexible to allow various levels of accuracy.

The approach to validation assessment is to perform a systematic comparison of CFD simulation results to experimental data from a set of increasingly complex cases. This approach is also called a building-block approach and it is recommended that it is followed in performing the validation assessment of complex systems. The approach consists of phases involving successively more complex flow physics, geometry and interactions. By comparing the CFD results to the experimental data, it is hoped that there is a good agreement, which increases confidence that the physical models and the code represent the real world for this class of simulations.

The physical models in the CFD code contain uncertainties due to a lack of complete understanding or knowledge of the physical processes as is the case with turbulence. In turbulent flows the uncertainty can be examined by running a number of simulations with the various turbulence models and examining the effect on the results.

3.10.3 Grid Independence (Convergence) Study

A method for determining the ordered discretization error in a CFD model is to examine the spatial convergence of the simulation by performing a grid convergence (or grid refinement) study. The method essentially involves performing the simulation on two or more successively finer grids.

As the grid is refined (grid cells become smaller and the number of cells in the flow domain increase) and the time step is refined (reduced) the spatial and temporal discretization errors, respectively, should asymptotically approach zero, excluding any computer round-off error.

In many cases however the aim is not to determine the exact solution but to establish the error band for the engineering quantities obtained from a certain grid solution. If for example the CFD simulations are part of a design study that requires a number of simulations, the use of a coarser grid may be more realistic and less time consuming and so it is more practical to determine the error on that coarser grid. The issue is what level of grid resolution is appropriate. The appropriate grid resolution is a function of the flow conditions, type of analysis, geometry and other variables.

Even if the appropriate grid resolution is determined it is essential to recognize the distinction between a numerical result which approaches an asymptotic numerical value and one which approaches the true solution. It is hoped that as the grid is

refined and resolution improves the computed solution will not change much and approach an asymptotic value. However, there still may be error between this asymptotic value and the true physical solution to the equations.

Methods for examining the spatial and temporal convergence of CFD simulations have been reviewed by Roache (1998). Most methods are based on the use of Richardson's extrapolation. A description of the procedure of the most widely accepted method, the Grid Convergence Index (GCI), is presented next.

3.10.4 Grid Convergence Index (GCI)

Roache (1998) suggests a Grid Convergence Index (GCI) to provide a consistent manner in reporting the results of grid convergence studies and provide an error band on the grid convergence of the solution. The GCI can be computed using two levels of grid; however, three levels are recommended to accurately estimate the order of convergence and to check solutions are within the asymptotic range of convergence.

The GCI is a measure of the percentage the computed value is away from the value of the asymptotic numerical value. It indicates an error band on how far the solution is from the asymptotic value and indicates how much the solution would change with a further refinement of the grid.

The procedure for calculating the GCI on a set of three different grids where h is the grid size and $h1<h2<h3$, as given by Roache (1998) is:

> *'Firstly simulations are performed for every grid size in order to determine the values of the key variables for the different grid sizes. It is desirable that the grid refinement factor, defined as* $r=h_{coarse} / h_{fine}$, *is greater than 1.3'.*

Assuming velocity u as the key variable, the apparent order p of the method is calculated using the following expression:

$$p = \frac{\ln\left(\frac{u_3 - u_2}{u_2 - u_1}\right)}{\ln(r_{21})} \qquad \textit{(Eq. 3-7)}$$

Having calculated the apparent order of grid refinement p, the GCI can then be determined as:

$$GCI_{12} = \frac{F_s|\varepsilon_{12}|}{r_{12}^p - 1} \qquad \textit{(Eq. 3-8)}$$

where:

$$\varepsilon_{23} = \frac{u_3 - u_2}{u_2} \qquad \textit{(Eq. 3-9)}$$

$$\varepsilon_{12} = \frac{u_2 - u_1}{u_1} \qquad \textit{(Eq. 3-10)}$$

and Fs is a safety factor. The safety factor is recommended[7] as Fs=3.0 for comparisons of two grids and Fs=1.25 for comparisons over three or more grids.

If a desired accuracy level is known and results from the grid resolution study are available, it is possible to estimate the grid resolution required to obtain the desired level of accuracy from the following equation:

$$r^* = \left(\frac{GCI^*}{GCI_{23}}\right)^{1/p} \qquad \textit{(Eq. 3-11)}$$

In equation *3-11*, r^* is the refinement factor between the finest grid resolution and the grid resolution required for the desired level of accuracy and GCI^* is the desired Grid Convergence Index.

[7] Safety Factor values recommended by Roache (1998)

The extrapolated value of the velocity magnitude at specified locations can then also be calculated using the following equation as:

$$u_{ext}^{21} = (r_{21}^{p} u_1 - u_2)/(r_{21}^{p} - 1) \qquad \textit{(Eq. 3-12)}$$

This extrapolated velocity value is the value that would be obtained if the grid size was equal to zero.

The GCI calculation above is called the local grid convergence index as it provides the convergence at one selected location for a specific variable – velocity magnitude in the given example. Depending on the requirements of the validation the procedure can also be applied for several points on a cross section, or random points inside the domain. The procedure can also be applied for several variables of interest at the same location. When the GCI at a location is determined for more that one variable it is called a global GCI.

Chapter 4. Experiments on Turbulent Jets

The experiments performed as part of the study and the results obtained are described in this Chapter. The overall goal of the experiments was to provide experimental data sets to be used for the validation of computational fluid dynamic simulations of buoyant turbulent jets. The experimental measurements focused primarily on density distributions that indicate mixing caused by the buoyant jets. In total nine experimental runs were conducted investigating buoyant surface jets and heavy wall jets.

4.1. Experimental Arrangement and Instrumentation

4.1.1 The Experimental Arrangement

The experiments described in this Chapter were conducted in the hydraulics laboratory of the Department of Civil Engineering at the University of Liverpool. All the experiments were performed in a rectangular transparent glass walled flume. The length of the flume was 6m and depth and width were 1m and 0.3m respectively. Separate compartments were placed on either side of the main body of the flume to minimise vertical velocity components, arising from pumping the water into the flume, and to ensure the formation of a jet. More detailed dimensions of the experimental flume are shown in Figure 4.1. The inlet and outlet sides of the flume are illustrated in Photos 4.1 and 4.2.

On the inlet side of the flume (Compartment A), a filter was installed to further reduce turbulence induced by the vertical movement of the water and to hold any debris from the water storage tanks. Water was supplied to the flume through a 50mm diameter pipe that connected to a submersible pump in a supply water storage tank situated under the floor of the laboratory.

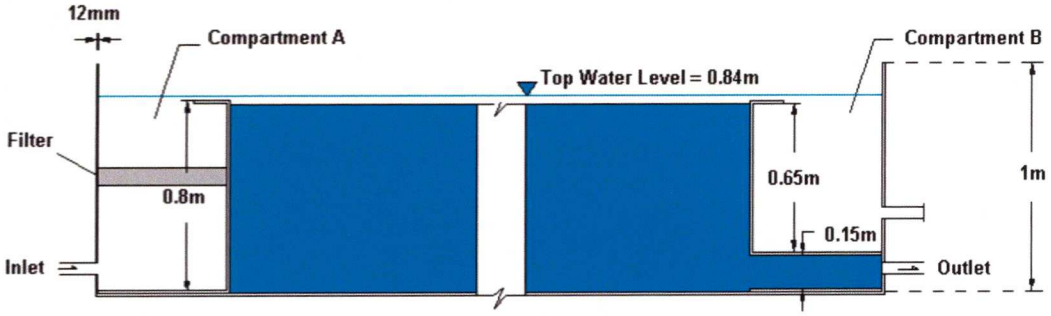

Figure 4.1: Flume Details

Photo 4.1: Experimental Flume - Compartment A (Inlet Side)

Photo 4.2: Experimental Flume - Compartment B (Outlet Side)

Water was drained from the flume through a 50mm diameter pipe that discharged into another tank also under the floor. The water tanks are shown in Photos 4.3 (a) and (b).

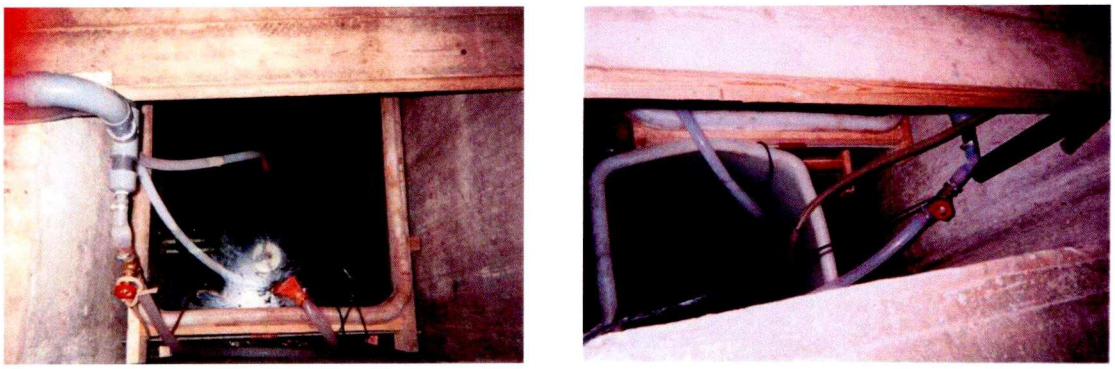

Photos 4.3 (a) and (b) – Water Storage Tanks

The supply storage tank was also used for the dilution of salt in fresh water for the production of saline water used in the experiments on heavy jets. For most of the experimental runs salt was diluted in fresh water to achieve a saline water density of 1025 kg/m^3. This saline water density value was chosen as it is similar to sea water density normally encountered in nature.

To enable visualisation of the flow Rhodamine, a water soluble tracer dye, was diluted in the saline water. The dye gave the saline water a deep pink colour that could easily be seen and photographed to capture the mixing process. The high concentration of Rhodamine dye meant that visualisation of the interface mixing layer was also possible. An example of Rhodamine dyed water is shown in Photo 4.4. Depending on the experiment undertaken the salt and Rhodamine were added to the water either in the supply storage tank or to the flume itself.

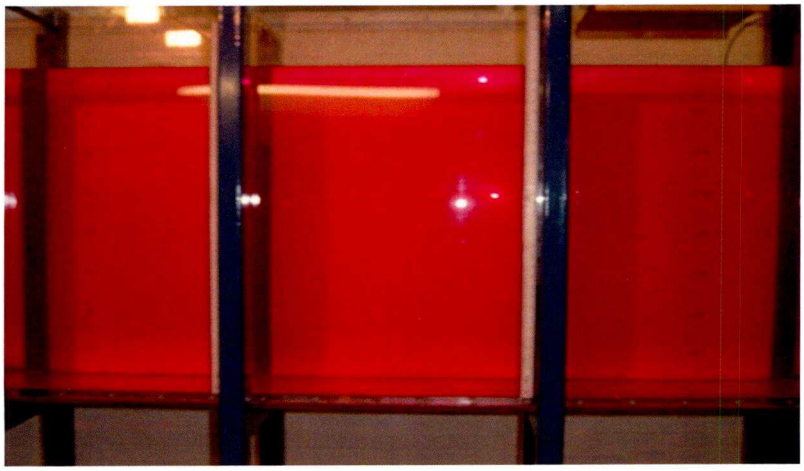

Photo 4.4: Rhodamine Dyed Saline Water

4.1.2 Instrumentation

The main instruments used in the experiments were propeller velocity meters for velocity measurements, a handheld density meter for density measurements and gauge meters for determining the location of the velocity and density measurements in the flume.

4.1.2.1 Velocity Measurements

The required velocity measurements were obtained with the use of Nixon miniature propeller velocity meters. The propeller meters are specifically designed for measuring water velocities in hydraulic models.

The Nixon miniature propeller meter comprises a probe and an indicator connected with a cable. The probe head has a five bladed PVC propeller, 11.6mm in diameter, mounted on a hardened stainless steel shaft which runs on bearings mounted in a protective cage. The cage is joined to a long thin tube with an insulated gold wire inside that projects to within 0.1mm of the tips of the blades. When the propeller rotates in a conductive liquid, the movement of the blades past the end of the wire varies the impedance between the wire and the tube. The indicator generates the carrier signal for the probe and displays the frequency of rotation of the propeller.

The propeller frequency displayed on the indicator is related to water velocity over its linear range with the use of a calibration chart provided by the manufacturer, a reproduction of which is attached as Appendix A.

According to the manufacturer, the Nixon miniature propeller meters can measure a linear velocity range of 6 cm/s to 150 cm/s with a nominal minimum velocity of 3 cm/s. The accuracy of the velocities obtained from the meters is given by the manufacturer as ± 2%.

The indicator and probe of the Nixon miniature propeller meters are shown in Photos 4.5 and 4.6.

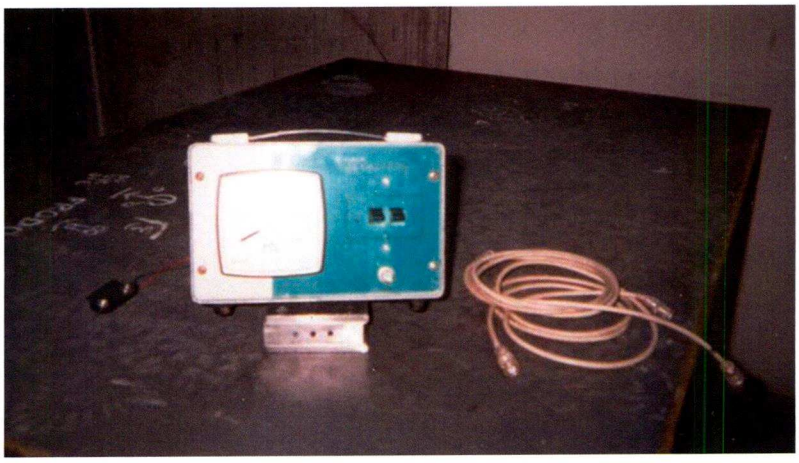

Photo 4.5: Velocity Meter Indicator

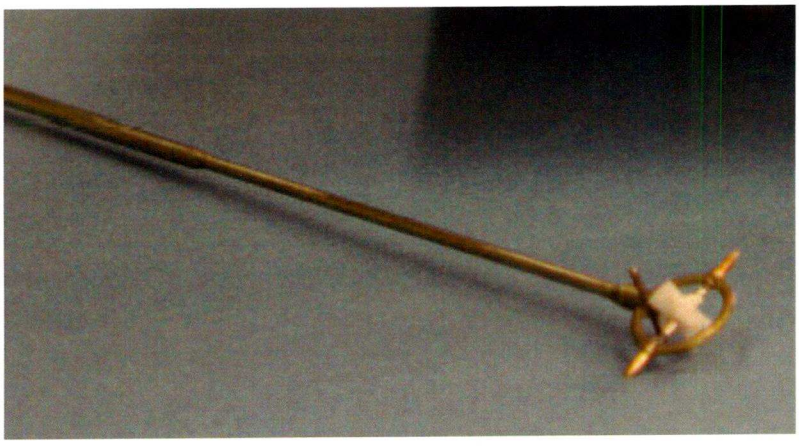

Photo 4.6: Velocity Meter Probe

Although a standard method for obtaining velocity profiles, propeller meters have several limitations. One such limitation is the low velocity threshold required for the meter to operate. Another significant limitation is their unidirectional measuring capability. The propeller rotates about an axis parallel to the flow giving the velocity magnitude along this direction, with readings measured in the case of re-circulating flows characterised by great instability.

4.1.2.2 Density Measurements

The required density measurements were obtained with an Anton Paar DMA 35N digital handheld density meter as shown in Photo 4.7. This particular meter is a handheld battery powered instrument based on the mechanical oscillator technique. A sample of approximately 2ml is transferred through suction to the device by pressing a lever on a built in pump. The sample to be measured is then introduced into a hollow U-shaped oscillator made of borosilicate glass.

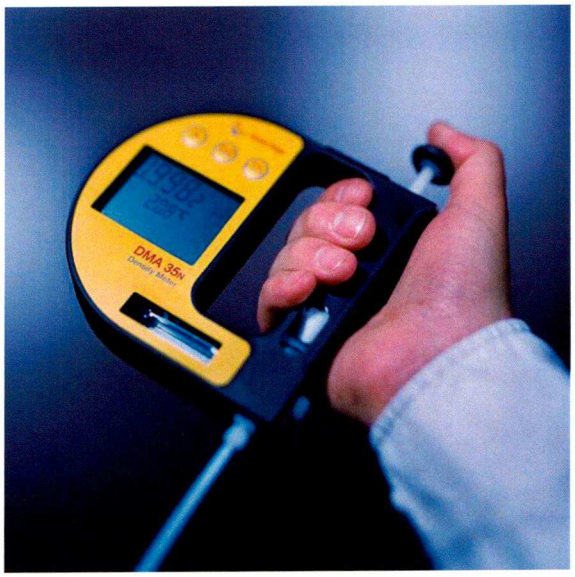

Photo 4.7: Anton Paar DMA 35N Handheld Density Meter

Since the volume of the sample participating in the vibration is kept constant by the constriction of the oscillator, the oscillating period depends only on the sample's density and the temperature of the sampling tube. To eliminate the temperature

coefficient of the oscillator, the temperature of the oscillator is also determined. From these periodic measurements, a built in digital processor calculates the density according to the following equation giving the true density of the sample:

$\rho = A\left(T^2 - T_o^2\right)$ where: T is the actual period, T_o is the period of the empty oscillator (constant) and A is a constant. T_o and A are determined by the manufacturer and are stored in the processor's non-volatile memory.

The range of densities that can be measured with the Anton Paar DMA 35N meter varies from 0 to 1.999 g/cm^3, whilst the temperature range is 0 – 40°C. The density value indicated on the display screen corresponds to the true density at the measured temperature within an error range of ±0.001 g/cm^3.

A significant weakness of the device is the long time required for the meter to provide the measurement taken. The manufacturer states that the meter has a typical measuring time of 30 seconds. The time between measurements however is significantly higher due to a shortcoming of the handheld density meter in the need to flush clean the collection tube after every reading before being able to test another sample. This can lead to long periods between measurements, making it practically impossible to obtain simultaneous measurements.

Because of the inadequacy of the available density meter for use in time related measurements a technique had to be developed to overcome the limitations of the device. This was done by obtaining the water samples at all the locations simultaneously at precise times during the course of the experiment through a pipette type suction device and storing the samples in test tubes. The density of the samples was then measured after the end of the experiments and the results recorded. This method is described in further detail in Section 4.1.3 – Measurement Methods.

4.1.2.3 Depth Gauges

The location of the velocity and density measurements is of great importance for the experiments in the study. For this reason Vernier depth gauges were used for more accurate determination of the depth of the measurements inside the flume.

One Vernier depth gauge was located at the flow inlet and used to measure the depth of the flow. Depth gauges were also used at the locations of the velocity measurements. The probes of the velocity meters were attached to the depth gauges' arms and then lowered to the required depths. Attaching the velocity meter probes to the depth gauges ensured there was no horizontal movement of the probes during measurements, as the gauges were fixed on bases positioned at set locations on top of the flume.

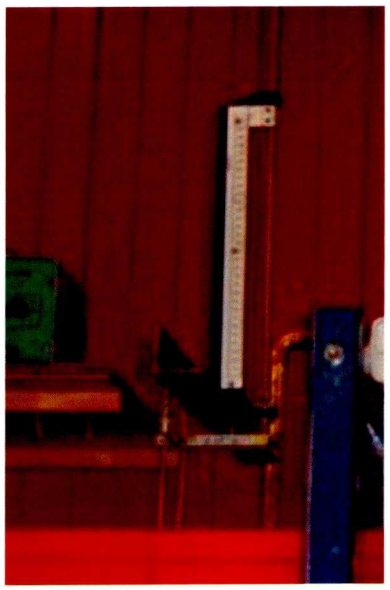

Photo 4.8: Vernier Depth Gauge

4.1.3 Measurement Methods

Velocity Measurements

Velocity measurements were taken at the inlet at the core of the jet for all the experimental runs. Determination of the inlet velocity is of great importance as it is the main parameter that determines the flow pattern. To obtain a velocity

measurement using a propeller velocity meter, the propeller has to be fully submerged in the water. For the inlet velocity measurement the meter was placed so that the propeller was fully submerged just under the water surface and centrally located with respect to the flume width at the exit point of the jet.

For any other velocity measurements the propeller meters were attached to Vernier depth gauges. The gauges enabled the accurate determination of the position of the propeller in the flume.

As there were insufficient propeller meters available to obtain measurements at all the points two velocity meters were fixed at two locations downstream of the inlet. These propeller meters were then lowered and any further measurements along that vertical axis were taken. The fact that the meters were fixed on the Vernier gauges, which in turn were fixed on the flume, meant there was no horizontal displacement of the meters when they were lowered to get the further readings.

The velocity measurements were not simultaneous without this being an issue. Once the jet developed it was expected that the velocity profiles would remain principally the same as long as the mass influx and velocity at the inlet remained constant.

Density Measurements

A requirement to facilitate the comparison of the experimental measurements with the computational results was the simultaneous capture of the density profile along the depth of the flume at more than one location. This could not be accomplished by measuring the density manually with the density meter at the required times. For this reason a technique had to be developed to enable the simultaneous measurements.

The problem was overcome as follows: A frame was installed over the flume and thin plastic tubes of corresponding lengths were lowered to the required depths. The samples were automatically drawn at specific times by pressing a button through a pipette type mechanism and were then put into test tubes for measurement at the end of the experimental run.

This method ensured that all the samples were taken from the exact locations and at the same time. The drawback of the method was the fact that the plastic tubes were an obstruction to the flow, possibly causing additional turbulence around the tubes. This however was deemed to be negligible in comparison with the turbulence of the flow and to have no significant effect on the results obtained.

A further aspect to be considered was the temperature of the water. Both the water entering the flume and the water in the flume should have the same temperature to ensure the buoyancy forces were the result of difference in density only and not differences in temperature. Temperature for both was ensured by having the tanks and flume filled overnight thus ensuring temperatures in both were the same.

4.2. Problems Encountered

During the course of this study several problems were encountered that affected the initial intentions for the study. The problems were mainly to do with the instruments intended for use in the experiments and the experimental facilities

The first problem encountered was with instrumentation and in particular with the device planned for use to obtain velocity profiles. The original intention was to acquire the velocity profiles by utilising an Ultrasonic Velocity Profiling (UVP) method. The UVP equipment would have enabled the measurement of instantaneous

velocity profiles along the whole depth of the flow area, including the capturing of velocity profiles at areas of re-circulating flows.

The University of Liverpool owns a UVP XW device manufactured from MET-FLOW SA in Switzerland. The device was acquired by the University in the 1980s and had been in disuse for a few years prior to the commencement of the study. Despite the disuse it was, at first, assumed the equipment was functioning properly. Attempts to obtain velocity profiles indicated the equipment was faulty and did not provide acceptable results.

The equipment was sent for repair; At first to the manufacturer's local representative in the UK, and later to the manufacturer in Switzerland. The repairs resulted in major delays, in excess of nine months, to the original schedule for the experiments. However, even after the repairs, problems with the equipment persisted and unfortunately its utilisation had to be abandoned.

This caused problems, as validation of velocity profiles could not be performed for every experiment conducted due to limitations with the propeller meters that could not provide readings on several occasions due to various impediments such as re-circulating flow or low values of velocity magnitude.

Other difficulties encountered with the experimental procedures were eventually resolved without causing significant problems or major delays to the project. One example was obtaining instantaneous density profiles; resolved by the construction of a sample 'drawing in' device as described in *Section 4.1.3 – Measurement Methods.*

Other developments affected the content of the project. During the course of the study the University implemented a restructuring of the Department of Engineering that

involved the relocation of the laboratories. In this restructuring the hydraulics laboratory had to be temporarily moved to another building before being permanently set up at its destined location. The relocation caused some minor delays but the major effect of the restructuring was that any experiments had to be completed by a certain date, after which the hydraulics laboratory would not be available for an extended period.

4.3. Experiments and Results

In total nine experimental runs were undertaken. Three runs on the surface buoyant jet and six on the heavy wall jet. The number of experiments was limited mainly because the aim of the experimental part of the study was not to extensively experimentally investigate these types of jets, which has already been done by several researchers, but to gather data on some critical variables that would enable the validation of simulations performed using Computational Fluid Dynamics (CFD). The experimental results were however compared with existing experimental data from other researchers to establish their reliability and check on their suitability for use as part of the validation of the simulations performed using the *FLUENT* CFD software.

The comparison of the experimental data with previous results was somewhat difficult as there are a limited number of previous studies on water buoyant jets that could be used. Although there are many studies on buoyant jets very few of these studies provide results comparable to these of the present study as the majority of previous studies involve other types of fluids (mainly air) and different turbulence levels and buoyancy differences. The comparisons with theory and experimental

results from other sources, however, provided confidence in the experimental data and any subsequent comparisons with computational results.

The main aim of the experiments of the study, to validate the computational simulations and to investigate how reliably CFD can be used to predict flow patterns and mixing caused by positively and negatively buoyant jets in realistic time scales, could be achieved with the use of the experimental data obtained.

All experiments were carried out in the flume described in Section 4.1.1. Different experimental set ups were used to account for the different buoyant jet types that were investigated and represent different mixing scenarios in natural environments. The experiments and the data are described in subsequent sections.

4.3.1 Experiments on the Buoyant Surface Jet (BSJ)

In total three experimental runs were conducted on the buoyant surface jet. The runs are labelled BSJ I, BSJ II and BSJ III. For each of the runs density profiles were obtained at three locations (5cm, 30cm and 160cm) downstream of the inlet. Density profiles were captured for all three runs 15 minutes after the start of the experiment. Profiles were also obtained 30 minutes from the start for the second run (BSJ II). Density measurements for both the fresh and the saline water were taken before the start of the experiments. The saline water density was measured as 1025 kg/m^3 and the fresh water density was 998.2 kg/m^3 for all three runs. The salt water density of 1025 kg/m^3 was chosen as it is usually the level of density encountered in sea water. Conditions under which each run was performed are summarised in Table 4.1.

Table 4.1: Summary of Experimental Runs on the Buoyant Surface Jet

Run Name	u_o (cm/s)	Ri_o	Measurement timings (min from start of run)	Measurement locations (distance from inlet)
BSJ I	20.50	0.050	15	5cm / 30cm / 160cm
BSJ II	8.00	0.128	15 / 30	5cm / 30cm / 160cm
BSJ III	15.00	0.065	15	5cm / 30cm / 160cm

Before each run the flume was filled with saline water (1025 kg/m^3 density) and dyed with Rhodamine to enable flow visualisation. The velocity at the inlet was measured with a propeller meter located exactly at the origin of the core of the jet. The density of the discharging fresh water was also measured before the experiments.

The original objective was to also capture velocity profiles of the buoyant surface jet for every run. This was attempted but could not be achieved using the propeller velocity meters. The limitation of the equipment to obtain measurements at areas of re-circulating flows and low velocities resulted in measurements with great uncertainty that were in the end deemed unsuitable for use.

4.3.1.1 Experimental Run 1 - BSJ I

The first experimental run on the buoyant surface jet was BSJ I. For this run the velocity at the inlet was measured as 20.5cm/sec, giving a densimetric Richardson number of 0.05 at the inlet. The salt water in the flume was sampled and confirmed to have a density of 1025 kg/m^3 while the fresh water had a measured density of 998.2 kg/m^3.

During the course of the experiment the density of the water was measured at several vertical locations at 5cm, 30cm and 160cm from the inlet. The measurements were taken after 15 minutes from the start of the experimental run. The exact locations and

density values of measurements taken can be found in Appendix B. The density profiles obtained from the measurements at the three locations downstream of the inlet are presented in Figure 4.2.

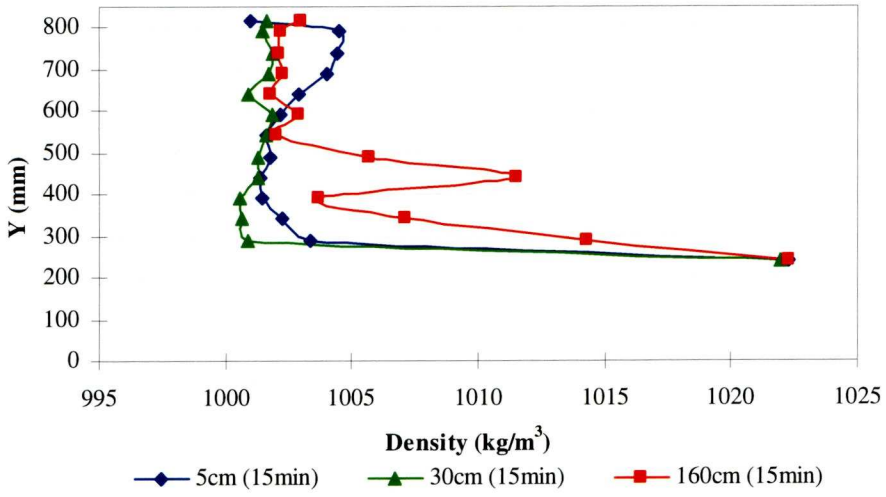

Figure 4.2: BSJ I - Density Profiles

Looking at the plotted the profiles, 15 minutes into the run there had already been significant displacement of the saline water. The interface between the two phases had moved downwards to the middle of the flume. The width of the interface between fresh and saline water seems to be different at each location with the widest interface observed at the furthest distance from the inlet section. Generally the measurements display some scatter, but, bearing in mind the difficulties with the instrumentation, they seem to be suitable for comparisons.

There were, however, some technical hitches during the course of the run that introduced uncertainty to the obtained measurements. A few minutes into the BSJ I run the fresh water level in compartment A started to fluctuate, due to a fault in the pump supplying water from the underground storage tank to the flume. The problem was immediately detected, action was taken and the water level was stabilised. Although the fluctuations of the inlet water level did not last for long they introduce additional uncertainty to the results.

Another element of uncertainty, acknowledged during this first run and applying to all further experimental runs conducted, was the determination of the velocity magnitude at the inlet. The pointer of the velocity meter normally fluctuates between a range of values and the decision for the average value lies with the operator taking the reading. This makes the readings more prone to human error; thus introducing uncertainty.

4.3.1.2 Experimental Run 2 - BSJ II

The second experimental run was BSJ II. For this run the jet velocity at the inlet was measured as 8cm/sec giving an initial Richardson number Ri_o=0.128.

Density measurements were taken at the same three locations downstream of the inlet as for BSJ I, at 5cm, 30cm and 160 cm. Two sets of density measurements were taken 15 minutes and 30 minutes after the start of the run. The profiles obtained from the measurements are presented in Figure 4.3.

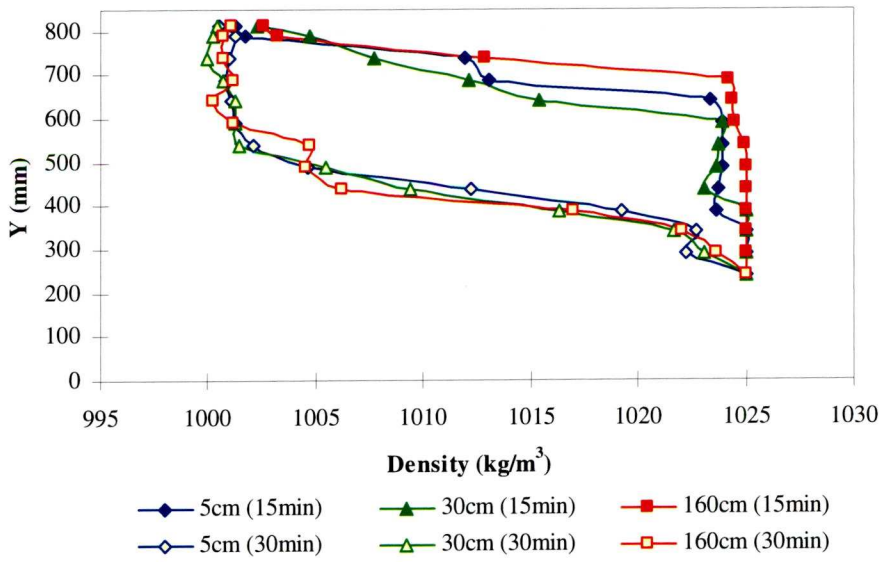

Figure 4.3: BSJ II - Density Profiles

The plot shows that in the 15 minutes between the two sets of measurements the migration of the density interface was roughly 200mm. Although after 15 min the

width of the interface varies at the three locations, the density profiles after 30 minutes show that the interface width between fresh and saline seems to be similar at all three downstream locations.

In addition to the density measurements taken after 15 and 30 minutes from the commencement of run, the location of the interface between the two phases was recorded and photographs of the interface were captured at five minute intervals. These photographs can be found in Appendix C. The measurements were then plotted and used to trace the interface development, presented in Figure 4.4.

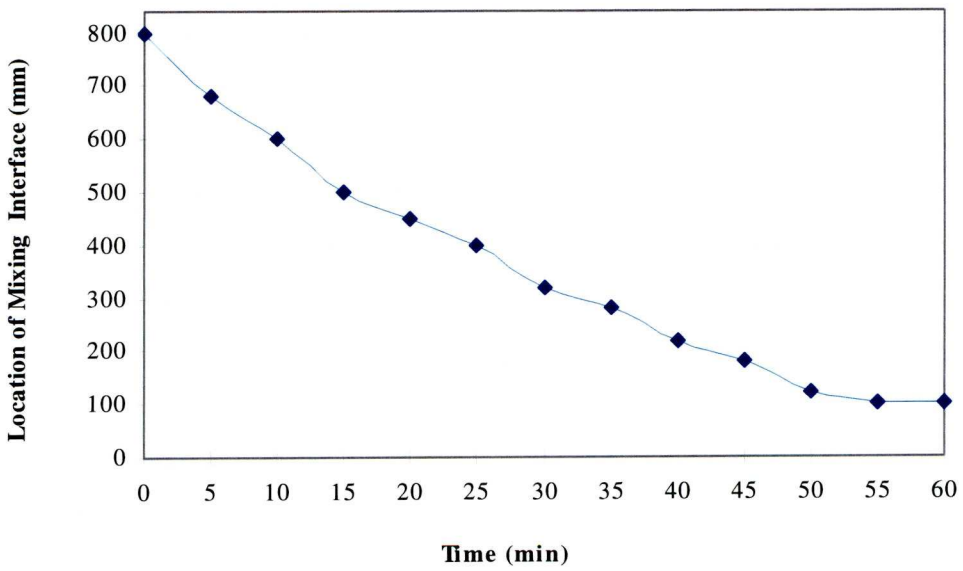

Figure 4.4: BSJ II - Migration of the Interface with Time

From the plotted interface locations with time it can be seen that the migration of the interface could be assumed to follow a linear development. With closer observation however, it can be seen that the profile closer to the top of the flume seems to have a steeper gradient, suggesting that the jet accelerates mixing whereas at the bottom of the flume mixing occurs mainly due to the density difference and mass influx.

4.3.1.3 Experimental Run 3 - BSJ III

The third and final run on the buoyant surface jet was BSJ III. For this run the inlet velocity was measured as 15cm/sec giving an initial Richardson number Ri_o=0.068. Similarly to the two previous runs on the buoyant surface jet, density measurements were taken at three locations (5cm, 30cm and 160cm) downstream of the inlet. The density measurements taken 15 minutes after the start of the experiment are plotted in Figure 4.5.

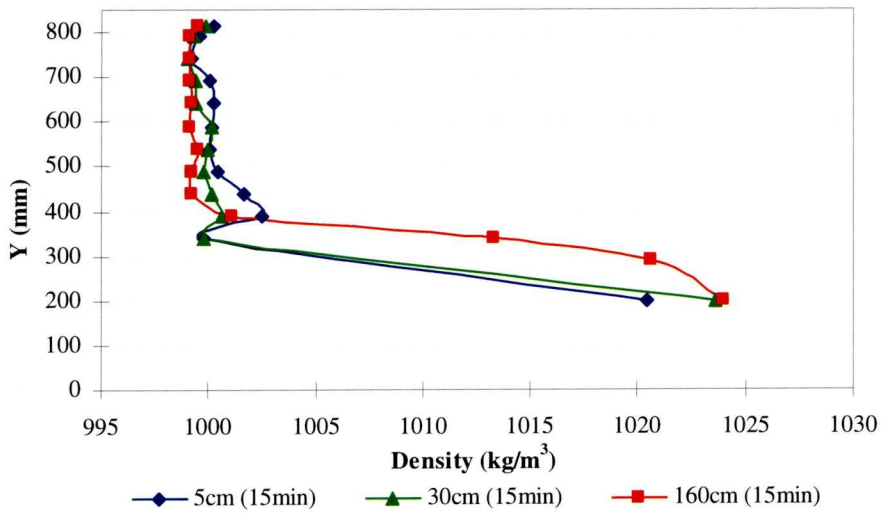

Figure 4.5: BSJ III - Density Profiles

The density profiles are again very similar to the previous two runs on the BSJ. The interface after 15 minutes had moved down towards the middle of the flume and was located between 200mm and 400mm from the bottom of the flume giving a mixing zone between the two fluids of roughly 200mm.

4.3.2 Discussion and Comparison with Studies on the Buoyant Surface Jet

To gain confidence that the experimental results on the buoyant surface jet were suitable for comparison with the simulation results, they were compared with experimental results from previous similar studies. A review of literature indicated

there are not many other experimental studies that could provide benchmarks. The most similar widely recognised studies on water mixing due to turbulent jets have been undertaken by Dr. N. Rajaratnam, in collaboration with various other researchers, and these studies were used for the comparisons.

For the experimental results to be comparable with results from previous studies the density profiles obtained were normalised. The process of normalisation is applied to experimental data with the aim to convert each measurement to a dimensionless quantity so that the data becomes comparable to other studies. Normalisation of the buoyancy, or the obtained density measurements, involved dividing the density difference ($\Delta\rho$) observed at each measurement point with the maximum density difference ($\Delta\rho_m$) at each section. Normalisation of the location was undertaken by dividing the depth of the location of the measurement (y) by the jet half width (b) at each section. The jet half width being the location where $\Delta\rho = \Delta\rho_m / 2$.

The dimensionless buoyancy (or density) defect profiles for the sets of measurements obtained for all three runs are presented in Figures 4.6, 4.7 and 4.8 for BSJ I, BSJ II and BSJ III respectively.

From the figures it can be observed that the buoyancy defect profiles deviate significantly from the Gaussian distribution that Rajaratnam and Subramanyan (1985) suggest, based on their observations and observations made by Chu and Vanvari (1976). It is noted that the researchers mentioned suggest the Gaussian distribution after verifying it with velocity measurements and have assumed that buoyancy defect follows the same trend as the velocity defect. No experimental studies could be found on buoyant surface jets where the buoyancy defect is analysed in detail. In the majority of the studies the focus is on the velocity field of the jet

which has been quite extensively researched experimentally. The transition from one fluid to the other and the decay of buoyancy seems to be more sudden and not follow the Gaussian distribution of the velocity decay.

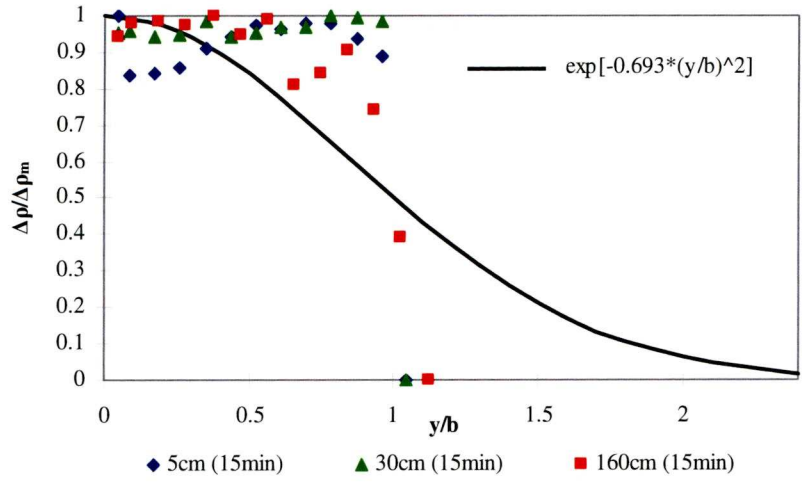

Figure 4.6: BSJ I - Dimensionless Buoyancy Defect Profiles

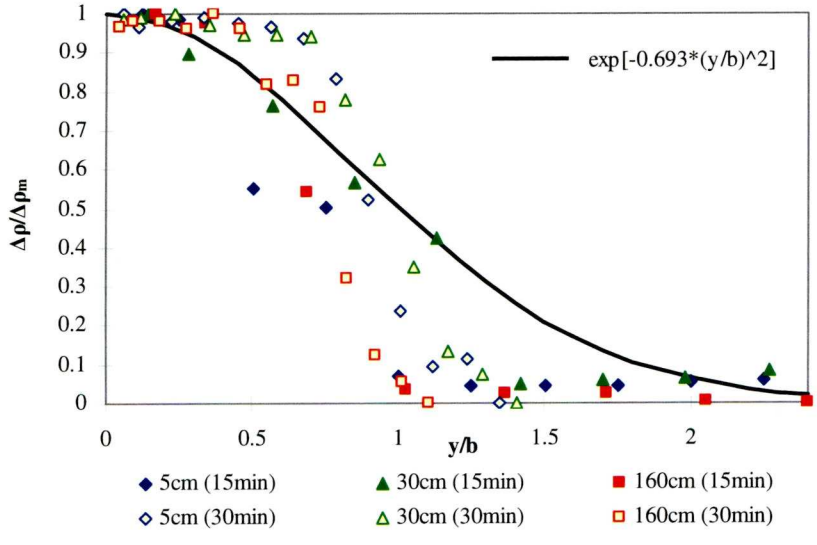

Figure 4.7: BSJ II - Dimensionless Buoyancy Defect Profiles

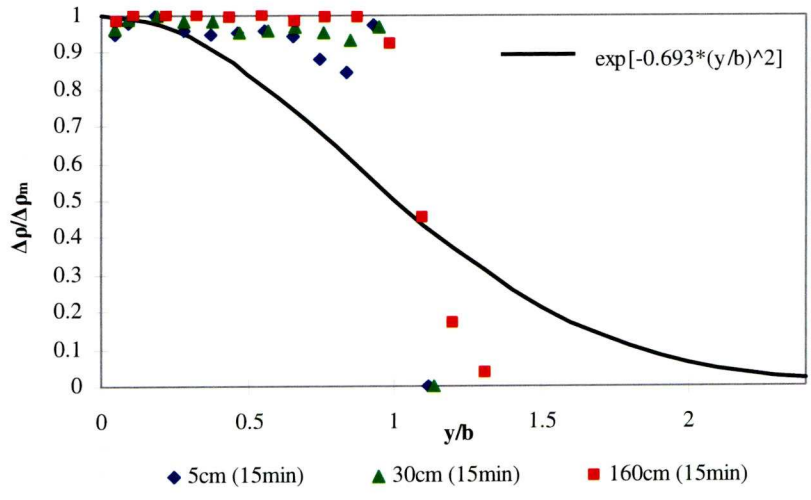

Figure 4.8: BSJ III - Dimensionless Buoyancy Defect Profiles

It also appears that the buoyancy, and in this case more specifically density, defect is also dependant on the inlet conditions and in particular the Richardson number. Looking at Figures 4.6 to 4.8 it can be seen that only in the case of BSJ II where the inlet velocity is significantly lower, and the Richardson number higher, than the other two runs, do the density defect profiles seem to follow a Gaussian pattern. Figure 4.6 and Figure 4.8 suggest that the transition between the two phases is not smooth but there are rapid changes in density suggesting that the mixing layer is not very wide and the flow is characterised by strong stratification.

No attempts were made to determine a relationship between the inlet *Ri* and the density distribution across the mixing interface as there was limited data available and such an investigation would require experiments that cover a range of Richardson numbers obtained with as accurate as possible instruments.

Overall, the experimental data obtained on the buoyant surface jet seem to compare well with results of previous studies and be adequate for comparisons with computational results.

4.3.3 Experiments on Heavy Wall Jet (HWJ)

Following the experiments on the buoyant surface jet, six experiments were performed for the collection of data on the heavy wall jet. The first four runs involved saline water of density of 1025 kg/m^3. Of the four runs with a saline water density of 1025 kg/m^3, two were carried out with the introduction of a 40cm long baffle, positioned 10cm from the inlet.

Two further runs were performed; one with saline water of 1010 kg/m^3 density and one with saline water of density of 1005 kg/m^3. These two runs were aimed to

gathering data for a flow when the buoyancy effect was not as dominant. For both these runs a 5cm long baffle was introduced to aid the direction of the flow towards the bottom of the flume and, as a result, aid the formation of the wall jet at the bottom of the flume.

The experimental runs, similarly to the surface buoyant jet experiments, were labelled HWJ I to HWJ VI and density profiles were obtained at various locations downstream of the inlet side of the flume. For the first two experiments on the heavy wall jet velocity profiles were also captured and are discussed in the relevant sections.

Table 4.2 gives a summary of the experimental runs performed on the heavy wall jet.

Table 4.2: Summary of Experimental Runs on the Heavy Wall Jet

Run Name	u_o (cm/s)	Ri_o	Measurement timings (min from start of run)	Measurement locations (distance from inlet)
HWJ I	20.00	0.051	15 / 30 / 45	30 cm / 280cm
HWJ II	22.00	0.047	15 / 30	30 cm / 280cm
HWJ III	20.50	0.050	15 / 30 / 60	30 cm / 172.5cm
HWJ IV	31.25	0.033	10/ 20 / 40 / 60	30 cm / 172.5cm
HWJ V	30.00	0.034	6 / 16	12 cm/ 60 cm/ 113 cm/ 164 cm
HWJ VI	28.50	0.036	6 / 16	12 cm/ 60 cm/ 113 cm/ 164 cm

4.3.3.1 Experimental Run 4 - HWJ I

The first experimental run to be carried out on the heavy wall jet was HWJ I. Density measurements were obtained at two locations downstream from the inlet (at 30cm and 280 cm). In total three sets of measurements were taken during the course of the run at 15 minutes, 30 minutes and 45 minutes from the commencement of the experiment. The density profiles at both locations and for both times are given in

Figure 4.9 overleaf. Figure 4.9 shows that similar levels of mixing occur at both downstream sections with the density profiles at the same times being similar at both sections.

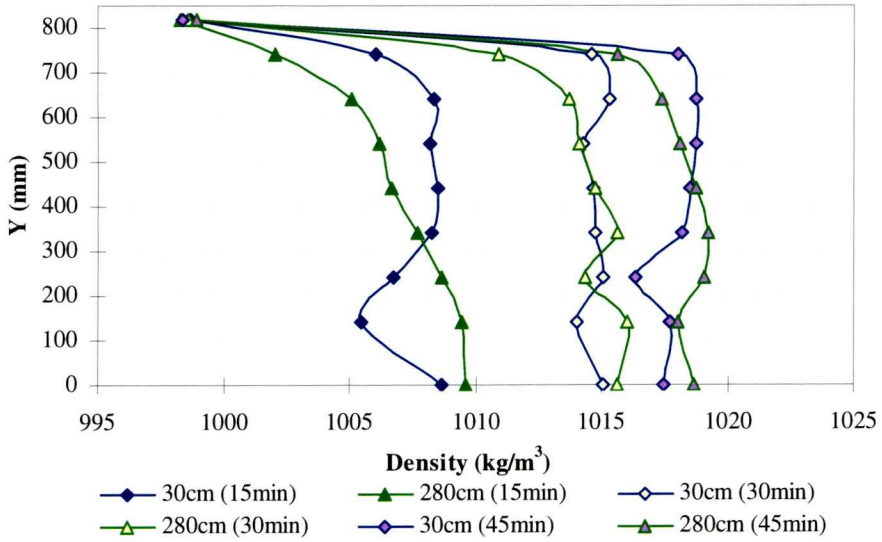

Figure 4.9: HWJ I - Density Profiles

Velocity profiles for HWJ I at the same two downstream locations (30cm and 280 cm) were also captures and are plotted in Figure 4.10.

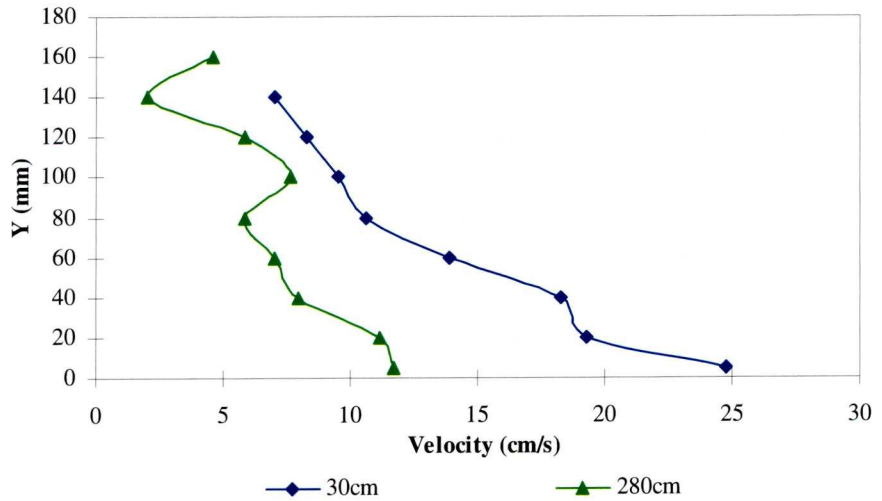

Figure 4.10: HWJ I - Velocity Profiles

Velocity measurements could not be taken for a wider section, either because the velocity was below the 6cm/s limit of the propeller meter, and no indication was given on the meter, or, because of high turbulence and re-circulation at the edges of

the jet, the meter indicator was too unstable to provide a reasonable measurement. The measurements, of both density and velocity, show some irregularities but do not seem unrealistic or unsuitable for comparisons.

4.3.3.2 Experimental Run 5 - HWJ II

Density profiles for the second run on the heavy wall jet were taken at the same locations as for HWJ I at 30cm and 280cm from the inlet side of the flume. This run did not last as long as HWJ I so measurements were only taken at 15 minutes and 30 minutes. Plots of the density profiles for HWJ II are given in Figure 4.11. The profiles are very similar to the density profiles of HWJ I indicating mixing along the whole depth of the flume.

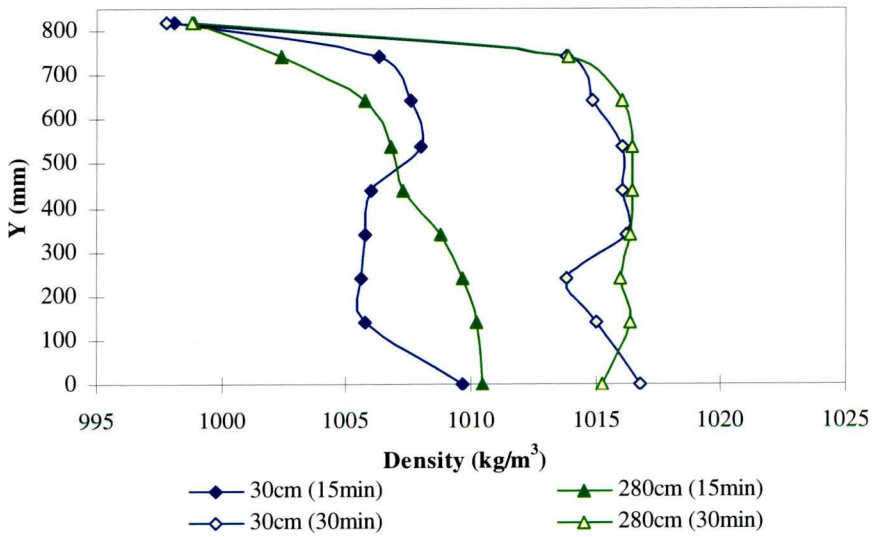

Figure 4.11: HWJ II - Density Profiles

As for HWJ I, velocity profiles along the axis of the heavy jet were also captured for HWJ II, and these profiles are given in Figure 4.12.

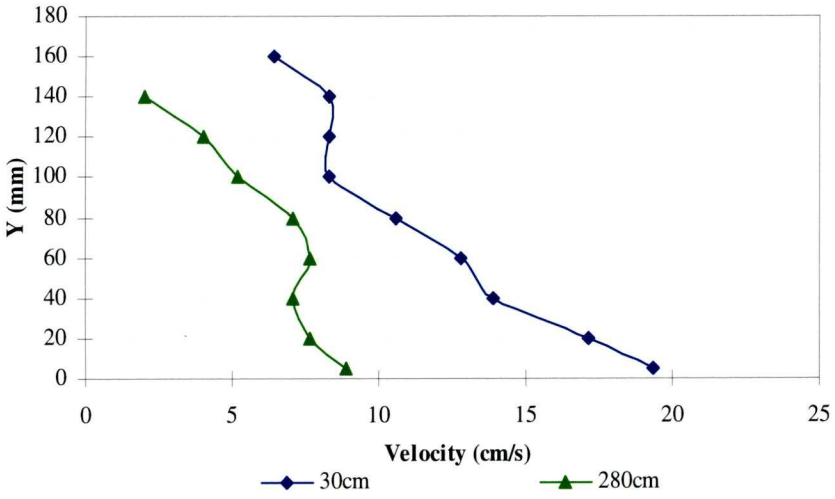

Figure 4.12: HWJ II - Velocity Profiles

The velocity profiles for HWJ II were again very similar to the ones for HWJ I. In both cases the maximum jet velocity at 280cm was measured to be approximately half the maximum velocity at 30cm.

It has to be noted however that the velocities at the second section, located 280cm from the inlet side of the flume, are very close to the propeller velocity meters minimum measured velocity capability of 6cm/s. The measurements were characterised by great instability of the indicator and this is very likely to be a source of error.

4.3.3.3 Experimental Run 6 - HWJ III

For the following two runs on the heavy wall jet (HWJ III and HWJ IV) a 40 cm deep baffle was introduced 10cm from the inlet side of the flume, as shown in Photo 4.9.

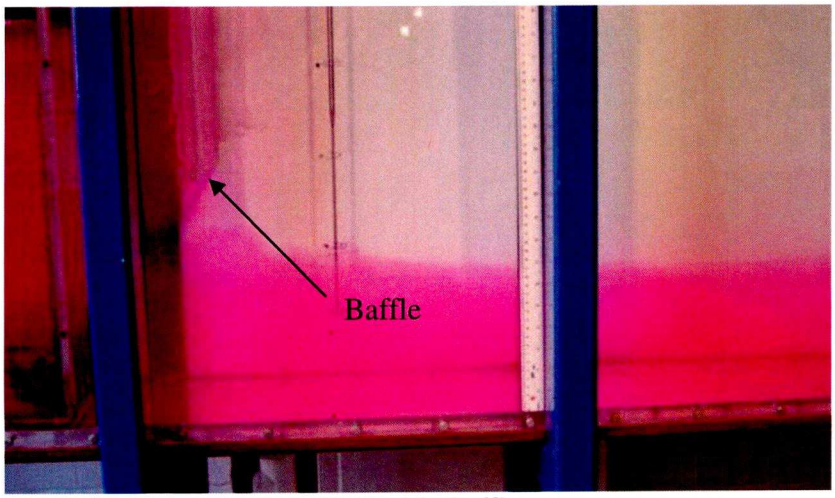

Photo 4.9: Baffle

The introduction of the baffle aimed to force the flow to the bottom of the flume, aiding the development of the heavy wall jet.

For HWJ III the density was measured at two locations downstream of the inlet side of the flume at 30cm and 172.5cm. Measurements in this case were taken at 15 minutes, 30 minutes and 60 minutes into the experimental run. The density profiles at each of these times are given in Figure 4.13.

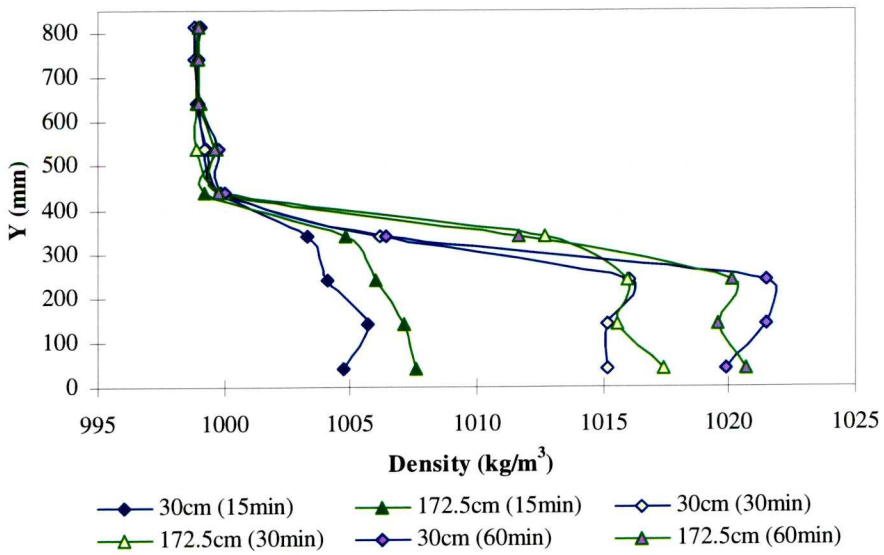

Figure 4.13: HWJ III - Density Profiles

The density profiles show the progressive mixing with density along the bottom of the flume increasing with time. Mixing appears to be uniform along the bottom of the flume with no mixing occurring above the level of the baffle. This is also demonstrated in Photos 4.10 (a) and (b) that were taken 60 minutes after the start of the run. The photographs show that the Rhodamine dyed saline water does not extend above the level of the baffle indicating a very strongly stratified layer.

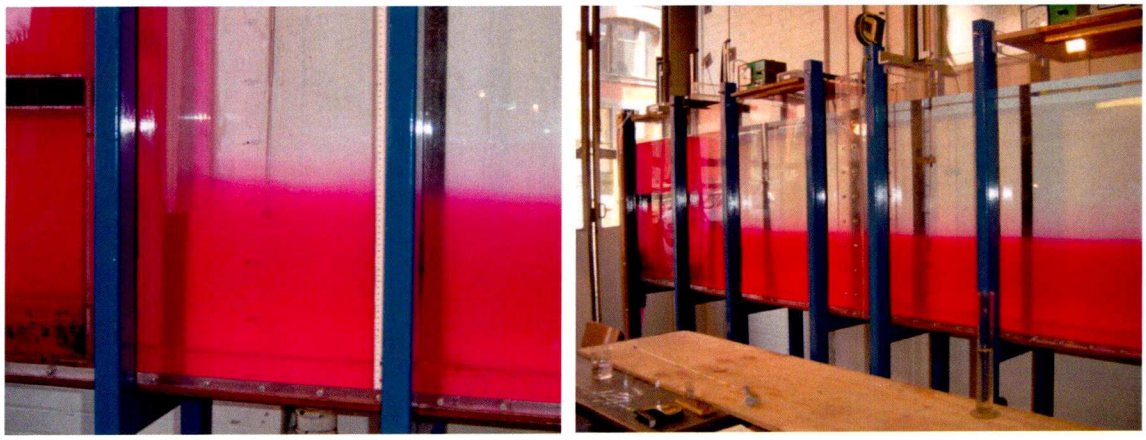

Photos 4.10 (a) and (b): Effect of the Baffle on the Interface between the Two Phases

4.3.3.4 Experimental Run 7 - HWJ IV

A further run, HWJ IV, was carried out on the heavy wall jet with the use of the 40 cm long baffle. Similarly to HWJ III density was measured at 30cm and 172.5cm downstream from the inlet side of the flume this time at 10min, 20min, 40min and 60 minutes after the start of the run. Density profiles captured during this run are given in Figure 4.14.

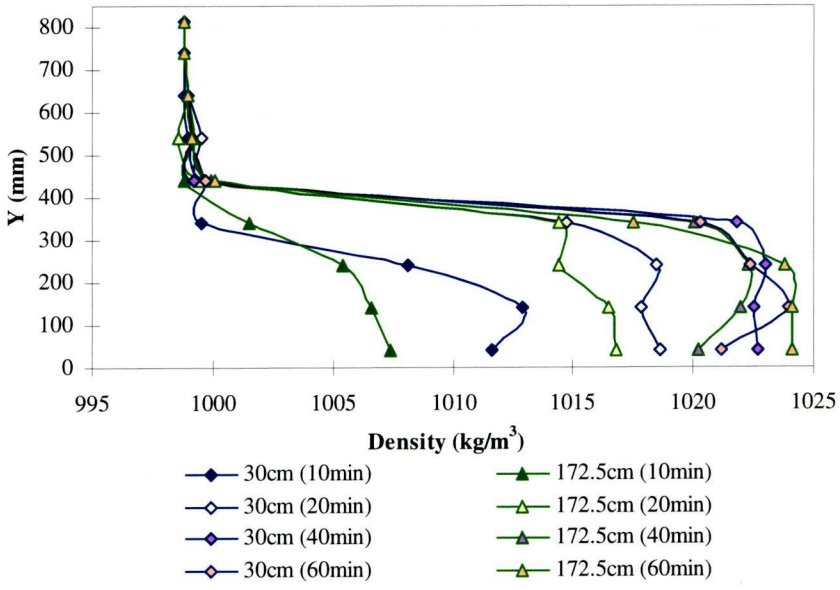

Figure 4.14: HWJ IV - Density Profiles

The profiles of both HWJ III and HWJ IV show that the baffle plays a significant role in the mixing occurring in the flume by creating a stratification interface between fresh and saline water which seems to extend only to the level the baffle is submerged in the water in the flume. Although the presence of the baffle aided the formation of the heavy wall jet, it restricted the mixing occurring in the flume.

4.3.3.5 Experimental Run 8 - HWJ V

The last two experimental runs (HWJ V and HWJ VI) were performed varying the density of the saline water to 1010 kg/m^3 and 1005 kg/m^3 respectively. A 5cm deep baffle was introduced 10cm downstream of the inlet with the aim again to direct the flow to the bottom of the flume and aid the development of the heavy jet.

Similarly to all the previous experimental runs density profiles were measured at locations downstream of the inlet. For HWJ V the density was measured at 12cm, 60cm, 113cm and 164cm. The way in which HWJ V differed from the previous runs was the saline water density that was reduced to 1010 kg/m^3. Density measurements

were taken at 6 min and 16 min into the run and are presented graphically in Figures 4.15 and 4.16.

The measurements were split into two separate graphs as the smaller density difference meant that the spread of the data was not as wide as for the previous runs and plotting all on the same graph resulted in a very congested figure.

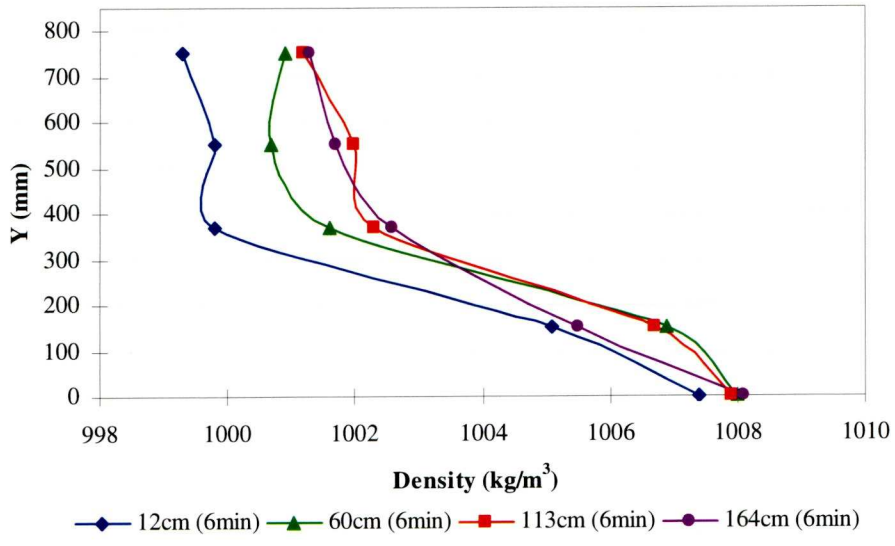

Figure 4.15: HWJ V - Density Profiles (t=6 min)

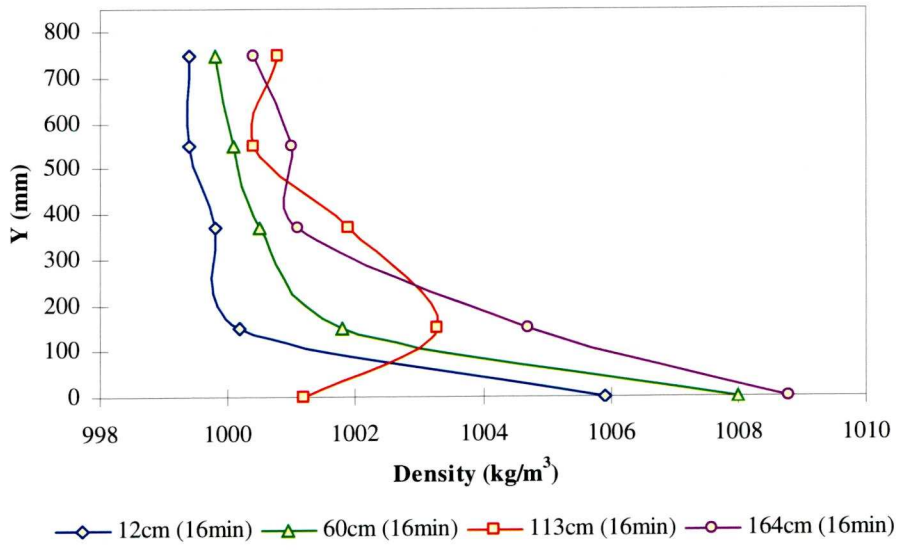

Figure 4.16: HWJ V - Density Profiles (t=16 min)

A discrepancy was noticed between the density measurements after 6min and after 16 min from the start of the run. Comparing the two sets of data it was found that higher densities were measured after 6min contrary to what was expected. This could be either the result of recirculating flow or some fault of the equipment when taking the density measurements.

4.3.3.6 Experimental Run 9 - HWJ VI

The final experimental run (HWJ VI) used saline water of a density of 1005 kg/m^3. As was the case with HWJ V, a 5cm deep baffle was introduced 10cm downstream of the inlet with the aim to direct the flow to the bottom of the flume and the density measurements were taken at 12cm, 60cm, 113cm and 164cm from the inlet side of the flume at 6 min and 16 min from the start of the experiment. Measurements taken are again split into Figures 4.17 and 4.18 for clearer presentation.

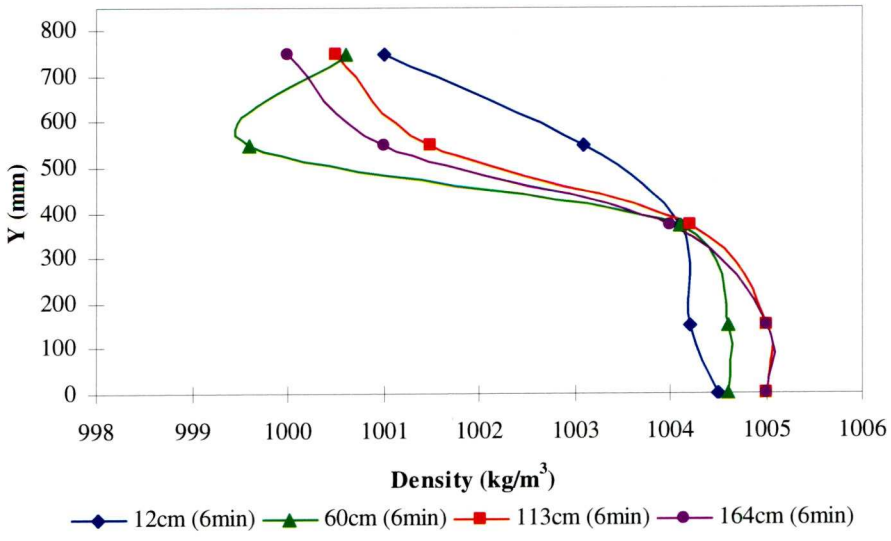

Figure 4.17: HWJ VI - Density Profiles (t=6 min)

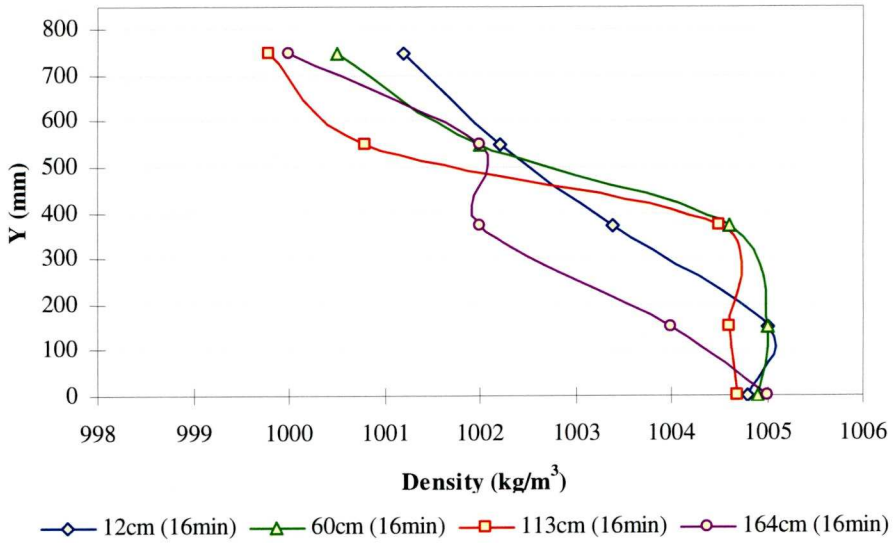

Figure 4.18: HWJ VI - Density Profiles (t=16 min)

4.3.4 Discussion and Comparison with Studies on HWJ

All the data acquired on the HWJ and described in the previous sections were normalised and compared with results of a similar experimental study on the plane wall jet by Ead and Rajaratnam (2002).

The first comparison involved the velocity distributions for HWJ I and HWJ II. Ead and Rajaratnam (2002) suggest that normalised velocity profiles follow a Gaussian type distribution as illustrated in Chapter 2 (Figure 2.8).

Following normalisation of the velocity profiles by dividing the velocity at each point by the maximum velocity at that cross-section and dividing the distance of each point from the wall with the jet half width Figure 4.20 was produced.

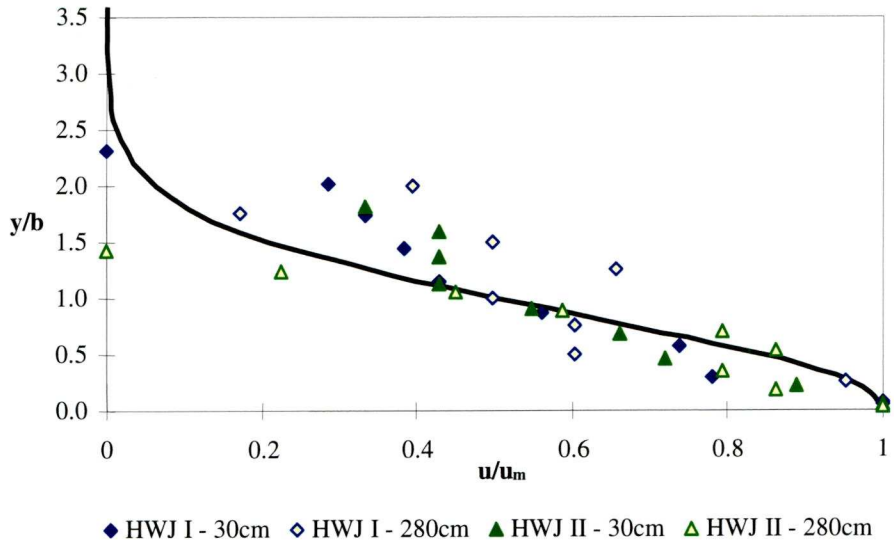

Figure 4.19: HWJ I and HWJ II Normalised Velocity Profiles

Although the data exhibit great scatter in comparison to the experimental data by Ead and Rajaratnam they do follow the expected trend. The scatter could be justified by the simple method used to get the velocity measurements and the fact that measurements were limited. Overall however the comparison of the velocity measurements with another much more extensive and detailed experimental study provides some assurance that the data is suitable for use in comparisons with computational results.

Further comparisons were performed with Rajaratnam and Subramanyan's (1986) study on buoyancy profiles of the heavy wall jet. Although in Rajaratnam and Subramanyan's study buoyancy was due to temperature difference, and not salinity difference as for the present study, it is assumed that both follow the same principle. Rajaratnam and Subramanyan's normalised experimental results have already been discussed and displayed in Figure 2.9. It is obvious from their results that although generally buoyancy defect profiles are assumed to follow the same defect pattern as velocity, this is not the case. Buoyancy seems to change more rapidly than velocity

in their experiments and the same was observed from the experimental data of this study.

The density profiles for all six runs on the heavy wall jet were normalised and are presented in Figure 4.20 for comparison with Rajaratnam and Subramanyan's results. The results show great similarities with Rajaratnam and Subramanyan's results suggesting that buoyancy does not follow the same pattern as velocity as is generally assumed. The similarity of the results with results from Rajaratnam and Subramanyan's study gives them some validity and enables their use for comparisons with results of the simulations performed and described in Chapter 5.

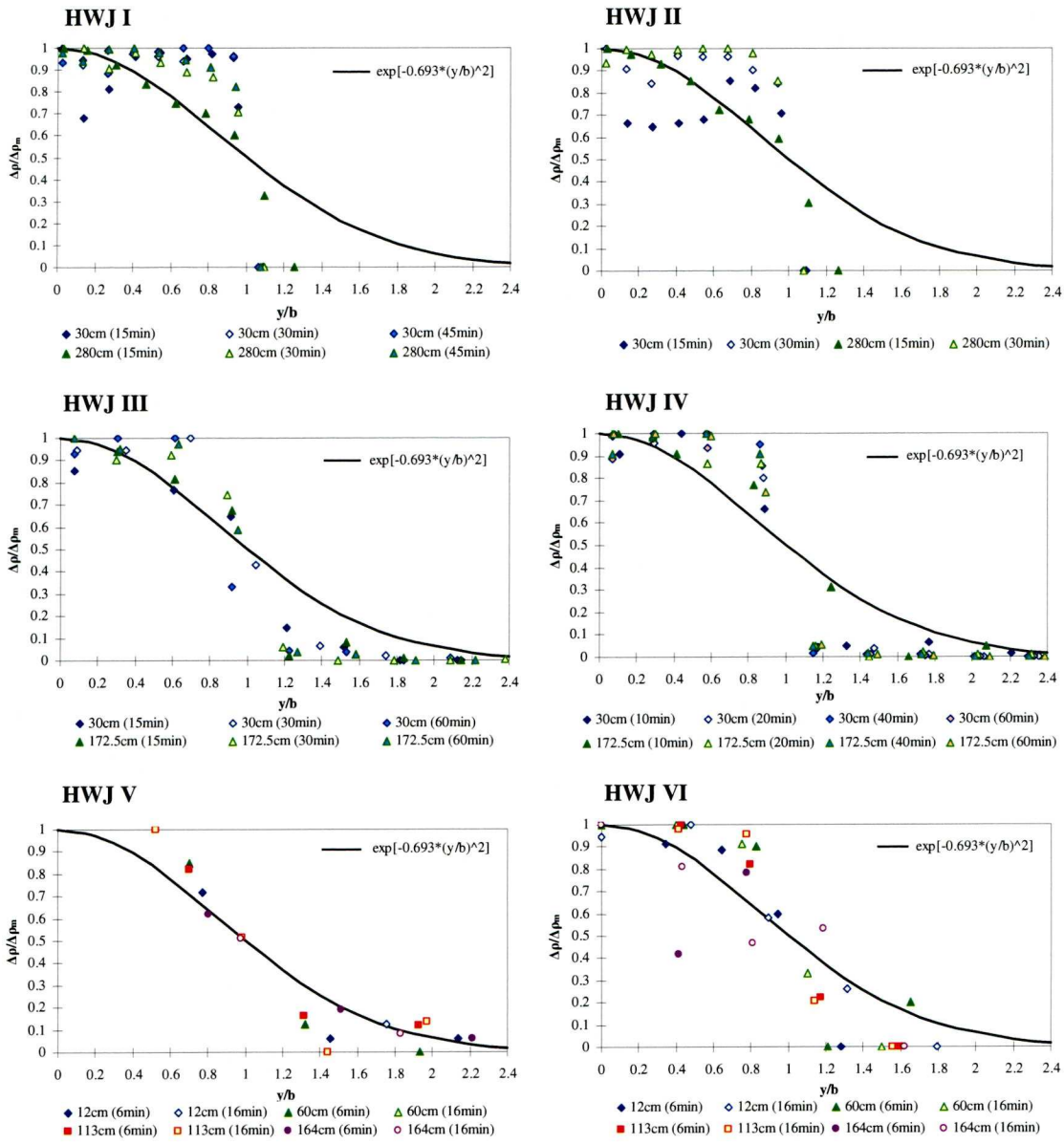

Figure 4.20: HWJ - Dimensionless Buoyancy Defect Profiles

The heavy wall jet expansion as was visualised using Rhodamine was photographed during the experimental run and is shown in Photo 4.11 overleaf.

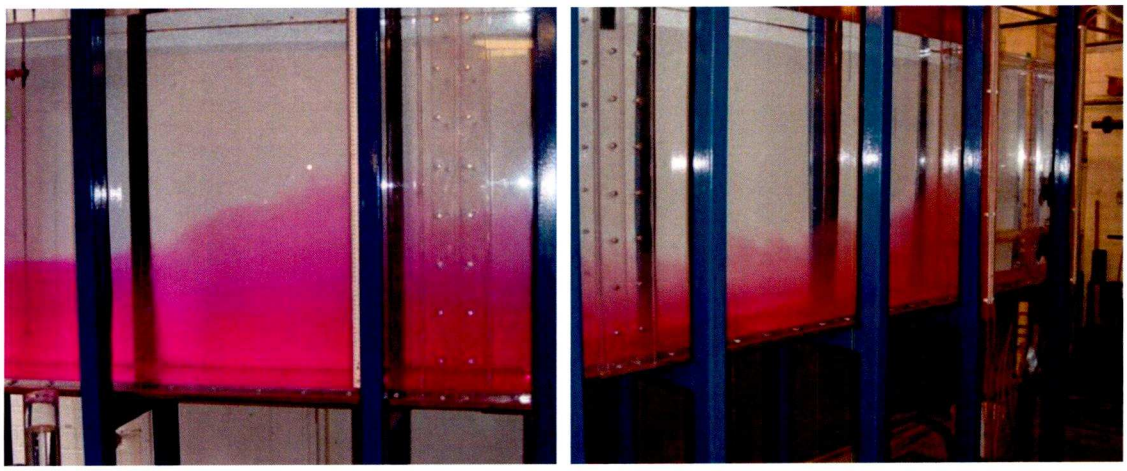

Photo 4.11: Heavy Wall Jet Expansion

4.4. Summary

In total nine experiment runs were carried out examining buoyant jets. A summary of the experimental runs and information about data obtained is given in Table 4.3.

Table 4.3: Summary of Experiments

Run	u_o (cm/s)	Saline water density (kg/m^3)	Baffle	Measurement locations (x distance from inlet)
BSJ				
BSJ I	20.50	1025	-	5cm / 30cm / 160cm
BSJ II	8.00	1025	-	5cm / 30cm / 160cm
BSJ III	15.00	1025	-	5cm / 30cm / 160cm
HWJ				
HWJ I	20.00	1025	-	30cm / 280cm
HWJ II	22.00	1025	-	30cm / 280cm
HWJ III	20.50	1025	40cm	30cm / 172.5cm
HWJ IV	31.25	1025	40cm	30cm / 172.5cm
HWJ V	30.00	1010	5cm	12cm / 60cm / 113cm / 164cm
HWJ VI	28.50	1005	5cm	12cm / 60cm / 113cm / 164cm

Overall, great scatter was observed in the experimental data due mainly to the simple instrumentation used to obtain the data. The trends followed the expected pattern from theory or previous experimental results although the accuracy of the measurements could be debated. The data is deemed adequate for rough comparisons

but care should be taken before drawing any final conclusions regarding any comparisons with CFD model results.

The experimental data does, however; provide the point of reference required for comparisons with computational results as presented in the following chapter.

Chapter 5. CFD Modelling of Buoyant Turbulent Jets

CFD models using the *FLUENT* CFD package were created to simulate the experiments on jets performed as part of this study and described in the previous chapter. The methodology followed for the setting up of the *FLUENT* models and the difficulties experienced are described in the present chapter. The obtained results are compared with the experimental data for each of the different setups and observations are discussed.

5.1. Setting up the FLUENT CFD Analysis

Before embarking on undertaking any CFD analysis certain decisions have to be made according to the requirements of the simulation and the features of the flow that will be analysed. Such considerations are the variables of interest of the flow that will be monitored, the accuracy required from the simulation results and the approach to be adopted towards the model development in more complex cases. These are discussed in the following sections where the setting up of the *FLUENT* CFD simulations of the present study is discussed.

5.1.1 Monitoring Variables

An important decision to be made when preparing a CFD analysis is the determination of the flow parameters that will be monitored and validated with experimental data, as well as the critical locations within the CFD domain. In the case of jets the velocity distribution along the axis of the jet is the main variable of interest. The decay and spread of the velocity with the associated transfer of momentum from one fluid to the other is the focal characteristic of jet flow. Furthermore, as velocity measurements are relatively easy to obtain, the velocity distribution along the axis of jets has been extensively researched experimentally compared to other features of the flow and the results can more easily be checked

against theory providing a good benchmark. Due to the above stated reasons velocity profiles along the axis of the jets were chosen as one of the key variables for comparison between experimental and simulated data.

Buoyant jets, however, have the additional important characteristic of the difference in density between the discharging and receiving fluid. This density difference can greatly influence the flow and even become the force determining the flow pattern. For this reason density distributions with time were identified as the central variable of interest in the case of buoyant jets.

5.1.2 Accuracy

Another issue to consider before starting the analysis is the desired accuracy of the model. Accuracy in CFD can have two meanings. There is the accuracy with which a simulation represents the solution of the equations used, known as numerical accuracy, and the accuracy with which the models represent reality, known as model accuracy. Although the scope of this study was to investigate model accuracy, numerical accuracy always needs to be checked and established before comparing simulated results against real data.

One indication of numerical accuracy is the residuals of the equations being solved. As the residuals decrease (converge) the calculated result for each equation approaches its real solution. The convergence level is dictated by the rate of change of residuals and the results can be said to have converged when the rate of change of residuals approaches zero. The compromise between computational time and solution accuracy describes a convergence criterion that is an acceptable overall error ratio compared to the bulk result. This means that although a solution may not have fully converged, further iterations will not significantly change the result.

The *FLUENT* software vendors and literature suggest that a convergence criterion for the governing equations produces valid results when the residuals have been reduced by at least three orders of magnitude. This recommendation was initially adopted, however, after initial tests it was established that a reduction of the residuals of three orders of magnitude was not adequate when modelling turbulent jets.

After trials a convergence criterion of decrease of residuals of five orders of magnitude ($1x10^{-5}$) was adopted for the residual components of velocity and turbulence. This was found to be the criterion beyond which the level of convergence did not influence significantly the results of the models. Further reduction of the residuals was not considered to be beneficial as the computational time would increase without the solution obtained being notably different.

This significant change of the variables with the further decrease of residuals below the literature suggested values of three orders of magnitude is displayed in Figure 5.1 using plots of velocity contours. It is obvious that after decrease of three orders of magnitude the jet has not fully developed and the pattern of velocity bears no resemblance to the expected pattern as it is greatly underestimated.

The steep gradients in velocity values between neighbouring grid cells arising from the jet discharge, complicate convergence and the choice of adequate residual decrease is fundamental. Logic checks have to be performed before deciding whether convergence is adequate and if unsure checks have to be made with theory or experimental data if available.

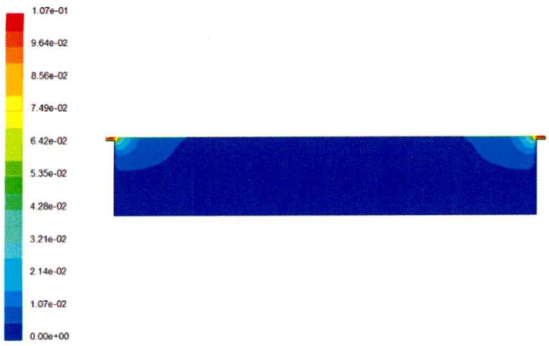

Contours of velocity magnitude after $1x10^{-3}$ reduction in residuals of velocity and turbulence

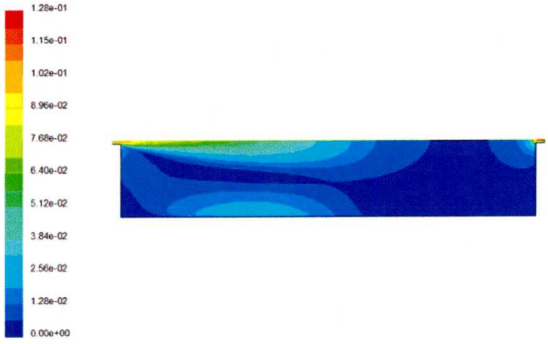

Contours of velocity magnitude after $1x10^{-5}$ reduction in residuals of velocity and turbulence

Figure 5.1: Influence of Convergence Criterion on the Solution (Homogeneous Jet)

5.1.3 Approach to Model Construction

The study required the creation of *FLUENT* models of different degrees of difficulty to simulate the types of jets studied. This enabled the adoption of a building block approach for the construction of the models. Sequential models were created starting with the simplest model, being that for a homogeneous jet, and progressing to the buoyant surface jet and finally the heavy wall jet. Modelling multiphase turbulent flows, as is the case for a buoyant turbulent jet, is technically more challenging to set up and more demanding computationally, making it more difficult to obtain satisfactory results. This is even more so in cases where other forces, besides the momentum of the discharging flow, play an equally important role in determining the development of the flow. This is the case with the force of gravity in the formation of the heavy wall jet.

5.2. Problems Encountered

A first attempt at modelling turbulent jets involved the plane surface jet in homogeneous conditions. This first model was relatively uncomplicated and not many problems were encountered at this stage. The homogeneous surface jet model was used to test different turbulence models and grid sizes in order to obtain the

turbulence model that was suitable and the grid size that was adequate for the more complicated simulations.

In the case of buoyant jets however, in addition to velocity profiles, density profiles at different time steps were also required to determine the validity of the *FLUENT* model. Unlike velocity, the density distribution in the flume is a time dependent variable that indicates the level and efficiency of mixing in the flume caused by the buoyant turbulent jet making the accurate mixing time prediction a key parameter for the model performance.

The main problem encountered during the simulations was that initial trials showed that *FLUENT* was greatly underestimating mixing times. Because of the significance of the mixing time prediction this had to be further investigated and solved. Numerous trial runs were performed investigating the effect of many different model parameters such as grid resolution, time step size, turbulence models etc on the mixing time. None of these parameters, however, was found to have a significant effect on the time. The parameter that was found to determine the mixing time was the turbulence kinetic energy (TKE) specified at the inlet.

Normally when setting up a CFD analysis an assumption is made on either the turbulence kinetic energy or the turbulence intensity of the flow made based on either experience or common estimation principles. Such a general assumption might show that a solution to the problem has been achieved, during this study, however, it was discovered that a general assumption is not adequate to accurately predict the mixing time. Checks of other parameters or numerical checks did not indicate that the obtained solution was not realistic. The turbulence kinetic energy has been investigated for every simulation described in the present chapter and it was found

that for every simulation a turbulent kinetic energy of 0.01 m^2/s^2 produced reasonable results. This value was an estimate that emerged from trial and error simulations as the available experimental data was not adequate to determine the turbulence kinetic energy. The effect of the turbulence kinetic energy is examined in more detail in Section 5.7 where the performance of the buoyant surface jet models is discussed. The effect of TKE on the solution is also demonstrated.

5.3. Initial Trials

Initial trials were performed by modelling a homogeneous surface jet. The homogeneous jet is the simplest of the turbulent jets and consequently less demanding computationally. This type of jet only involves a single phase leading to fewer equations having to be solved. The initial trials were performed in order to determine the appropriate grid resolution for the problem and examine the performance of the available turbulence models for this type of flow. The variable studied to determine the suitability of the grid resolution and turbulence model was the velocity distribution along the axis of the jet.

The homogeneous jet provided the stepping stone of the analysis enabling the gradual introduction of the more complex flow patterns involved in the buoyant jets. The modelling of the buoyant jets was performed using the building block approach from the model constructed for the homogeneous jet.

5.3.1 Grid Resolution

Adopting an adequate grid resolution is a significant parameter in performing a successful CFD analysis. Defining a coarser than required grid can greatly influence the solution and even provide unrealistic results. On the other hand a very fine grid can increase significantly both the time and difficulty of obtaining a solution to the

problem. Striking a right balance between adequate grid size and accuracy is an area of concern and investigation without clear definitions about what this balance is.

Three grid sizes were created on the same geometry (detail shown in Figure 5.2) in order to investigate the effect of grid size to the solution. The grids were structured quadrilateral grids with a cell size of 0.02m by 0.02m, 0.01m by 0.01m and 0.005m by 0.005m respectively.

In order to investigate the appropriateness of the three grids, a grid dependence study was performed using the Grid Convergence Index (GCI) method as defined by Roache (1998). The GCI is considered the most reliable method for checking and reporting uncertainty associated with the solution at particular grid resolutions.

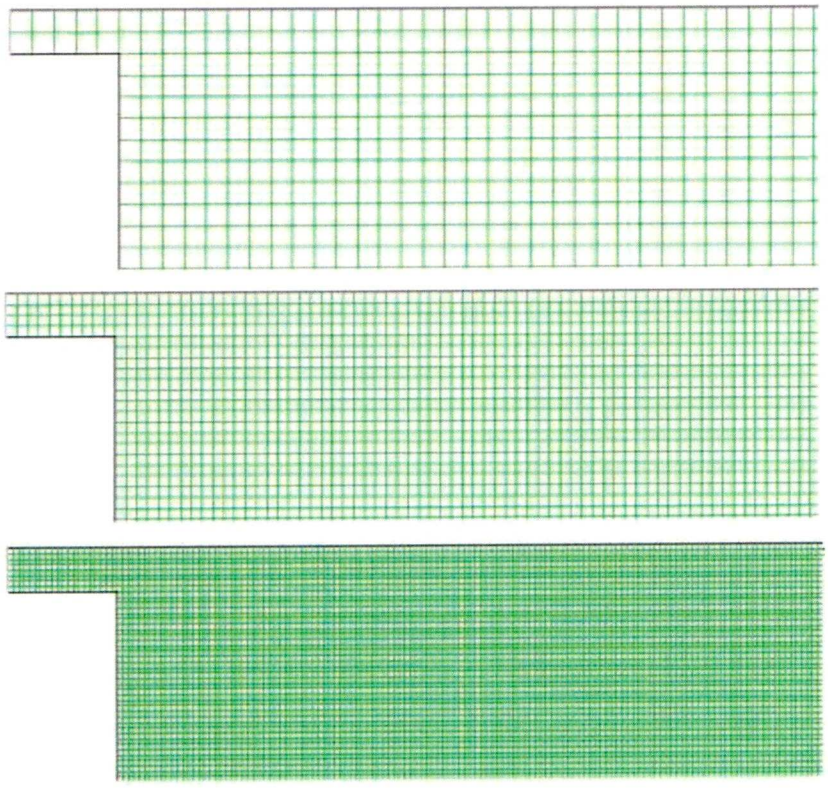

Figure 5.2: Detail of Grids Used (at the Inlet)

5.3.2 Effect of the grid size on the solution

The grid resolution is the first factor that can have a significant impact not only on the accuracy of the results obtained from a model, as mentioned previously, but also the computational time required to reach the solution.

The effect of the grid size on the computational time needed was investigated by setting up the exact same model and running for the three different grid sizes studied for as long as needed to obtain the convergence criterion adopted of decrease in velocity and turbulence residuals of five orders of magnitude. The results of this investigation are given in Table 5.1 below.

Table 5.1: Number of iterations and time required for different grid resolutions

	Grid resolution (m)	Number of cells	Number of iterations to convergence	Time to convergence (in hours)[8]
h1	0.02 x 0.02	13,520	9,720	2.7
h2	0.01 x 0.01	54,080	26,729	11.2
h3	0.005 x 0.005	216,320	119,057	132.3

Velocity magnitude profiles were extracted at 20cm, 40cm, 60cm, 80cm, 100cm, 120cm, 150cm and 200cm from the inlet for each of the three grid sizes to investigate the effect of the grid resolution on the velocity field. At a first glance the velocity profiles produced with all three grid sizes seemed plausible with the velocity pattern being very similar to the expected from theory velocity distributions.

A comparison of the extracted velocity magnitude profiles at the different sections for the three grid sizes is presented overleaf in Figure 5.3.

[8] Using a Pentium4 2 GHz processor with 1GB of memory

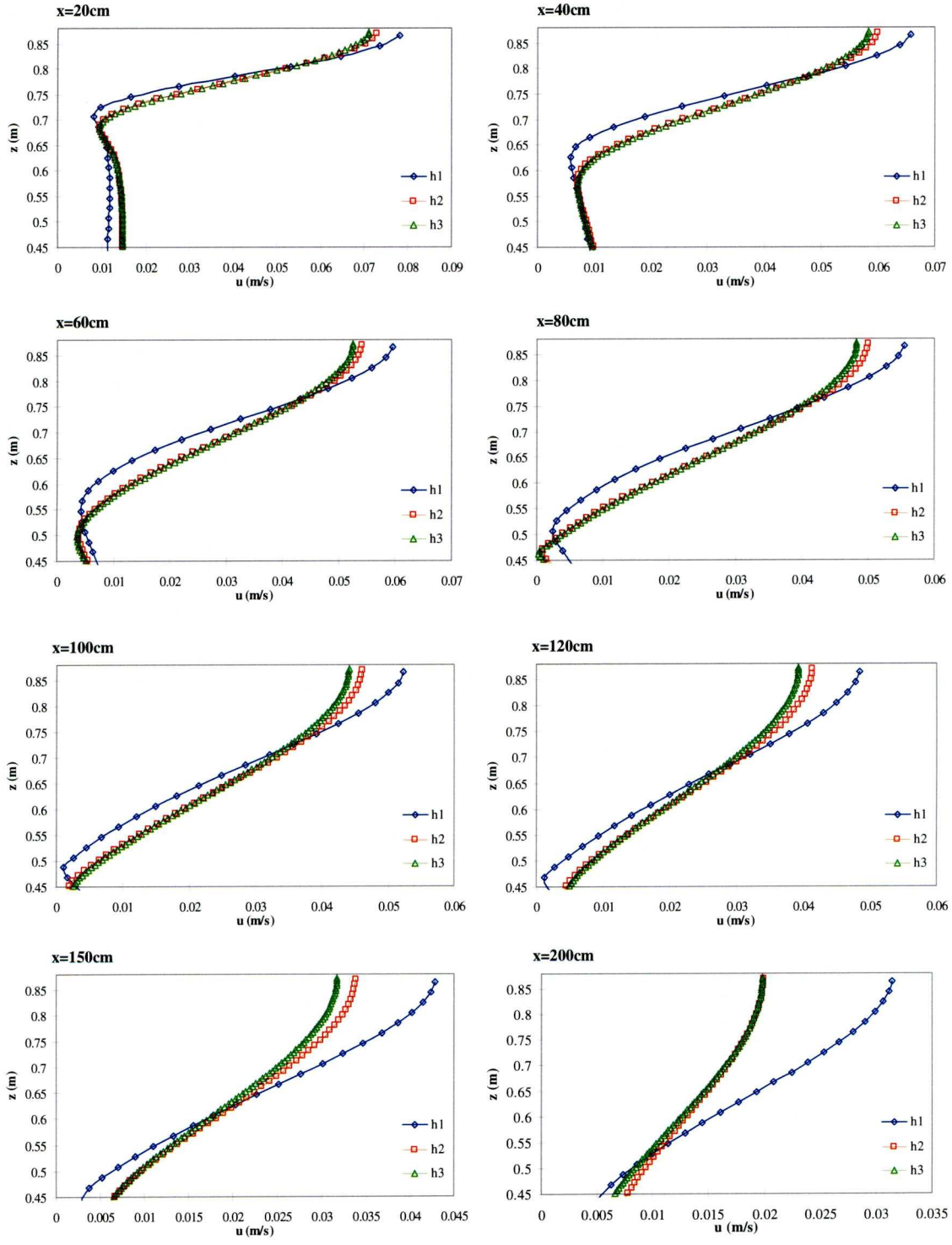

Figure 5.3: Plane Surface Jet - Velocity Profiles at Different x Stations from the Inlet (Coarse, Medium and Fine Grid Sizes, h1>h2>h3)

From an initial observation it is obvious that the solution obtained with the coarse grid (h1) differs significantly from the solutions obtained with the two finer grids (h2 and h3), with the differences becoming more apparent at distances further from the inlet. The solutions of the two finer grids seem to compare well indicating a convergence towards a solution. Such a comparison however cannot signify whether they solutions also represent an accurate numerical solution. To ensure that the solutions reached were numerically accurate enough and to determine the level of spatial convergence error, a grid convergence study was performed as described in the next section.

5.3.3 Grid Convergence

The method selected for the grid convergence study was the Grid Convergence Index (GCI) as defined by Roache (1998).

For the three different grids created the grid size was defined as h, with h1>h2>h3. In accordance with the above condition the grid refinement factors were calculated as:

$$r_{21} = \frac{h_2}{h_1} = \frac{0.02}{0.01} = 2 \qquad \textit{(Eq. 5-1)}$$

and $$r_{32} = \frac{h_3}{h_2} = \frac{0.01}{0.005} = 2 \qquad \textit{(Eq. 5-2)}$$

The exact same analysis was performed on the three grids and the velocity magnitudes in the x axis direction were obtained as demonstrated in Figure 5.3. Having chosen the velocity magnitude as the key variable to be reported, at certain selected locations from the inlet, the order of the grid refinement was calculated at each point as:

$$p = \frac{\ln\left(\frac{u_3 - u_2}{u_2 - u_1}\right)}{\ln(r_{21})} \qquad \textit{(Eq. 5-3)}$$

$$GCI_{12} = \frac{F_s|\varepsilon_{12}|}{r_{12}^p - 1} \qquad \textit{(Eq. 5-4)}$$

$$GCI_{23} = \frac{F_s|\varepsilon_{23}|}{r_{23}^p - 1} \qquad \textit{(Eq. 5-5)}$$

where:

$$\varepsilon_{23} = \frac{u_3 - u_2}{u_2} \qquad \textit{(Eq. 5-6)}$$

$$\varepsilon_{12} = \frac{u_2 - u_1}{u_1} \qquad \textit{(Eq. 5-7)}$$

and Fs is a safety factor taken as 1.25.

The grid convergence index (GCI) was calculated at several grid points at the selected monitoring locations of 20cm, 40cm, 60cm, 80cm 100cm, 120cm, 150cm and 200cm downstream of the inlet. Overall the average GCI_{23} between the medium and the fine grid was found to be 2.26%.

The extrapolated value of the velocity magnitude at each point was then calculated according to the following equation as:

$$u_{ext}^{23} = (r_{23}^p u_2 - u_3)/(r_{23}^p - 1) \qquad \textit{(Eq. 5-8)}$$

This extrapolated value is the value that would be obtained if the grid size was equal to zero. Detailed tables of the calculation of the GCI and the extrapolated velocity values can be found in Appendix D.

The velocity profiles at different sections were compared with the obtained extrapolated velocity profiles as shown in Figure 5.4. Error bands equal to 10% of the extrapolated velocity are included for better indication of the accuracy of the chosen grid size. The average difference between the velocity obtained from the chosen grid and the extrapolated velocities was 1.87%.

The velocity profiles with the chosen grid size were found to be consistently less than 5% of different from the extrapolated values, with only a few exceptions, indicating that the grid size was adequate for the simulations.

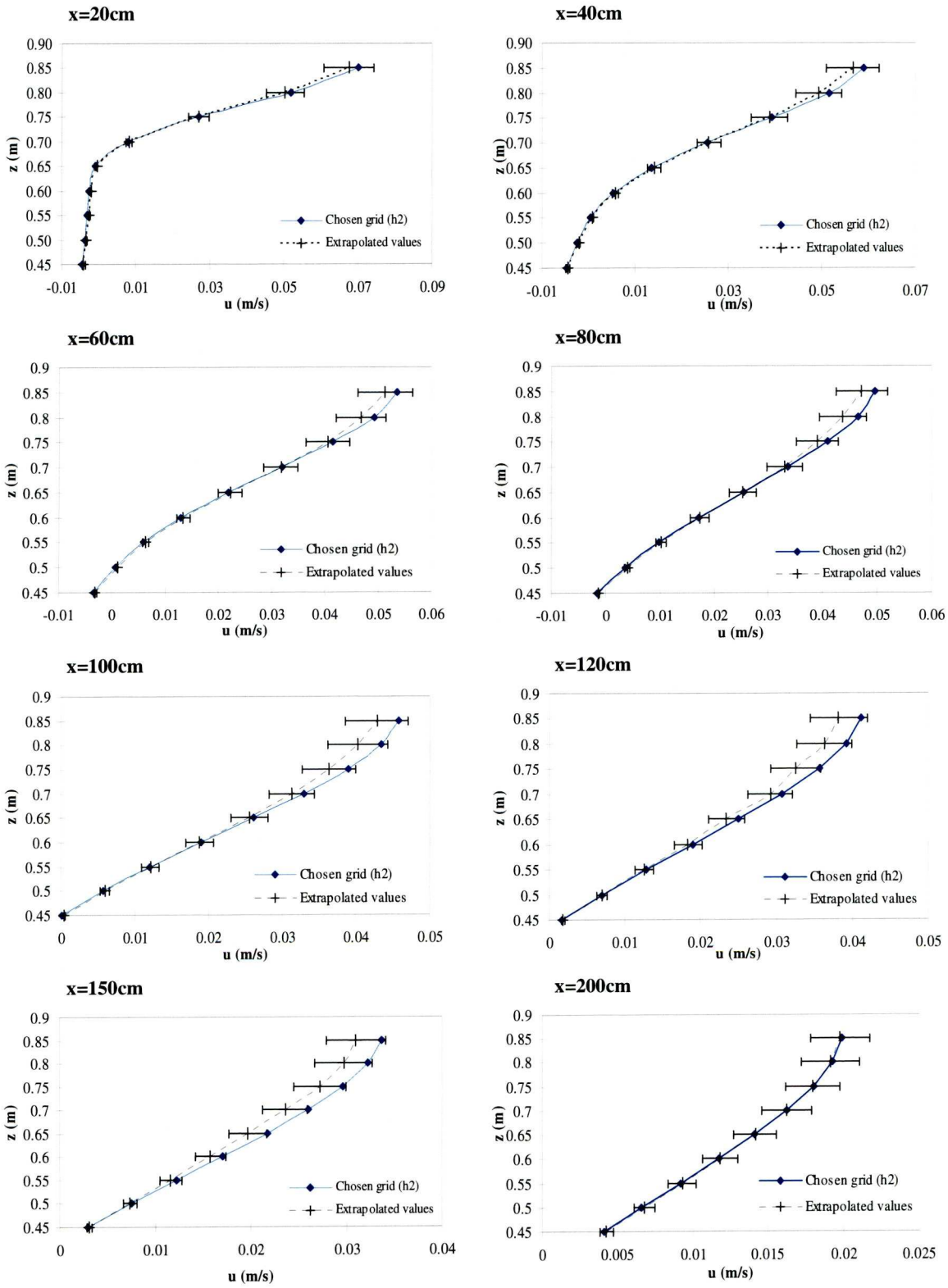

Figure 5.4: Chosen Grid (h2) vs Extrapolated Velocity Values

5.3.4 Boundary Conditions

Another major issue of concern in CFD simulations is the implementation of the right boundary conditions. Choosing the correct boundaries is fundamental in order to obtain realistic results. Boundary conditions, if implemented wrongly, can greatly influence the results as they can force the solution. The boundary conditions needed to be specified for the modelling are discussed below.

5.3.4.1 Inlet and Outlet Boundaries

The inlet and outlet boundaries were straightforward to implement. The inlet conditions were specified as a velocity inlet where only the velocity magnitude, the TKE, or turbulence intensity, and the flow direction need to be defined. The outlet boundary was implemented as a mass outflow boundary.

5.3.4.2 Wall Boundaries

The flume walls were described using a non-slip stationary wall boundary. The roughness height of the walls was assumed to be equal to zero as glass, the material of the flume, does not pose great resistance to the flow.

5.3.4.3 Free Water Surface Boundary

The most complex boundary that needed to be defined was the free water surface. The most accurate representation of real life conditions would be to specify an additional phase of air above the water. This option however, would require much more complicated equations to be solved by the software. By introducing more complex equations, with a view to eliminating assumptions made when simplifying a model, there is the risk of introducing additional computational error. Furthermore, the introduction of an additional phase increases computational time and computer power demand dramatically.

The alternative options identified to implement the free water surface boundary condition are discussed below.

The solution to modelling a free surface without the introduction of an additional phase is to model it utilising on of the two following assumptions:

- the free surface is a symmetrical boundary, or
- the free surface is a non-friction wall

Defining the free water surface as a symmetry boundary the surface is considered an internal axis and symmetry of the flow pattern is assumed on both its sides. By defining the free surface as a non-friction wall the surface is considered a frictionless wall that poses no resistance to the flow.

In a similar manner to the investigation of the grid size to the solution, the implementation of the free water surface boundary condition was examined.

From comparisons of the results obtained after performing simulations with both options it was found that the non friction wall boundary condition was forcing the solution to higher values of velocity magnitude. This was more apparent further away from the inlet, where the velocity field started to decrease, as is demonstrated in Figure 5.5.

The great difference in value between the first and the second cell of the grid indicates that the solution is greatly influenced by the wall boundary condition. The assumption of the non friction wall for modelling a free surface is generally valid but should not be implemented in this case as the area of interest of the flow is adjacent to the boundary and the relatively sudden decrease of the velocity scale cannot be modelled using the wall boundary condition.

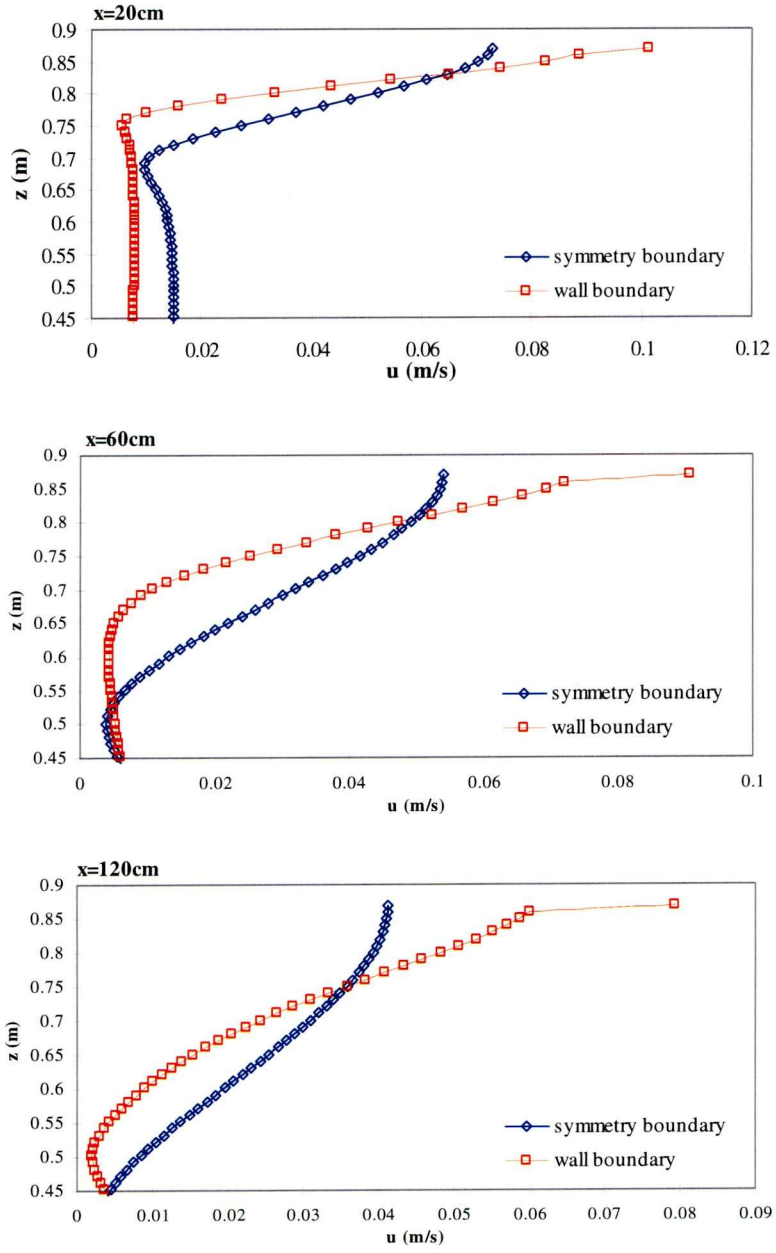

Figure 5.5: Comparison of Wall and Symmetry Boundary Conditions for the Free Surface Boundary

5.3.5 Turbulence Models

A critical concern in computational fluid dynamics simulations is turbulence modelling. The chaotic nature of turbulence itself and the lack of understanding fully the processes involved complicate the accurate prediction of turbulent flows. Turbulence models are based on assumptions that are derived usually from experimental study of specific types of flows. The fact that the assumptions used in

turbulence models are based on specific types of flows makes turbulence models applications limited to these flows and not universally applicable.

For application to the present study, three different turbulence models were tested, the standard k-ε model, the RNG k-ε model and the k-ω model. These models were found to be most likely suitable to model the flow according to the recommendations for the choice of turbulence models provided by *FLUENT* and given in Table 3.1 in Chapter 3. Initial trials with use of the Reynolds Stress Model indicated instability that led to divergence of the solution.

Testing the performance of the three turbulence models involved performing identical simulations and varying only the turbulence model used. Velocity profiles were then extracted at eight locations downstream of the inlet and comparisons between the three sets of data were made. These comparisons are presented graphically in Figure 5.6 following.

The comparisons show that the k-ε and the k-ω models produce very similar results at most downstream sections, with differences between the two becoming obvious only for the sections further away from the inlet at 150cm and 200cm. The RNG k-ε model produced different patterns for all sections mainly with regards to the jet expansion close to the jet source.

Although the results obtained with the standard k-ε and the k-ω models were more similar than the solution obtained using the RNG k-e model, this similarity was not enough to assess the performance of each turbulence model with regards to how realistic were the extracted profiles.

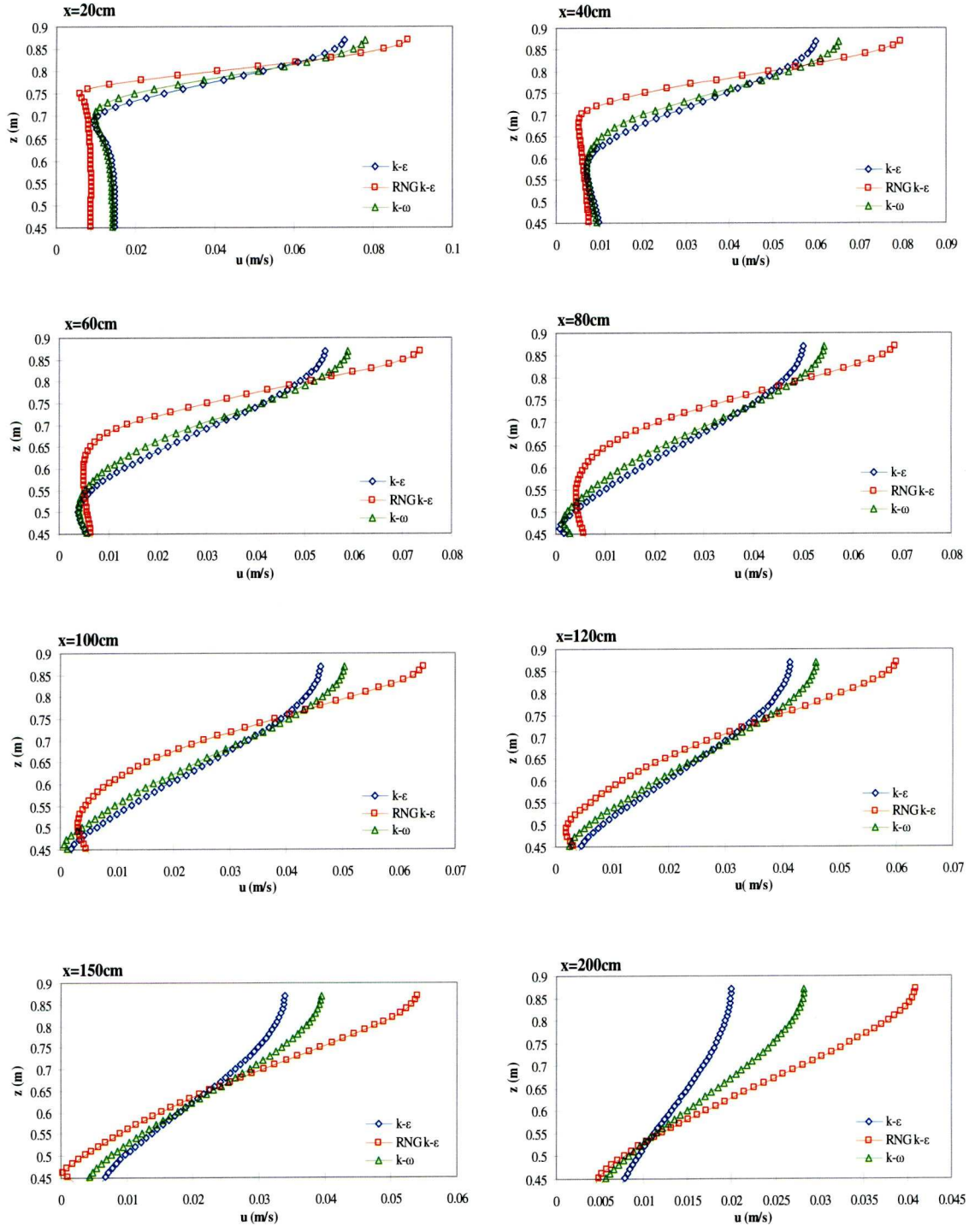

Figure 5.6: Comparison of Velocity Profiles Obtained with the Application of Different Turbulence Models (k-ε, k-ω and RNG k-ε)

In order to decide on the performance of each of the turbulence models tested, the velocity profiles obtained were subsequently compared against turbulent jet theory. The velocity profiles of each one of the solutions and at each location examined were normalised and plotted against a Gaussian curve, as given by Chu and Vanvari (1976). The normalisation procedure has already been described in the previous chapter. These comparisons are seen in Figure 5.7 overleaf.

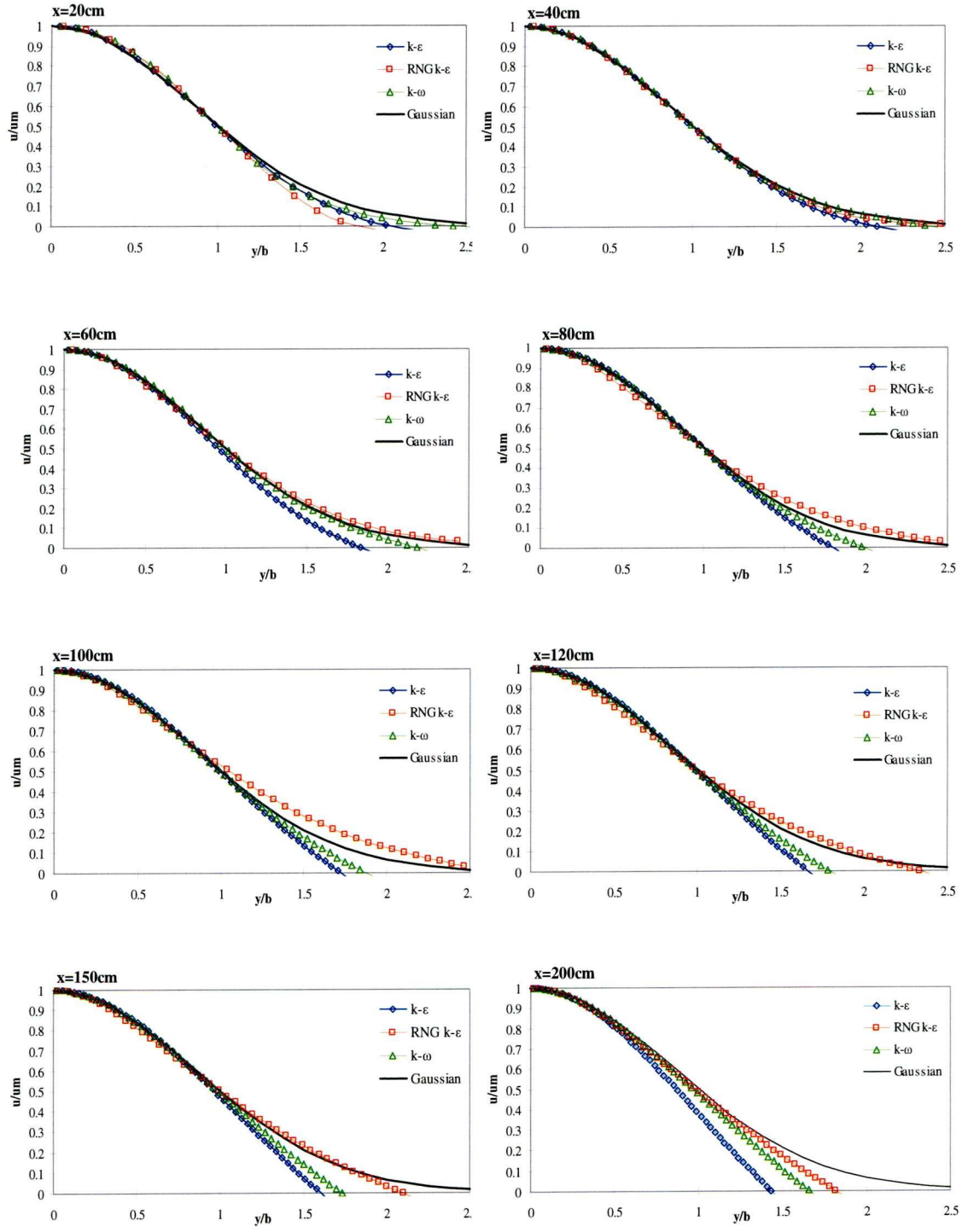

Figure 5.7: Comparison of Normalised Velocity Profiles Obtained with the Application of Different Turbulence Models (k-ε, k-ω and RNG k-ε)

From the comparisons it is apparent that all three tested turbulence models succeed in predicting the profile of the jet development velocity field, giving very similar results and making it difficult to reach any conclusions regarding their performance based only on this feature, although the performance of the RNG k-ε model seems to be marginally better than that of the standard k-ε and the k-ω models.

As the comparisons of the normalised velocity profiles were not adequate to provide a determining conclusion with regards to the performance of the different turbulence models, further comparisons were made with features of plane surface turbulent jets from theory.

The development of the jet's velocity field and the development of the jet width with the distance from the inlet were compared with the respective curves provided by Rajaratnam and Humphries (1984) as shown in Figure 5.8 and Figure 5.9. These comparisons enabled the final selection of the turbulence model that was later applied to further simulations.

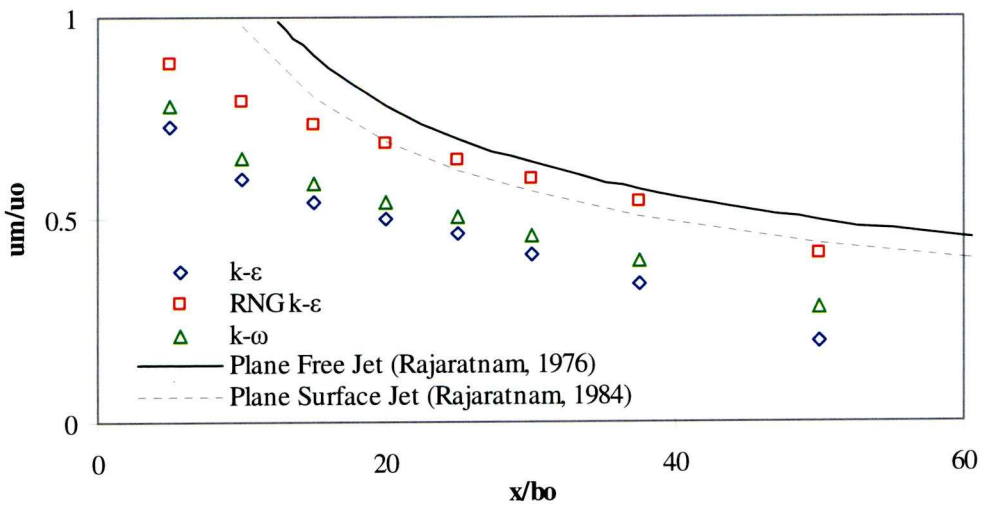

Figure 5.8: Comparison of Jet Development with the Application of Different Turbulence Models (k-ε, k-ω and RNG k-ε)

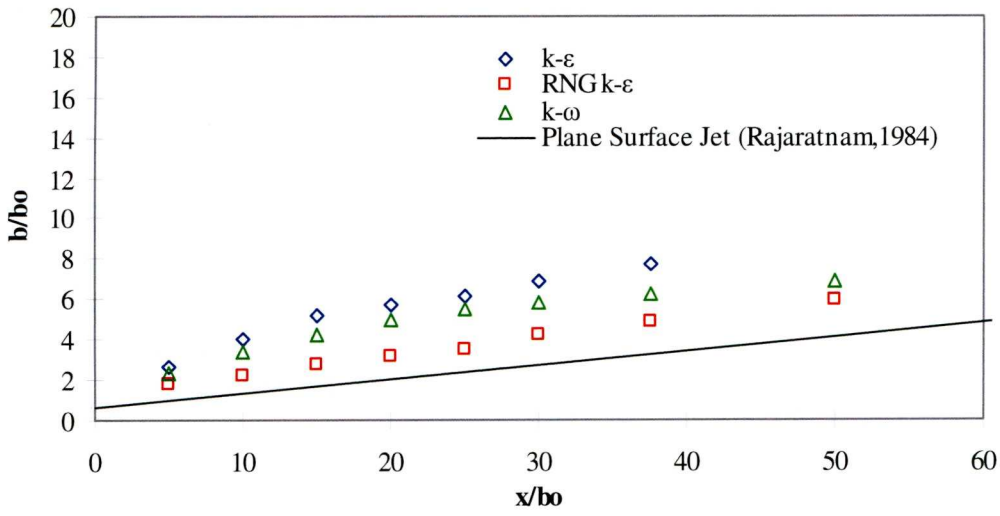

Figure 5.9: Comparison of the Jet Width Obtained with the Application of Different Turbulence Models (k-ε, k-ω and RNG k-ε)

The RNG k-ε model was found to perform better than both the standard k-ε and the k-ω models in both the development of the jet and the size of the jet width comparisons. Overall, the turbulence model that was found to perform better when compared with the theory of turbulent jets after the series of comparisons demonstrated above was the RNG k-ε model and which was selected as the turbulence model to be used in the subsequent simulations.

An observation made, however, was that all turbulence models tested failed to describe adequately the potential core region of the jet. This can be seen in Figure 5.8 as the normalised simulation results deviate more from the theoretical curve for distances close to the inlet in the potential core region following the same trend as sections further downstream. This feature is due to the nature of the computation of turbulent flows in CFD. When a turbulence model is applied, it corresponds to the whole flow domain and the calculation of turbulence starts at the very first cell from the inlet. This highlights the incapacity of CFD to adequately model transitional

flows, as the choice currently is either laminar of turbulent flow at the whole extent of the flow domain.

5.3.6 Summary of Results of Initial Trials

Summarising the initial trials performed and described in the previous sections the following conclusions were drawn.

- A grid size of 0.01m x 0.01m was found adequate for application to the simulations to be performed. Accuracy arising from further reduction of the grid size was found to be disproportionate to the time required for convergence to be achieved with the available computational resources.

- The boundary condition found to be most appropriate for the modelling of the free water surface was the symmetry boundary. The assumptions behind the simplification of the free water surface to a symmetrical boundary were found to give realistic results.

- The turbulence model that was found to perform best when compared with the theory of turbulent jets was the RNG k-ε model.

These findings and assumptions were used subsequently for the simulations performed on buoyant turbulent jets based on the experimental set-ups and conditions described in Chapter 4.

5.4. Homogeneous Surface Jet Modelling

Using the model setup that accrued from the initial trials, the first simulation performed was that of a homogeneous surface jet. Velocity profiles obtained from the simulation were compared against three different sets of experimental data. This simulation, being simpler than simulations of buoyant jets, was used to confirm that the assumptions and simplifications arising from the initial trials were appropriate.

The experimental data were taken from experiments performed by Chu and Vanvari (1976), Rajaratnam and Humphries (1984) and Papapostolou (2002). Chu and Vanvari in their studies on buoyant surface jets also included a single benchmark experiment on non-buoyant surface jet. Rajaratnam and Humphries performed a series of experiments on non-buoyant surface jets while the experiments by Papapostolou were conducted at the University of Liverpool, utilizing the same flume and experimental set up as the experiments described in Chapter 4 of the present study. The input data used for the simulation were the conditions of Papapostolou's experiment.

5.4.1 Velocity Profiles

Velocity profiles were extracted after the completion of the simulation at eight different sections downstream of inlet and are presented in Figure 5.10.

The extracted velocity profiles display the expected pattern with the maximum velocity being observed at the free surface and the velocity decreasing with the distance from the free surface following a Gaussian shape. The width, or spread, of the jet also increased with the distance from the jet source as was expected

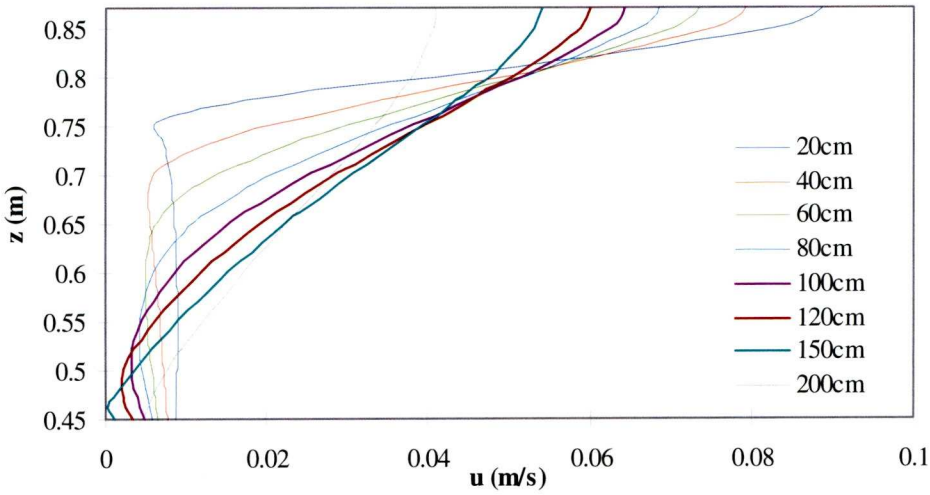

Figure 5.10: Homogeneous Surface Jet - Velocity Profiles at Different Distances from the Inlet

The velocity profiles obtained at the first four stations (at 20cm, 40cm, 60cm and 80cm) downstream of the inlet were normalised and compared with experimental data by Chu and Vanvari (1974). These comparisons are presented in Figure 5.11.

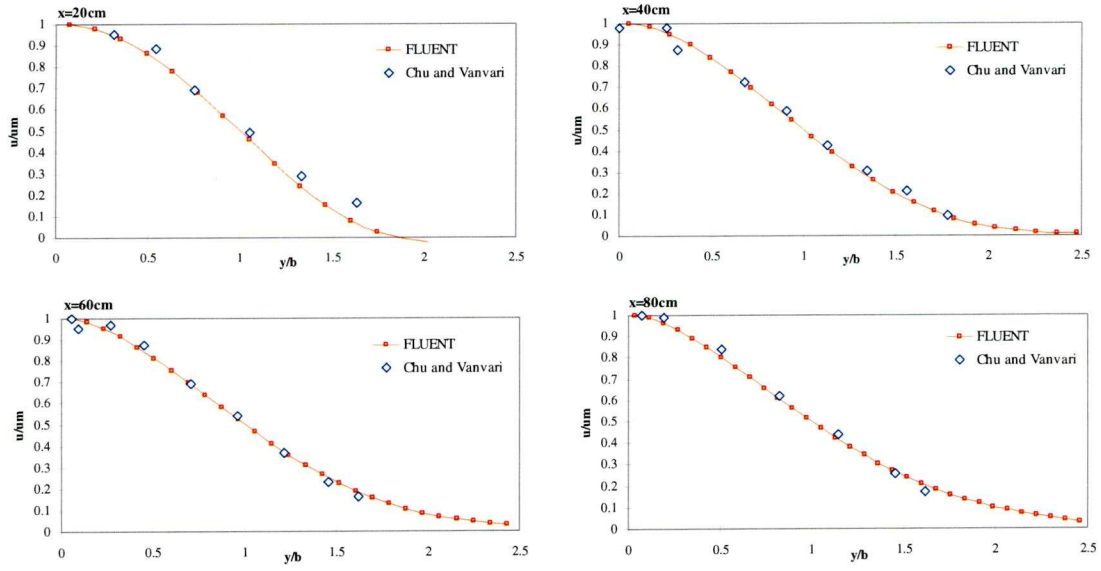

Figure 5.11: Computed Dimensionless Velocity Profiles vs. Experimental Data (Chu and Vanvari – 1976)

From the comparisons in Figure 5.11 it can be concluded that the chosen model set up results are in very good agreement with the experimental data. Similar

conclusions can be drawn from Figure 5.12 and Figure 5.13, where the computed jet velocity field development and jet width are compared with experimental data. Although the comparison between computed and experimental results is satisfactory, the experimental data display much greater scatter.

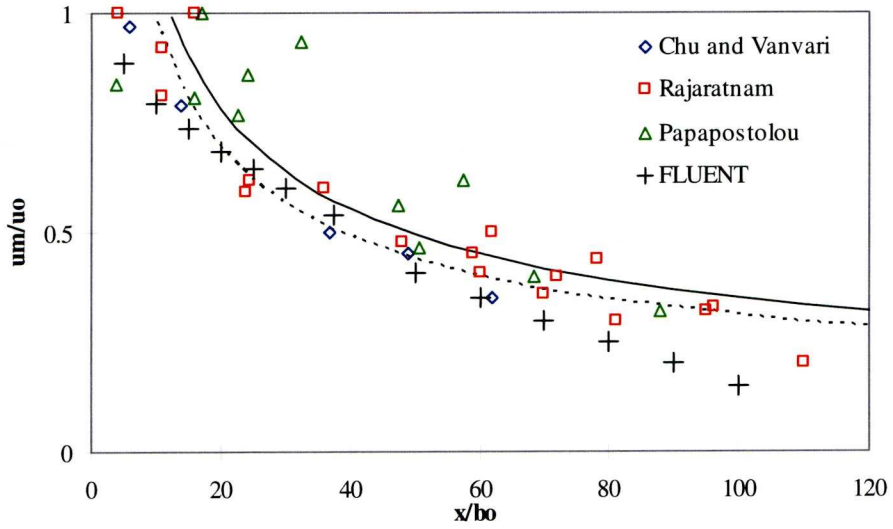

Figure 5.12: Homogeneous Surface Jet - Computed vs. Experimental Jet Velocity Field Development

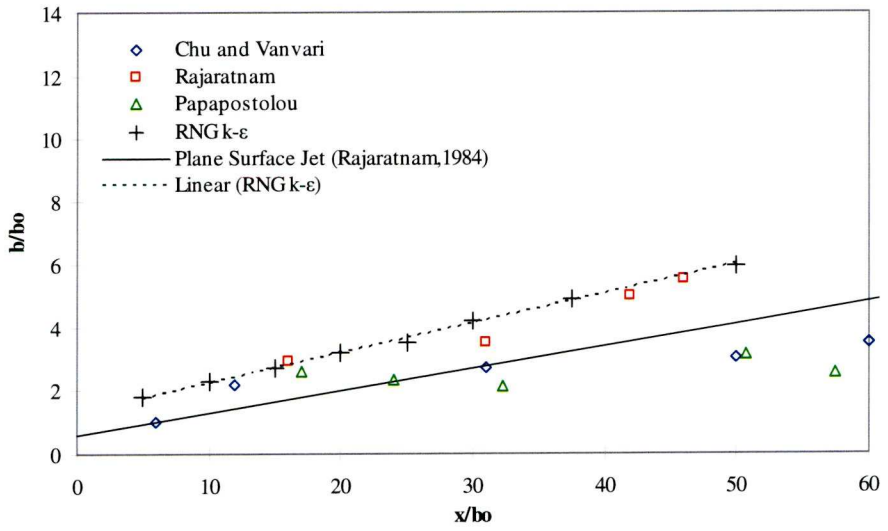

Figure 5.13: Homogeneous Surface Jet - Computed vs. Experimental Jet Width

5.5. Homogeneous Surface Jet Model Performance

From the simulation of the homogeneous surface jet it is derived that the chosen model set up in *FLUENT* succeeds in predicting the flow resulting from the inflow of a turbulent jet on the surface of ambient stagnant water.

The main features of the flow were fairly accurately predicted by the simulation. The assumptions and simplifications do not seem to have significant impact on the derived solution and comparisons with experimental results confirm this. In particular the velocity profiles at different sections are predicted with great accuracy.

5.6. Buoyant Surface Jet (BSJ) Modelling

5.6.1 Multiphase Model

The fundamental difference between modelling a homogeneous jet and modelling a buoyant jet is the presence of an additional fluid of different density. In modelling terms the simulation of a buoyant jet involves two phases. In the simulations described in the following sections these two phases (or fluids) are fresh water and saline water.

Saline water was not a readily available option in *FLUENT* and it had to be specified and added as an additional material in *FLUENT*'s materials panel. The density specified for saline water was 1025 kg/m^3, whilst the viscosity specified was *FLUENT*'s default for water and equal to 0.001003 kg/ms.

The basic difference in modelling a two phase flow in *FLUENT*, rather than a single phase simulations such as that of the homogeneous surface jet, is the introduction of an additional set of equations to be solved through an additional model called

multiphase model. The two multiphase models in *FLUENT* that could be applied in the present study are the VOF and the mixture models.

Trials with the two multiphase models indicated that both performed similarly. The mixture model was found to slightly better predict the width of the interface between the two phases and was chosen for the final simulations.

5.6.2 Density Profiles

5.6.2.1 Simulation 1 - BSJ I

The first simulation to be carried out examining the buoyant surface jet was based on experiment BSJ I. As mentioned in the experiments section in Chapter 4, there were some technical problems with the pump supplying fresh water to the flume at the beginning of the experimental procedure. This has consequently imposed additional uncertainty to the experimental results. For this reason, comparisons with results from the simulation of BSJ I required a more sceptical approach.

Although the experimental measurements were taken 15 minutes from the start of the run, as the results were surrounded by greater uncertainty due to the technical problems, comparisons were made with density profiles from the computational simulation after 10 minutes and 15 minutes to account for the possible effect of the pumping difficulties. The velocity magnitude specified at the inlet was equal to 20.5 cm/s on the x-axis, as measured during the experimental run, and the TKE was specified as 0.01 m^2/s^2. These comparisons are found in Figure 5.14, Figure 5.15 and Figure 5.16.

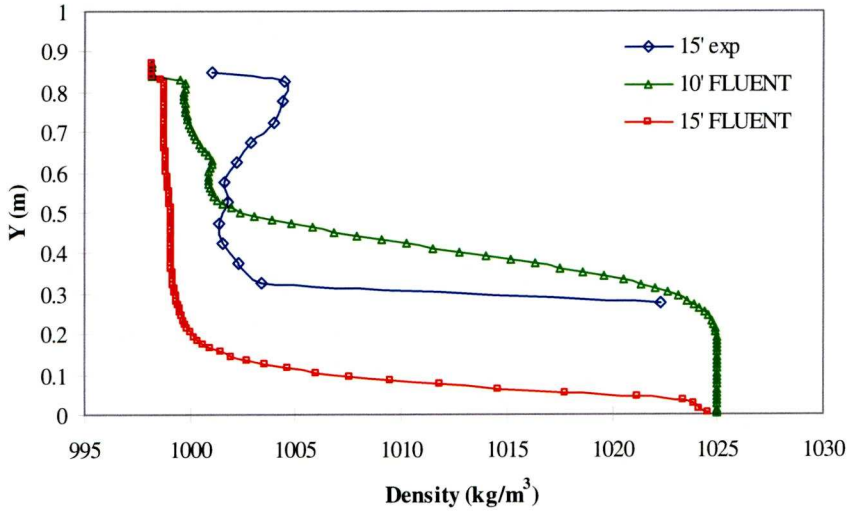

Figure 5.14: BSJ I - Experimental and Computed Density Profiles at 5cm from the Inlet

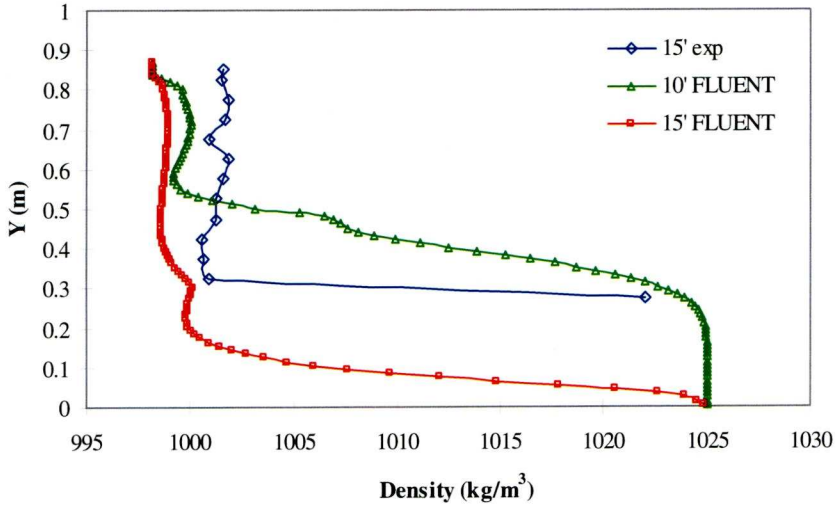

Figure 5.15: BSJ I - Experimental and Computed Density Profiles at 30cm from the Inlet

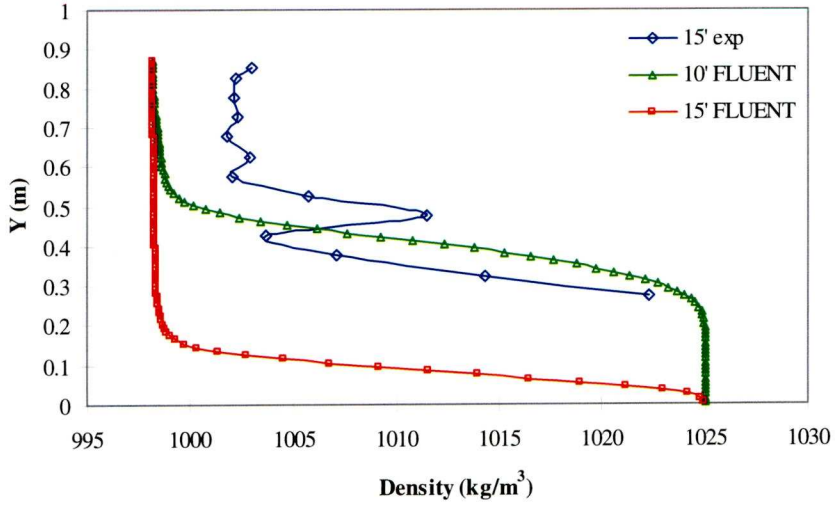

Figure 5.16: BSJ I - Experimental and Computed Density Profiles at 160cm from the Inlet

The computed results seem to be reasonable when compared with the experimental density profile, although in this particular case there is great uncertainty associated with the experimental data, making it difficult to draw any conclusions. The trend of both sets of data though seems to be roughly the same.

5.6.2.2 Simulation 2 - BSJ II

The following simulation was based on the second experiment on the buoyant surface jet, BSJ II. This experiment provided a more reliable set of experimental data as no problems were encountered during the experimental procedure. The inlet velocity for this experiment was measured as 8 cm/sec and this was specified also in *FLUENT* as the inlet velocity. The TKE at the inlet was set to 0.01 m^2/s^2.

Comparison of experimental and computational density profile data at the three locations for both measurements taken after 15 minutes and after 30 minutes show that there is very good agreement between the two sets of data.

The comparisons of the density profiles at distances equal to 5cm, 30cm and 160cm from the inlet after 15minutes and 30 minutes are presented below in Figure 5.17 to Figure 5.22 overleaf.

The comparisons show great agreement between computed and experimental density profiles and demonstrate the capability of *FLUENT* to accurately predict the mixing that results from a surface buoyant jet. Both density profiles and mixing times were realistic and comparable with good accuracy to experimental data.

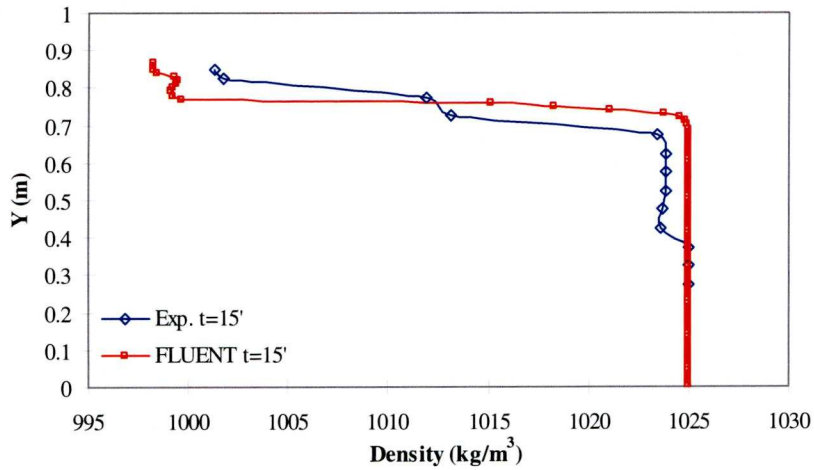

Figure 5.17: BSJ II - Experimental and Computed Density Profiles at 5cm from the Inlet (t=15 min)

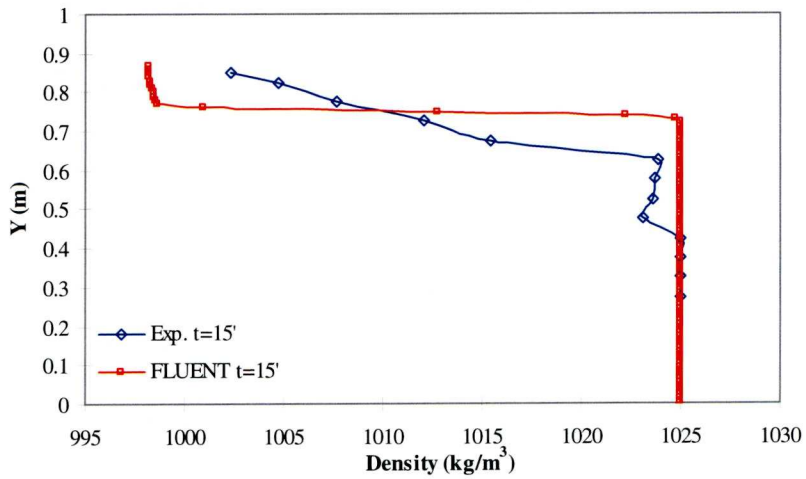

Figure 5.18: BSJ II - Experimental and Computed Density Profiles at 30cm from the Inlet (t=15 min)

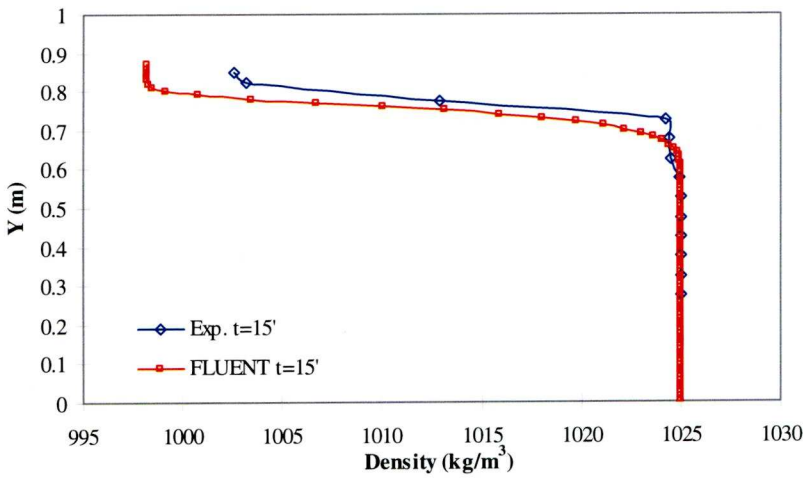

Figure 5.19: BSJ II - Experimental and Computed Density Profiles at 160cm from the Inlet (t=15 min)

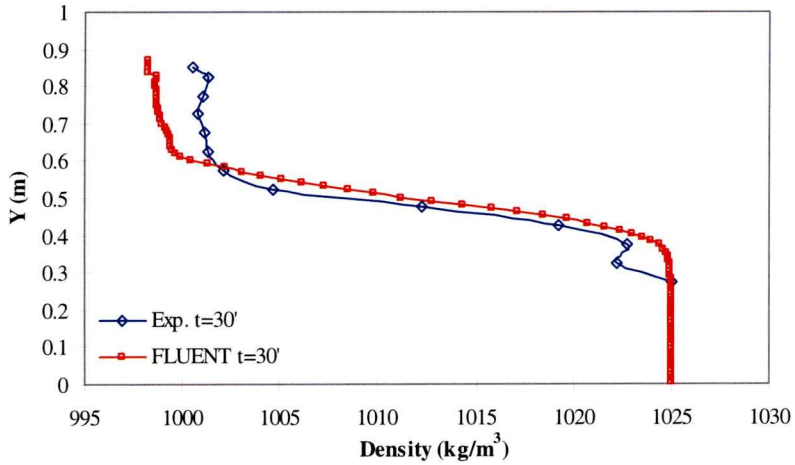

Figure 5.20: BSJ II - Experimental and Computed Density Profiles at 5cm from the Inlet (t=30 min)

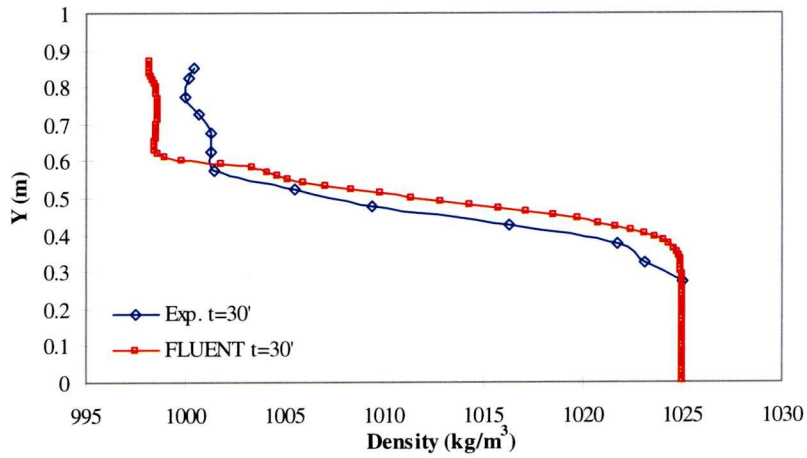

Figure 5.21: BSJ II - Experimental and Computed Density Profiles at 30cm from the Inlet (t=30 min)

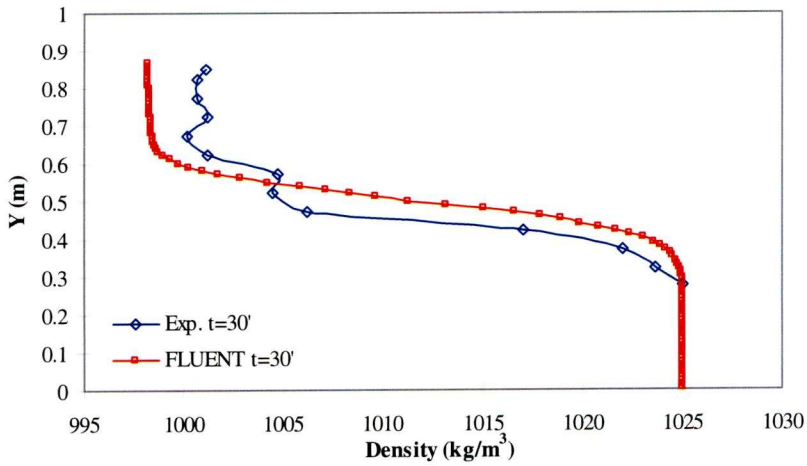

Figure 5.22: BSJ II - Experimental and Computed Density Profiles at 160cm from the Inlet (t=30 min)

5.6.2.3 Simulation 3 - BSJ III

The third and final simulation that was performed on the buoyant surface jet was based on experimental run BSJ III. As the experimental results of the first run on the BSJ were not reliable enough to draw conclusions with regards to the credibility of the simulation results, a further simulation would confirm the indication from the results comparisons of BSJ II that *FLUENT* is capable of accurately predicting mixing caused by a buoyant surface jet. The results of this simulation are compared with the experimental data for BSJ III in Figures 5.23 to 5.25 overleaf.

The computed results in this case do not compare as well as in the previous set up for BSJ II indicating that mixing occurs faster than measured during the experiments. The trends of density profiles however compare very well in all three sections and the mixing times are not completely unrealistic.

As has been already discussed, the right choice of models and initial conditions is imperative in order to obtain accurate results. Accurate flow rate, or velocity at the inlet, is not the only requirement as it was found that the factor that determines the mixing time is the turbulent kinetic energy specified at the inlet. As TKE was not measured in the current study and the TKE specified at the inlet was the result of trial and error simulations, it can be assumed that more accurate specification of the TKE at the inlet would lead to more accurate results.

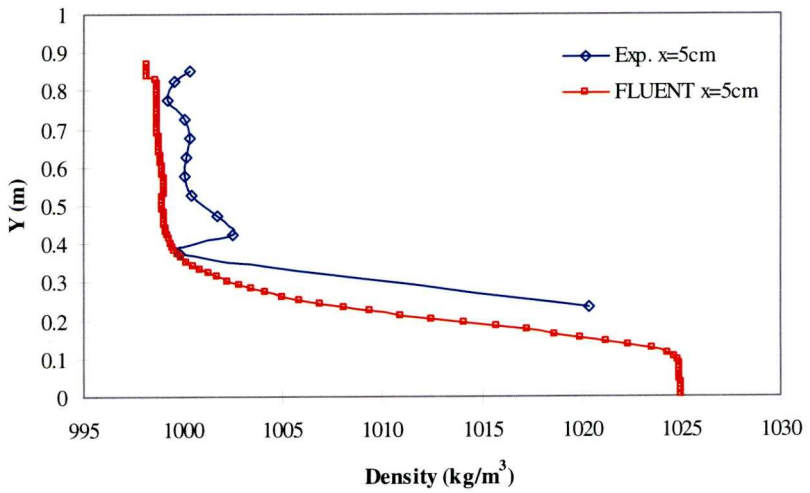

Figure 5.23: BSJ III - Experimental and Computed Density Profiles at 5cm from the Inlet (t=15 min)

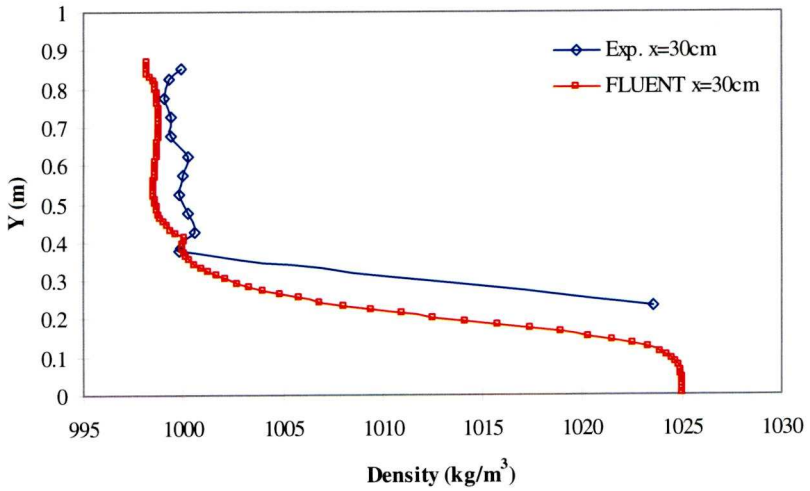

Figure 5.24: BSJ III - Experimental and Computed Density Profiles at 30cm from the Inlet (t=15 min)

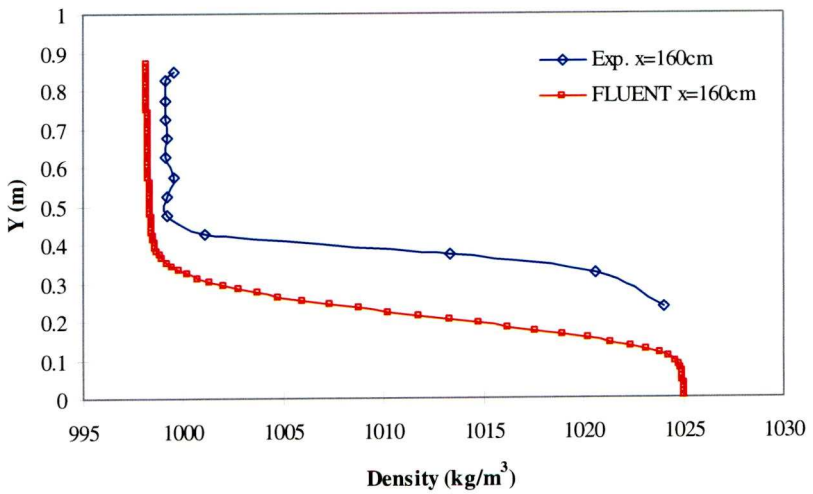

Figure 5.25: BSJ III - Experimental and Computed Density Profiles at 160cm from the Inlet (t=15 min)

5.7. Buoyant Jet Model Performance

The results presented in the previous section demonstrate that CFD produced satisfactory results in the case buoyant surface jets. A great difficulty however was encountered at the first attempts of the BSJ analysis. The difficulty was the fact that *FLUENT* was significantly underestimating the mixing times. Mixing was predicted by CFD to occur up to four times faster than the times observed in the lab.

As the source of this was not known several different trial and error simulations were performed using different options within the *FLUENT* code. The different scenarios involved the use of different multiphase models, refined time step and different turbulent kinetic energy values at the inlet. The property that was found to determine the mixing time in every case was the turbulent kinetic energy (TKE) at the inlet for simulations of all the experimental runs. The effect of time step was only marginal and a time step of 0.1s was adopted as it was found to be satisfactory and further reduction in the time step did not change to the obtained solution. The different multiphase models only influenced the interface between the two phases but not the mixing time.

After it was established that the parameter determining the mixing time was the TKE, trials using different values for the TKE at the inlet were performed. The trials indicated that a value of 0.01 m^2/s^2 for the TKE at the inlet produced realistic results for all three simulations performed on the BSJ. Further refinement of the TKE value was not attempted as it would require a large number of simulations and there was not an adequate number of experimental data to perform an analysis to investigate if there is a relationship between the velocity and the TKE at the inlet. A demonstration of the effect of TKE on the mixing time is given in Figure 5.26. The level of TKE of

0.01 m^2/s^2 is very low, although a low level of TKE at the inlet was expected from the experiments as one of the aims of the filter installed at the inlet compartment of the flume was to reduce turbulence and ensure the formation of a buoyant surface jet.

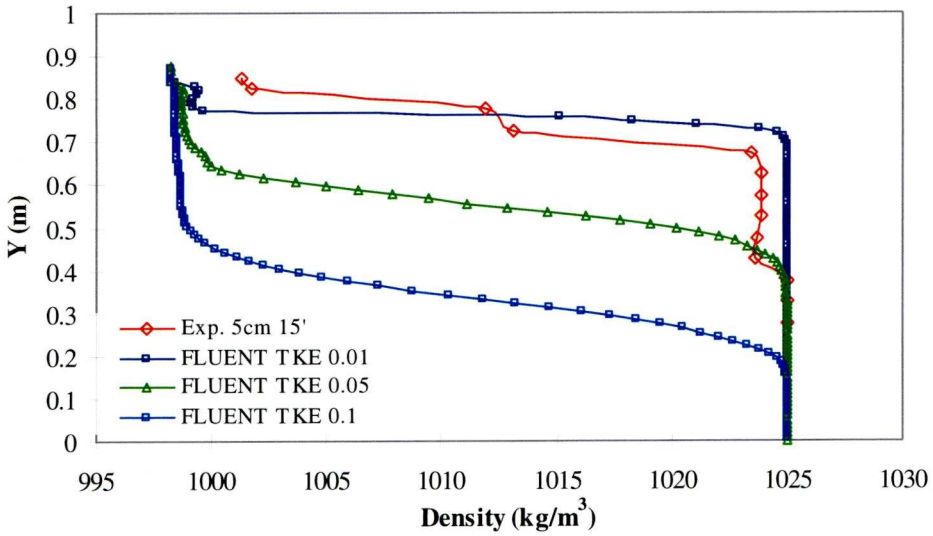

Figure 5.26 Effect of the Turbulence Kinetic Energy (TKE) on the Mixing Time (BSJ II - 5cm after 15 min)

The comparisons of computational and experimental results however confirm *FLUENT*'s capability to accurately predict the density profiles. The most accurate predictions using CFD simulations were obtained for the second simulation BSJ II. BSJ I demonstrates *FLUENT*'s capacity to predict the pattern of the density distribution in the flume but the uncertainty of the experimental results in this case prohibit any conclusions to be drawn. The comparisons of the third set of experimental data with computational results indicate that the predictions are not as accurate as those of BSJ II but are still within acceptable limits. In this case the computed results demonstrate a slight underestimation of the time scale required for mixing. This could be due to several causes, both in the simulation but also in the experimental data. Inaccurate measurement of the velocity magnitude at the inlet could be a likely reason, as could be a not accurate enough assumption about the

TKE specified at then inlet when performing the computational analysis. All the simulations results presented were performed by applying the same time step of 0.1s and turbulent kinetic energy at the inlet equal to 0.01 m^2/s^2.

Overall *FLUENT* seems to be capable of predicting both density profiles and mixing time scales reasonably well. It would be useful to attempt a further verification of the assumptions of this model with experimental results of better accuracy and actual measurements of the turbulent kinetic energy at the inlet before drawing any final conclusions. However, there is indication that *FLUENT*'s performance in this case is satisfactory.

5.8. Heavy Wall Jet (HWJ) Modelling

Modelling of heavy wall jets is a more advanced simulation in comparison with that of surface buoyant jets, as the main driving force determining the flow field is not only the momentum from the jet inlet but also the strong buoyancy and gravitational forces that act contrary to the jet flow.

5.8.1 Velocity Profiles

For modelling the heavy wall jet, the same conditions were applied for the free water surface as for modelling the buoyant surface jet. Due to the nature of the flow the water surface is not a region of interest in the case of the heavy wall jet so the conditions applied to the buoyant surface jet were considered to be adequate and no further investigations were required with regards to the free surface boundary condition. The region of interest for the heavy wall jet is the area near the wall boundary as the interaction between boundary and flow influences greatly the flow regime. For this reason the grid adjacent to the wall boundary was further refined to ensure the implementation of the boundary did not influence the results. A detail of the refined grid at the wall boundary is given in Figure 5.27 below.

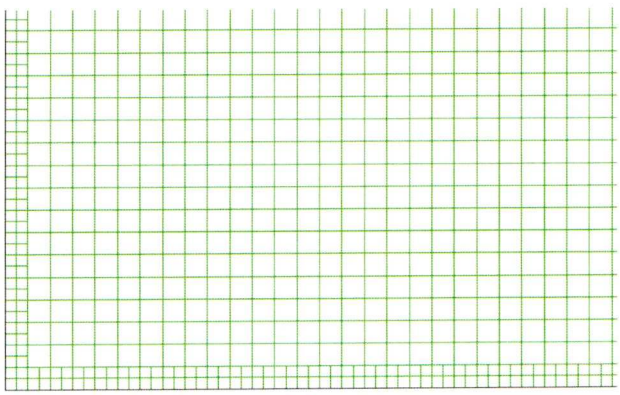

Figure 5.27: Detail of Grid Refinement at the Wall Boundary

The first test performed as part of the investigation of the performance of CFD against experimental results was the comparison of the variation of the maximum jet velocity with distance. The normalised maximum jet velocity for the first heavy wall jet run (HWJ I) was compared against an experimentally derived curve provided by Ead and Rajaratnam (2002). The results are shown in Figure 5.28 and it was observed that the CFD obtained results were in good agreement with the experimental data.

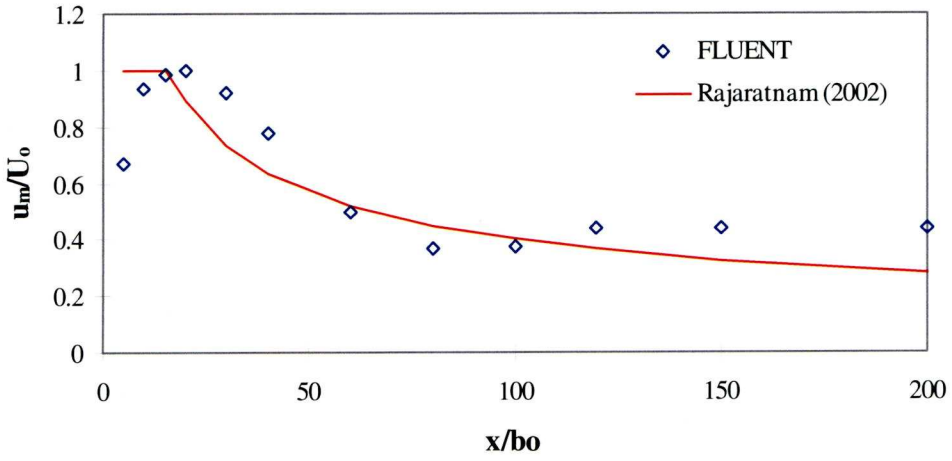

Figure 5.28: HWJ I - Variation of Maximum Jet Velocity with Distance

Ead and Rajaratnam's experimental results showed that the maximum velocity decayed in a logarithmic trend. The computed results seem to roughly follow the same pattern.

A further comparison was performed between the experimental velocity profiles and the velocity profiles extracted from *FLUENT*. The comparisons are found in Figure 5.29 for HWJ I and Figure 5.30 for HWJ II. Taking into account the built in uncertainty around the experimental data, the comparisons showed reasonable agreement between the two sets of data.

The comparisons show that the computed results show a much smoother velocity development and at the section located 280cm from the inlet the jet seems to have dissipated contrary to the experimental results.

It has to be noted however that the velocity magnitudes at this section are very close to the 6cm/s threshold of the propeller meter's measuring capacity and the experimental measurements were very unstable and more prone to user error at the specific section.

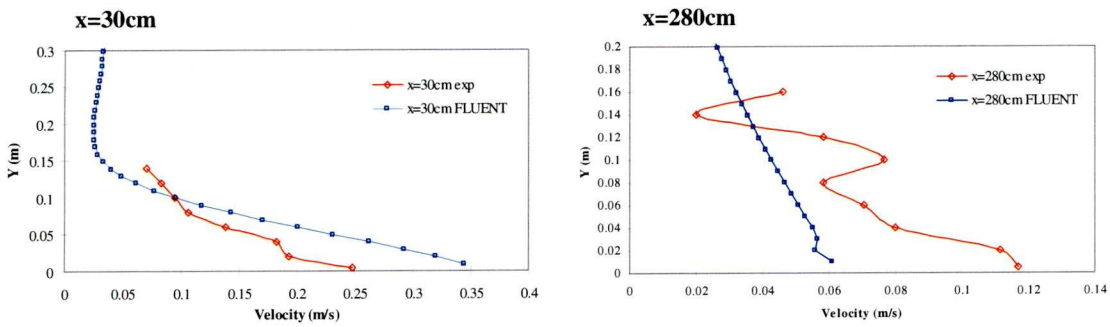

Figure 5.29: HWJ I - Experimental and Computed Velocity Profiles

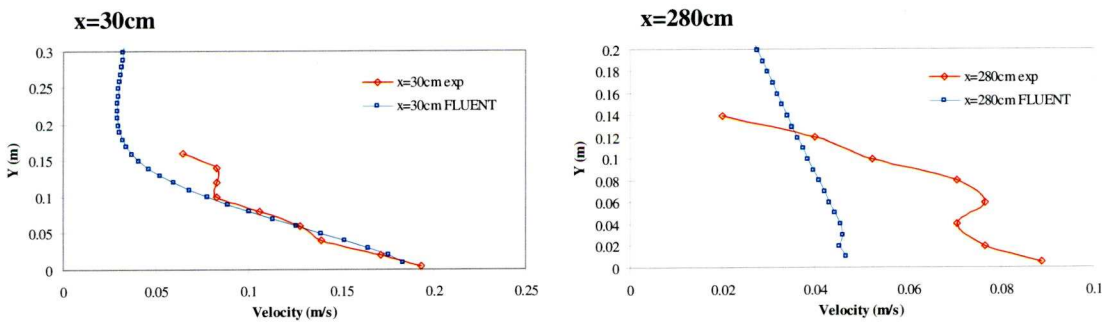

Figure 5.30: HWJ II - Experimental and Computed Velocity Profiles

Typical velocity vectors of the heavy wall jet as they are presented by *FLUENT* are displayed in Figure 5.31.

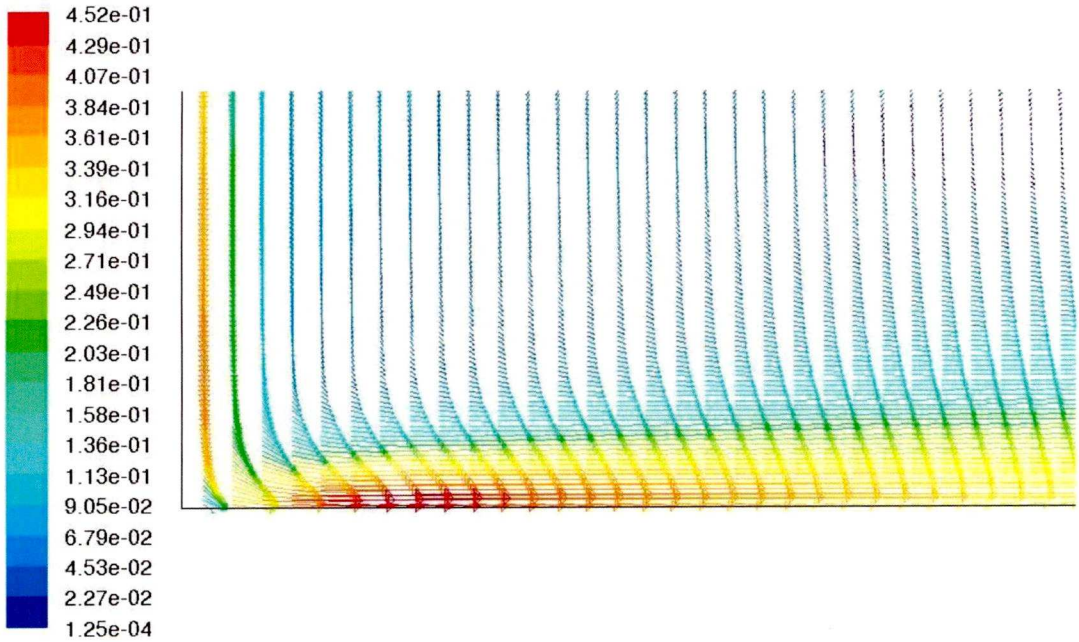

Figure 5.31: Typical Velocity Vectors for the Heavy Wall Jet

5.8.2 Density Profiles

In the following section comparisons of every density profile obtained for each of the heavy wall jet runs are made with the corresponding density profiles extracted from the CFD simulations.

5.8.2.1 Simulation 4 - HWJ I

In total six density profiles were acquired experimentally in two sections of the flume (30cm and 280cm from the inlet side) after 15, 30 and 45 minutes from the start of the run. Density profiles at the same locations and same times were extracted from the simulation and are plotted in graphs against the experimental density profiles in Figure 5.32 to Figure 5.34.

Overall the simulated results show good agreement with the experimental results, especially at the section closer to the jet source. The greatest difference between the two sets is observed at the bottom of the flume where the simulation results exhibit faster mixing, or rather displacement of the fresh water with saline water.

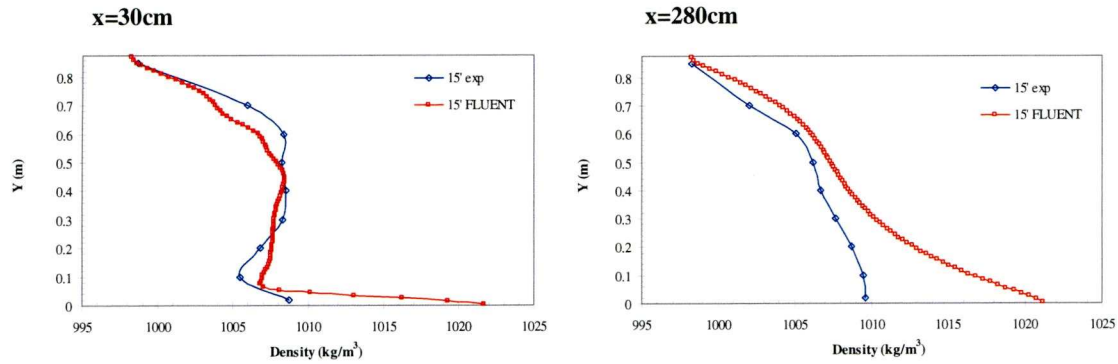

Figure 5.32: HWJ I - Experimental and Computed Density Profiles (t=15min)

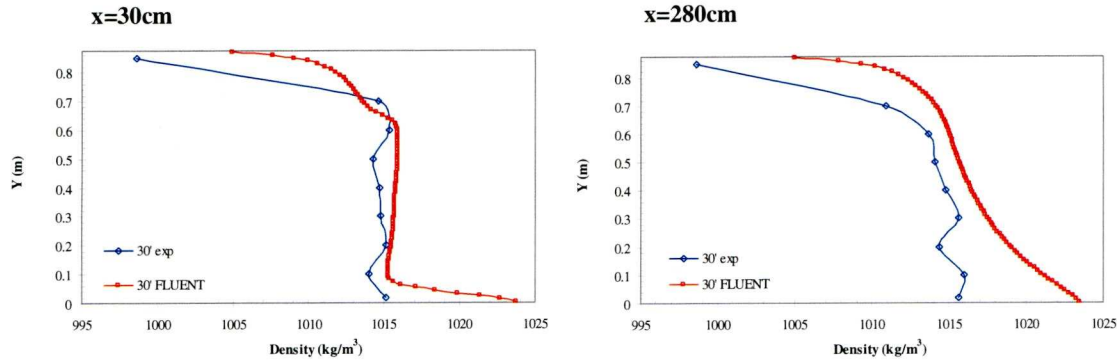

Figure 5.33: HWJ I - Experimental and Computed Density Profiles (t=30min)

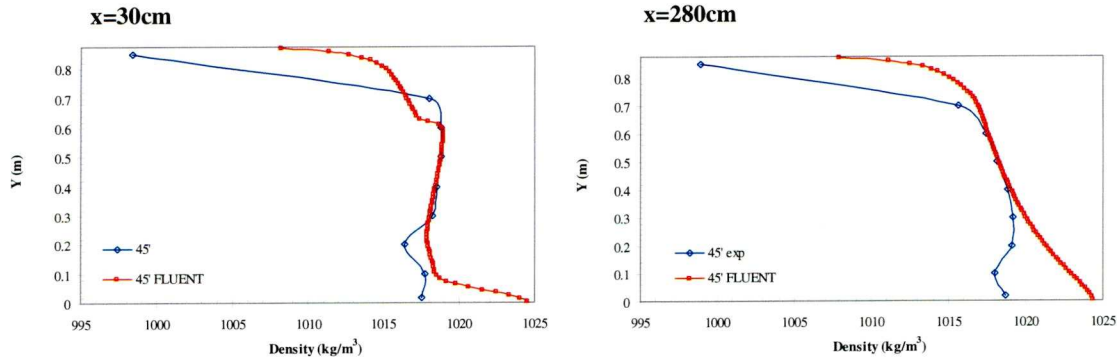

Figure 5.34: HWJ I - Experimental and Computed Density Profiles (t=45min)

From the comparisons it can be seen that *FLUENT* reasonably accurately predicts the density profiles at the section nearer to the jet source. Although better agreement with the experimental density profiles is observed at the first section, even at the section further away from the jet source *FLUENT* manages to predict the trend.

5.8.2.2 Simulation 5 - HWJ II

The second set of comparisons on the heavy wall jet was based on experiment HWJ II. Density profiles were again obtained experimentally at 30cm and 280cm from the origin of the jet and the corresponding profiles were extracted from the simulation after 15min and 30 min. The experimental and computational profiles are graphically compared in Figure 5.35 and Figure 5.36.

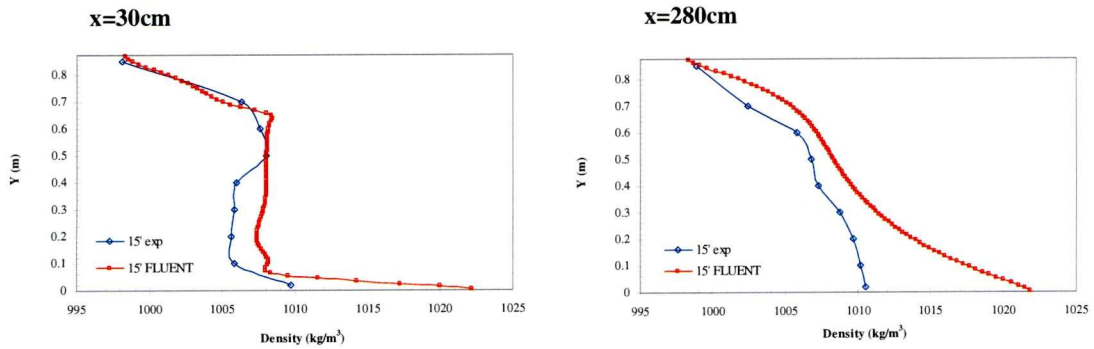

Figure 5.35: HWJ II - Experimental and Computed Density Profiles (t=15min)

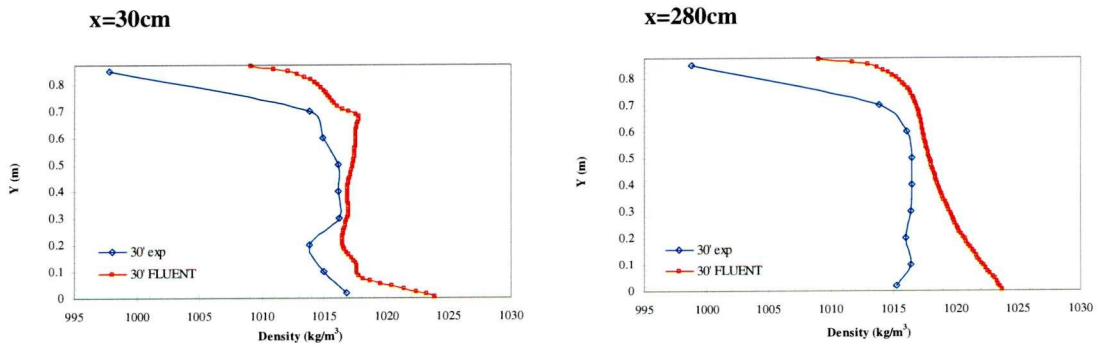

Figure 5.36: HWJ II - Experimental and Computed Density Profiles (t=30min)

The result of the comparisons is similar to that of HWJ I with *FLUENT* largely achieving to predict the mixing and the pattern of the density distribution in the flume. The most significant differences between the two sets of data are again observed at the bottom of the flume where the computed results indicate displacement of the fresh water by the saline water.

5.8.2.3 Simulation 6 - HWJ III

The third simulation on the heavy wall jet was based on experiment HWJ III and was the first of the runs to be undertaken with the introduction of a baffle at a distance of 10cm from the inlet. For this run a 40cm long baffle was used.

The experimental and computed density profiles are plotted along each other in Figure 5.37 to Figure 5.39. In Figure 5.38 it can be seen that *FLUENT* indicates that there is recirculation at the region above the jet flow which affects the density profiles at the location closer to the jet source. The experimental data however did not manage to capture such a flow pattern. It is likely that the distance between the experimental measurement locations was too large to capture the recirculation pattern.

In general the simulation managed to predict the location of the interface between the two phases, mixing at the bottom of the flume due to the jet, however, seemed to happen at a faster rate than that shown by the experimental results. It is odd that the experimental results, even at the section close to the jet source, display great dilution rather than displacement of the fresh water by the saline water jet.

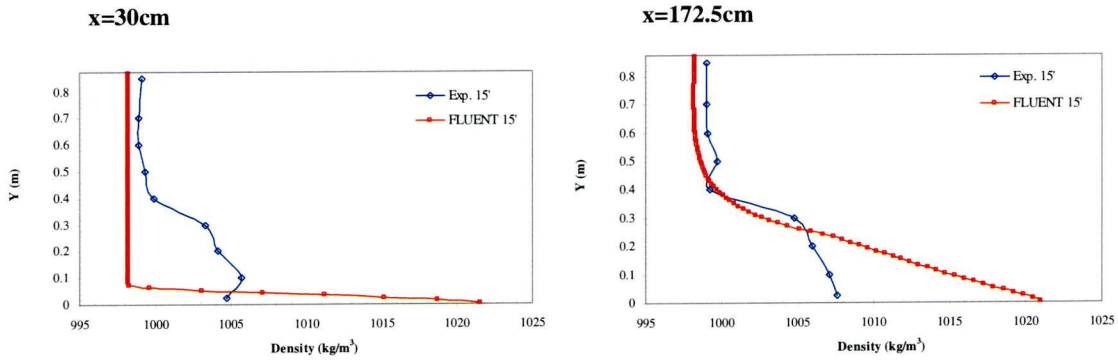

Figure 5.37: HWJ III - Experimental and Computed Density Profiles (t=15min)

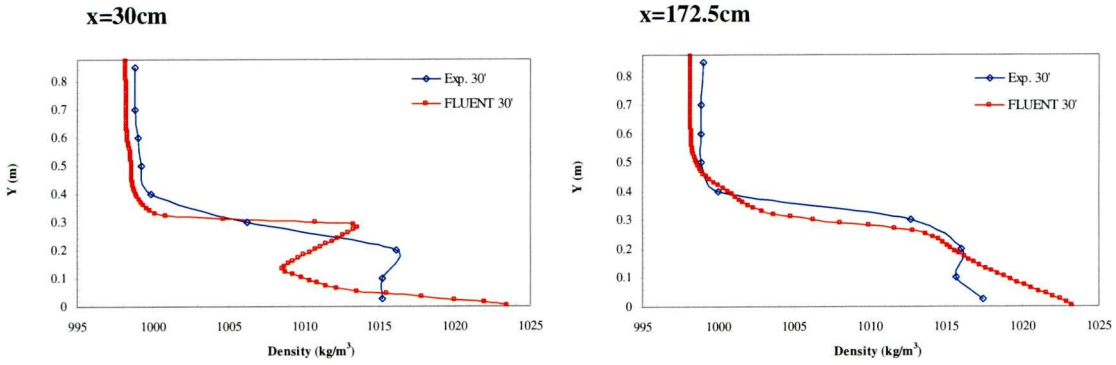

Figure 5.38: HWJ III - Experimental and Computed Density Profiles (t=30min)

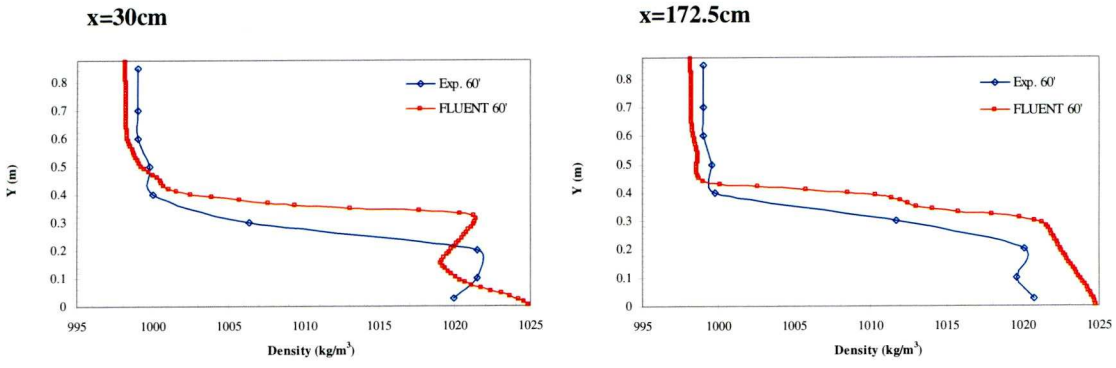

Figure 5.39: HWJ III - Experimental and Computed Density Profiles (t=60min)

5.8.2.4 Simulation 7 - HWJ IV

The HWJ IV experiment was very similar to HWJ III and as a result similar observations were also made for the simulation performed based on experimental run HWJ IV. Again *FLUENT* indicated recirculation at the section close to the jet source for the measurements taken after 10 and 20 minutes. The interface between the two phases was again predicted quite accurately. However, the simulation seemed to once again over predict the mixing rate at the bottom of the flume.

The experimental data and computed profiles are compared in Figure 5.40 to Figure 5.43.

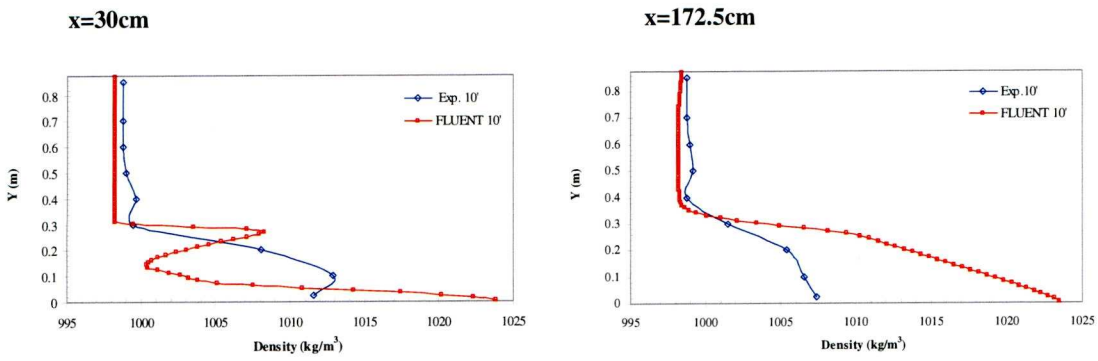

Figure 5.40: HWJ IV - Experimental and Computed Density Profiles (t=10min)

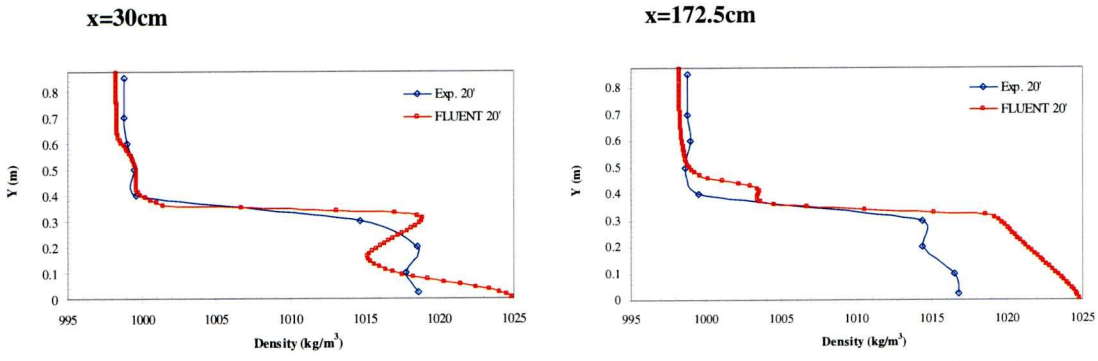

Figure 5.41: HWJ IV - Experimental and Computed Density Profiles (t=20min)

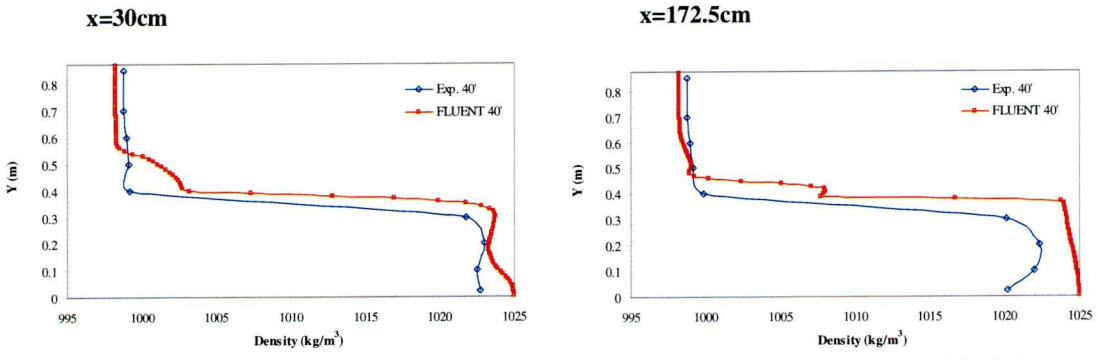

Figure 5.42: HWJ IV - Experimental and Computed Density Profiles (t=40min)

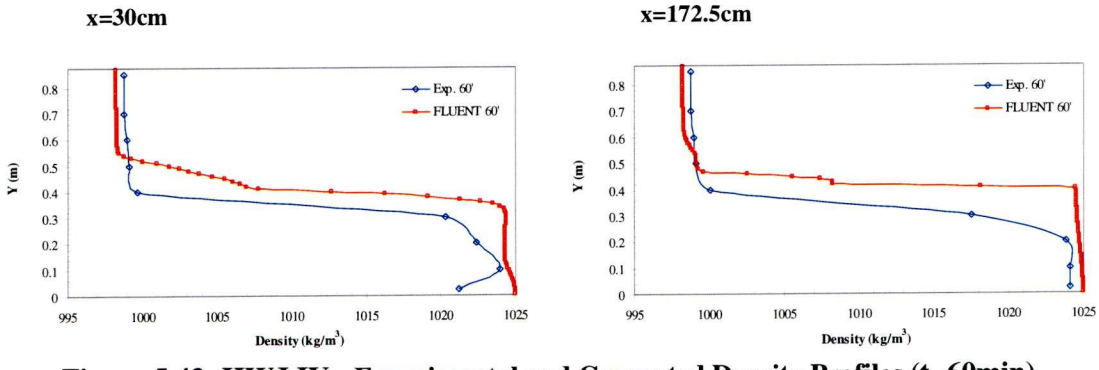

Figure 5.43: HWJ IV - Experimental and Computed Density Profiles (t=60min)

5.8.2.5 Simulation 8 - HWJ V

The HWJ V simulation was the first simulation that involved a lower density difference between the fresh and saline water. Investigations indicated that this model was much more sensitive to parameters that did not have a great impact on the previous models. One such example was the time step size as is demonstrated in Figure 5.44.

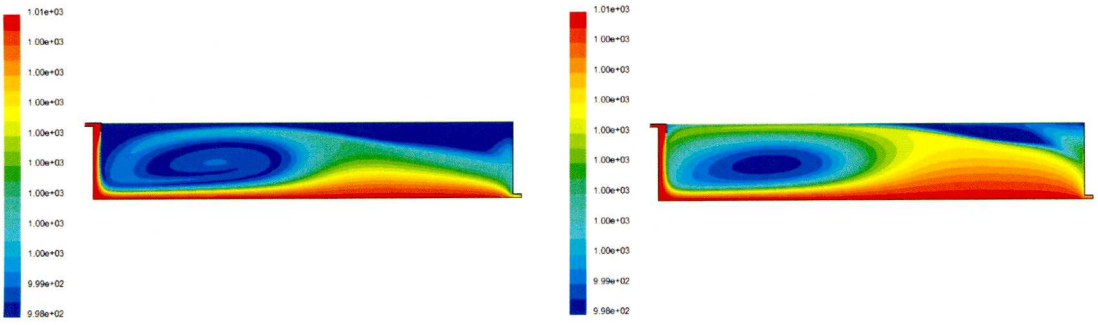

Density contours with 1s timestep (t=5min) Density contours with 0.1s timestep (t=5min)

Figure 5.44: HWJ V - Density Contours after 5min for time step 1s and 0.1s

The same model set up as used for the previous simulations however, did provide satisfactory results as shown Figure 5.45 and Figure 5.46.The same model conditions as for the previous models were applied and although the comparisons do not compare as well they still provide results that could be used to roughly predict mixing especially some time after the start of the run.

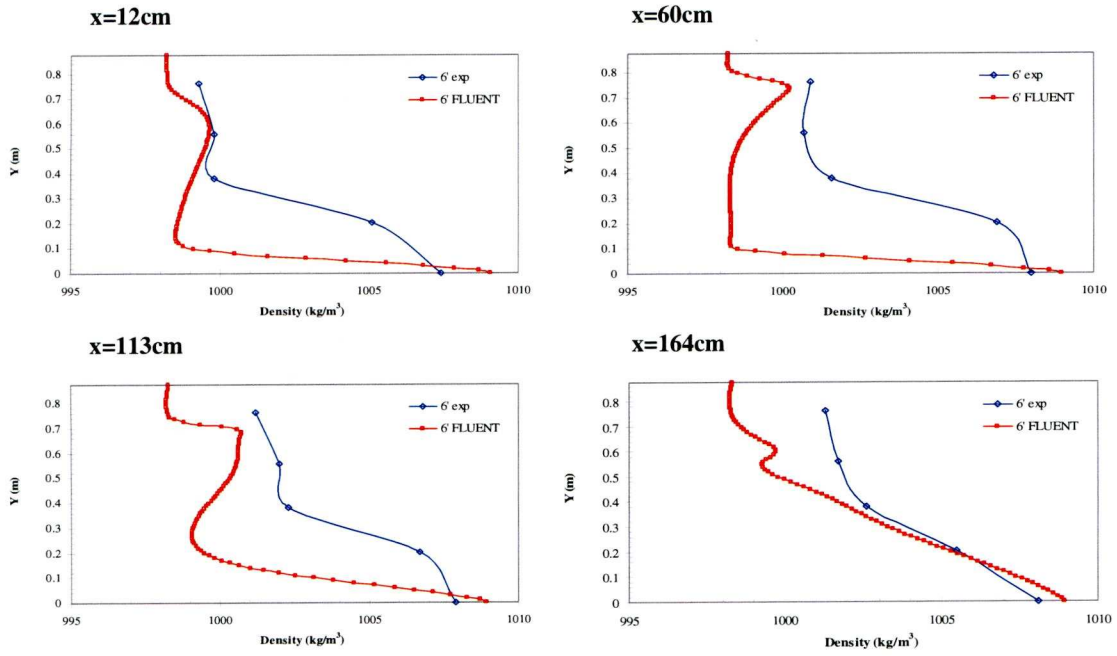

Figure 5.45: HWJ V - Experimental and Computed Density Profiles (t=6min)

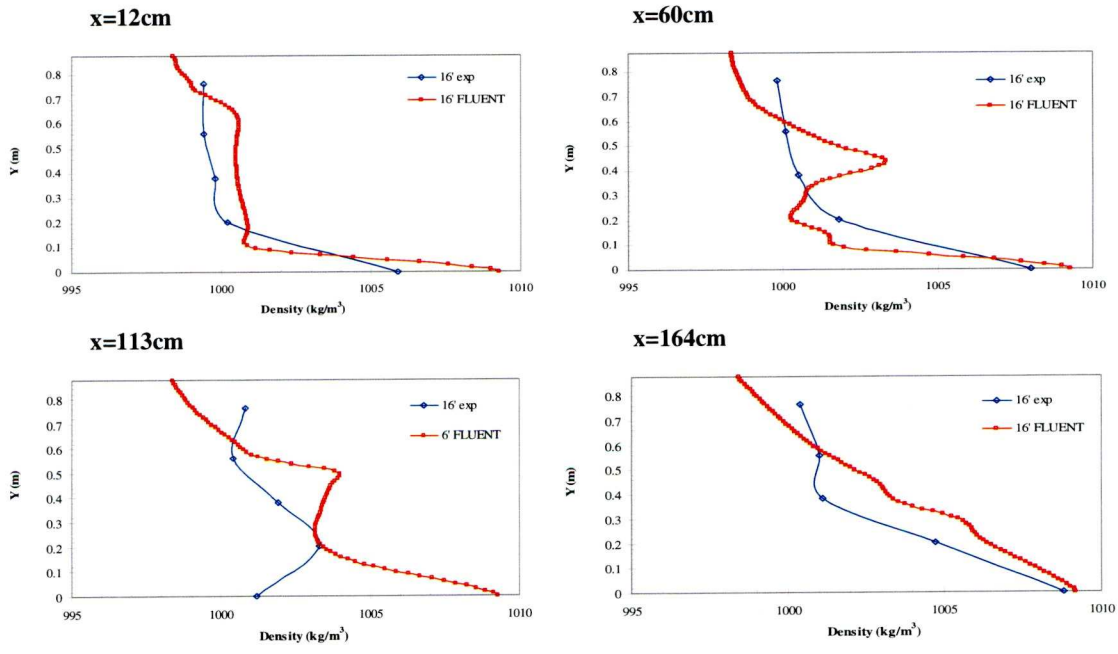

Figure 5.46: HWJ V - Experimental and Computed Density Profiles (t=16min)

Although the comparisons were not as accurate, the overall flow pattern produced by the simulation is very similar to the flow pattern caused by a heavy wall jet as given by Ead and Rajaratnam (2002) and demonstrated in Figure 5.47 overleaf.

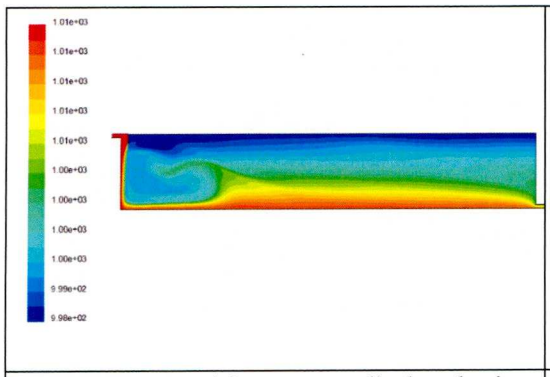

HWJ V Simulated flow pattern displayed using density contours

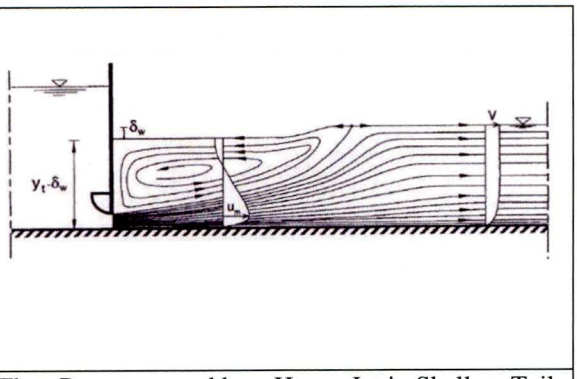

Flow Pattern caused by a Heavy Jet in Shallow Tail water (after Ead & Rajaratnam, 2002)

Figure 5.47: HWJ - Simulated and Experimental Flow Pattern Comparison

5.8.2.6 Simulation 9 - HWJ VI

The very last simulation on the heavy wall jet was based on experimental run HWJ VI. The density difference between the fresh and the saline water in this case was the lowest of all the runs. The saline water density of 1005 kg/m^3 used in the experiments gave a density difference of less than 1% (0.07%). This simulation proved to be the most challenging with the results being given from the computation being less similar to the experimental results.

The comparisons between experimental and computed density profiles at the four downstream locations are given in Figure 5.48 after 6 minutes and Figure 5.49 after 16 minutes. The computed density profiles taken after 6 minutes from the start of the run indicate very strong recirculation. Something like that was not captured by the experimental data.

Overall the computed results seem to be much weaker for the simulations with lower density differences between the two phases. However, as the experimental data were also uncertain, no conclusions could be drawn. There is nevertheless strong indication that *FLUENT* 's performance decreased for the the lower density differences.

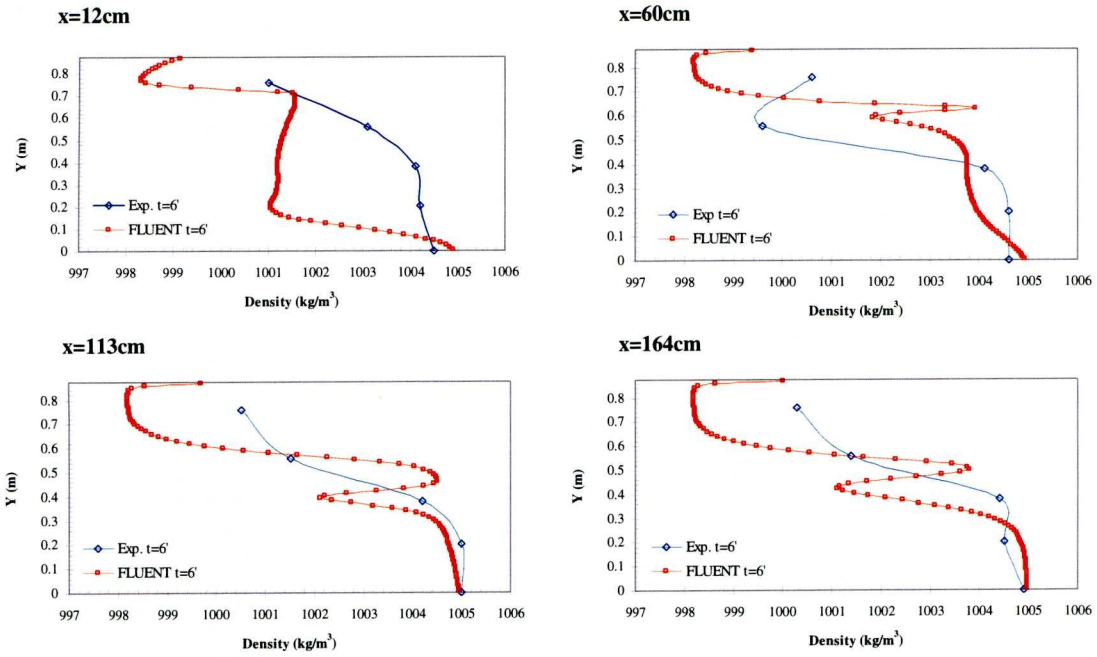

Figure 5.48: HWJ VI - Experimental and Computed Density Profiles (t=6min)

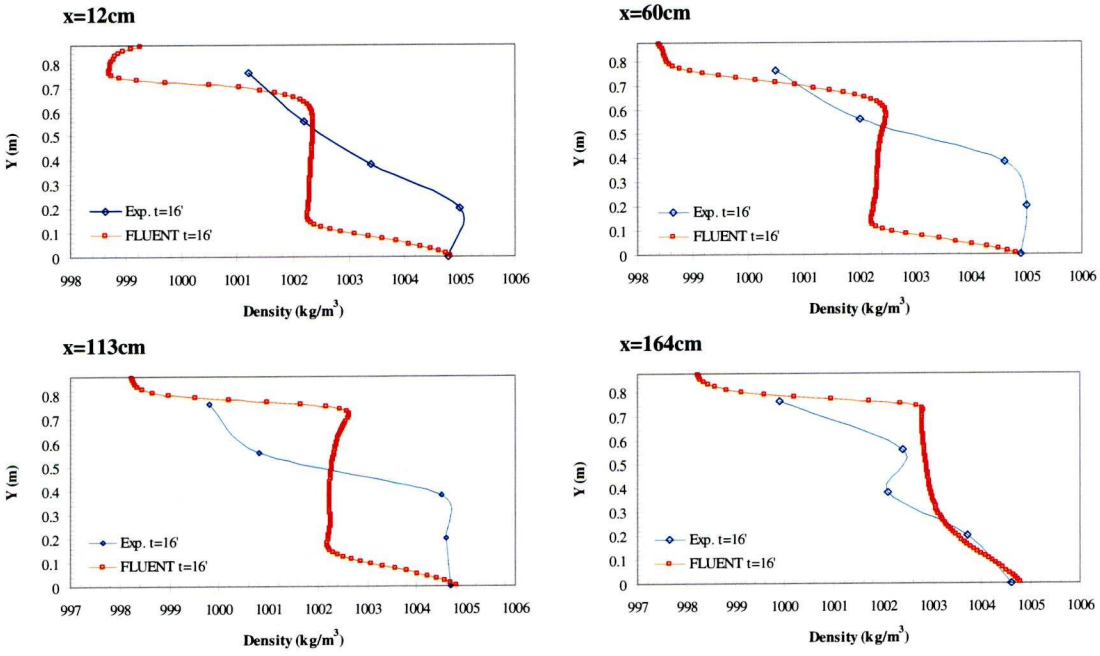

Figure 5.49: HWJ VI - Experimental and Computed Density Profiles (t=16min)

5.9. Heavy Wall Jet Model Performance

Overall the performance of the computational models in predicting the mixing caused by heavy wall jets was again reasonably satisfactory. *FLUENT* managed to predict the mixing times and density profiles reasonably well for all six experiments converted to simulations. It was observed however that the CFD simulations performed better when the density difference between the two fluids was higher.

For runs HWJ I to HWJ IV the density of the salt water was 2025 kg/m^3 meaning 2.68% higher than the density of fresh water which was 998.2 kg/m^3. The results of these simulations are generally in agreement with the experimental data, although some inconsistencies, especially at locations further away from the jet source were observed. For HWJ V and HWJ VI however the simulations do not seem to perform as well as for the first four runs in the heavy wall jet. In both these cases the only difference from the previous simulations was the lower density difference which was 1.18% for HWJ V and 0.68% for HWJ VI. These two simulations proved more challenging as the lower density difference signified less strong buoyant forces meaning there was no clear dominating power driving the flow.

This clear deterioration of the performance of CFD for lower density differences needs to be further investigated in order to enable the draw of any conclusions. There are however, strong indications that *FLUENT* does not perform the same when buoyant forces are not as strong. This highlights the concern that CFD cannot be deemed adequate from a single validation but needs to be validated over a range of different scenarios to ensure that results produced from an analysis are credible and can be used to predict various physical processes.

Chapter 6. Discussion and Conclusions

6.1. Discussion and Recommendations

The credibility of Computational Fluid Dynamics (CFD) simulations in predicting mixing of water bodies caused by turbulent buoyant jets using a standard commercial CFD code was investigated. The attempt to transfer the experimental conditions to simulations and predict the various characteristics of the flow was largely achieved for all the experiments. The results indicate that simulations could be a viable method to predict mixing in natural bodies with a view to CFD simulations eventually predicting the outcome of mixing processes in cases where experimental data is not available. However, the study demonstrates that CFD simulations at present cannot be deemed credible without comparisons to experimental data. There were several potential pitfalls identified during the course of the study that should be taken into account before conclusions are drawn from results provided by CFD simulations.

The study involved undertaking a set of experiments on buoyant turbulent jets (buoyant surface jet and heavy wall jet) to obtain experimental data that were subsequently used to validate CFD simulations. The conditions under which the experiments were performed were transferred to the computational models set up as initial and boundary conditions.

One significant shortcoming of the study, however, was that both the accuracy and the number of the experimental data used were not of sufficient quality and quantity to establish relationships between simulation performance and conditions used. The initial intention of making velocity as well as density comparisons for all

experimental runs did not materialise as significant technical problems emerged during the course of the study. This considerably limited the confidence with which conclusions regarding the credibility of the simulation results could be drawn. As there are large uncertainties in the proper application of CFD itself, especially with regards to turbulence models, the validation of CFD simulations requires experiments that are as reliable as possible. Comparisons of the experimental results of the study with theory of turbulent jets provided some assurance that there were no great discrepancies between the two. Although the experimental data were not accurate enough to be suitable for detailed examinations, in conjunction with previous experimental studies they provided a good guide and proved very useful in aiding the identification of significant pitfalls that could be encountered when attempting to predict mixing due to turbulent buoyant jets using CFD.

The first parameter of a simulation to be identified as a potential source of significant error that could lead to unrealistic results was the choice of convergence criterion. At the start of every simulation the user is asked to define the convergence criterion. The *FLUENT* software default value, which is also a value widely suggested as a rule of thumb, of reduction in residuals of three orders of magnitude was proven not to be adequate when modelling turbulent jets. Results of the present study indicated that a realistic solution was approached only after a convergence criterion of five orders of magnitude decrease in residuals. As turbulent jets are characterised by rapid changes a convergence criterion of three orders of magnitude was not sufficient for the flow to develop fully. This observation highlighted the fact that default values in the software or general recommendations should not be taken for granted and it would be advisable if they were questioned before being applied. To achieve that an

appreciation of the flow is required and sense checks should always be made even after a simulation seems to have reached a satisfactory solution.

As part of the study several checks were made to identify the suitability of different choices available in CFD for the modelling of turbulent buoyant jets. The first exercise was undertaken to determine the appropriate grid resolution for the problem. This was checked using the Grid Convergence Index (GCI) on three different grid sizes. The GCI is a recognized technique for the control of numerical accuracy. The verification exercise demonstrated that the GCI value was less than 3% for the downstream component of velocity for the medium and fine grid sizes investigated. As the GCI is akin to a 99.9% statistical confidence interval the uncertainty between the meshes could suggest that the numerical schemes were of an acceptable numerical accuracy to be used in predictive terms.

A further check was carried out to identify the most suitable turbulence model to describe turbulent jet flow. Three turbulence models (the standard k-ε, the RNG k-ε and the k-ω models) were identified as suitable for the flow and were subsequently tested against each other and against theory to determine which was the most apt for modeling turbulent jets. After comparisons of velocity profiles taken with the use of the three different models were made both between them and with turbulent jet theory and experimental results from previous studies, the RNG k-ε model was identified as the most suitable and was consequently applied to all the simulations. The choice of turbulence model is particularly complicated as there are no recognized methods for checking its appropriateness and the only way to evaluate a model's performance is to compare with theory or experimental results. Again an

appreciation of the flow is important as even after checks there is still a danger that the results might not be realistic.

This was experienced when comparisons between computational and experimental data on the time dependent density measurements were carried out. Although a grid convergence study was performed and exercises to determine the most appropriate turbulence model and boundary conditions were undertaken, and confirmed in some cases with velocity comparisons, the density comparisons were not in agreement. While comparisons of the velocity fields with theory displayed satisfactory accuracy of the obtained solution, the mixing time was completely unrealistic, with mixing happening up to four times faster than in the respective experiments.

Through trial and error simulations the determining factor of the mixing time scales was found to be the turbulent kinetic energy specified at the inlet. For accurate simulations it is not only important to know the mass influx and velocity magnitude at the inlet but also the turbulence intensity or the turbulent kinetic energy directly. The turbulent kinetic energy appears to be a function of the inlet conditions and further investigations to determine a relationship linking them directly would be desirable. This could not be achieved in this study as the variation of inlet velocities was not adequate for such an examination. Normally when setting up a CFD analysis an assumption is made on either the turbulence kinetic energy or the turbulence intensity of the flow based on either experience or common estimation principles. Such a general assumption however is not adequate to accurately predict the mixing time and although other parameters or numerical checks might show that a solution to the problem has been achieved this is not the case. The turbulence kinetic energy has been investigated for every simulation described in the following chapter and it

was found that for every simulation a turbulent kinetic energy of 0.01 m^2/s^2 produced reasonable results. This value was achieved by trial and error and was an estimate as the available experimental data was not adequate to determine the turbulence kinetic energy.

Although satisfactory results were obtained, the computational model did not perform equally in all cases investigated. One observation made was that the models seemed to give better results for the runs with higher density difference between the two fluids with the run with the lowest density difference between the two fluids performing the worst. This however could not be investigated further as only two of the nine runs were performed with a lower density difference.

A final observation was that CFD failed to predict certain characteristics of the flow, such as the potential core of the jet. This is something that the code has not yet the capability to fully address transitional flows.

The fact that the simulation results were realistic for all the investigated experimental setups, with various degrees of difficulty, is an indication of the consistency in the computational results. There are several aspects however that point out the fact that without extensive checks with theoretical results, the results obtained with the use of CFD can seem correct but not represent reality.

It could be argued that the process of hydraulic investigations would be significantly enhanced if the integration of CFD and experiments was much stronger. The scope of experimental measurements could be extended through CFD and the credibility of the simulation results enhanced by the availability of suitable measurements from experiments. The underlying perspective is that CFD studies will eventually be able

to predict the outcome of a physical event for which experimental data is not available. This sort of closer integration is however rare at present.

Further investigations and comparisons with experimental data to confirm the findings of the present study and investigate the relationship between TKE inlet conditions with mixing time and buoyancy levels with model performance are advisable. The uncertainty surrounding the experimental data used in the study makes it difficult to reach any detailed conclusions. Experimental data obtained with more advanced profiling techniques, both for velocity and density would be very useful, as well as greater computational power that would enable faster and more detailed computational modelling.

Furthermore, CFD application to problems of water and environmental engineering is still relatively new and benchmark experimental data is not readily available as is the case in other industries, like aerospace and automotive engineering, where CFD has been used for years. In many cases assumptions used in the commercial codes, such as factors in turbulence models, have been developed for applications in those traditional CFD industries and are not always suitable for other applications. Sets of experimental benchmark experimental results against which checks of computational models could be performed would be a great way of increasing confidence in computational simulations in a water and environmental engineering context. This is already the case in other fields of CFD applications. NASA for example has been providing freely available sets of benchmark cases for common aerospace applications. The development of such benchmark experimental results would be desirable also for common water and environmental engineering applications, such

as buoyant jets, so that there is a point of reference with regards to making various checks to confirm solution realism.

Another issue with CFD simulations is the fact that at present no best practice guidelines explicitly outline what parameters need to be checked to assume whether a simulation is credible. Following standard guidelines, the code can be verified by analysing the downstream component of velocity and undertaking a grid convergence index check. This however does not seem to address the accuracy of every aspect of the flow. Even though such an exercise was undertaken, it was demonstrated that it is still possible that the simulation has not been verified. Therefore, it would be beneficial if present guidelines were extended to cover more features of more complex flows, such as multiphase flows, and explicit guidelines were formulated about how the guidelines should be interpreted.

A final recommendation would be to perform a similar analysis of mixing due to turbulent buoyant jets by gathering experimental data and performing the CFD simulation in three dimensions. A validation of mixing due to turbulent buoyant jets through a three dimensional analysis would provide the assurance that CFD could be used to predict mixing also in more complicated geometries as is often the case in natural water bodies.

6.2. Conclusions

Overall it has been demonstrated that CFD is a viable solution to accurately predicting mixing of water bodies due to buoyant turbulent jets. The results are encouraging, and suggest that CFD can be useful and practical in more complex mixing applications that arise from turbulent buoyant jets. Commercial CFD codes,

such as *FLUENT*, if used with a sufficiently detailed mesh and thorough checking procedures seem to be capable to give reliable answers using standard two-equation turbulence models.

However, as the study has demonstrated, conclusions should be drawn only following careful consideration and after rigorous checks. Velocity measurements comparisons are not adequate to determine the performance of a buoyant jet model. The use of experimental investigations cannot at present be completely replaced by the use of CFD as it is possible that CFD results that appear correct do not represent reality. CFD simulations should at least be checked with previously validated generic flow cases when experimental data is not available. Additional care should be exercised when performing simulations of time dependent problems. The study has demonstrated that the turbulent kinetic energy is a significant parameter in time dependent CFD simulations of buoyant jets.

Appendix A Velocity Meter Calibration Chart

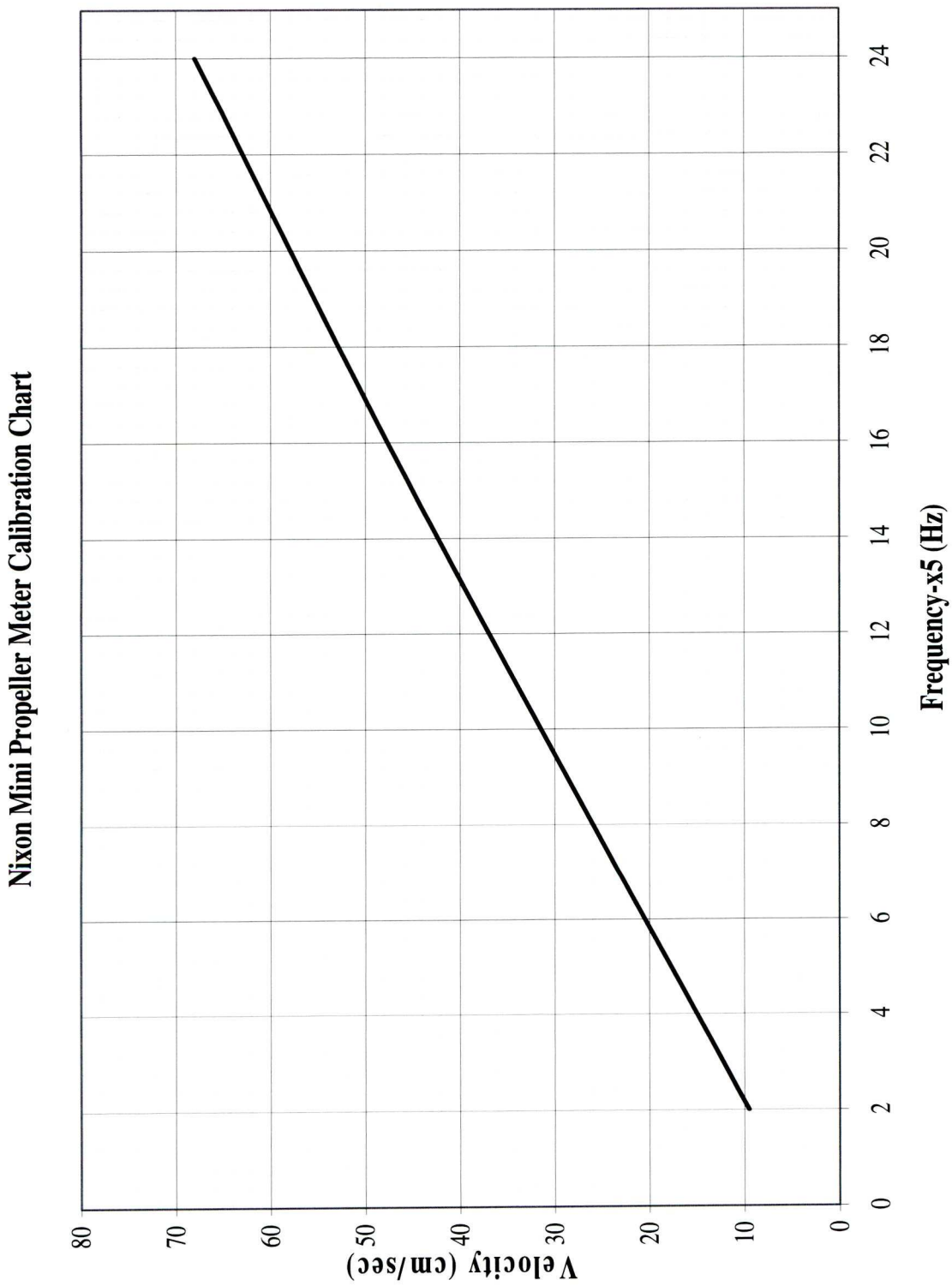

Appendix B Experimental Measurements

B.1 Buoyant Surface Jet Experimental Data

B.1.1 BSJ I

Table B.1: BSJ I - Density Measurements (t=15min)

Distance from flume bottom (mm)	Density (kg/m^3)		
	x=5cm	x=30cm	x=160cm
815	1001.0	1001.6	1003.0
790	1004.5	1001.5	1002.2
740	1004.4	1001.9	1002.1
690	1004.0	1001.7	1002.3
640	1002.9	1000.9	1001.8
590	1002.2	1001.9	1002.9
540	1001.6	1001.6	1002.0
490	1001.8	1001.3	1005.7
440	1001.4	1001.3	1011.5
390	1001.5	1000.6	1003.7
340	1002.3	1000.7	1007.1
290	1003.4	1000.9	1014.3
240	1022.3	1022.0	1022.3

B.1.2 BSJ II

Table B.2: BSJ II - Density Measurements (t=15min)

Distance from flume bottom (mm)	Density (kg/m^3)		
	x=5cm	x=30cm	x=160cm
815	1001.3	1002.3	1002.6
790	1001.7	1004.7	1003.2
740	1011.9	1007.7	1012.9
690	1013.1	1012.1	1024.2
640	1023.4	1015.4	1024.4
590	1023.9	1023.9	1024.5
540	1023.9	1023.7	1024.9
490	1023.9	1023.6	1025.0
440	1023.7	1023.1	1025.0
390	1023.6	1025.0	1025.0
340	1025.0	1025.0	1025.0
290	1025.0	1025.0	1025.0
240	1025.0	1025.0	1025.0

Table B.3: BSJ II - Density Measurements (t=30min)

Distance from flume bottom (mm)	Density (kg/m^3)		
	x=5cm	x=30cm	x=160cm
815	1000.5	1000.4	1001.1
790	1001.3	1000.2	1000.7
740	1001.0	1000.0	1000.7
690	1000.8	1000.7	1001.2
640	1001.1	1001.3	1000.2
590	1001.3	1001.3	1001.2
540	1002.1	1001.5	1004.7
490	1004.6	1005.5	1004.5
440	1012.2	1009.4	1006.2
390	1019.2	1016.3	1017.0
340	1022.7	1021.7	1022.0
290	1022.2	1023.1	1023.6
240	1025.0	1025.0	1025.0

B.1.3 BSJ III

Table B.4: BSJ III - Density Measurements (t=15min)

Distance from flume bottom (mm)	Density (kg/m^3)		
	x=5cm	x=30cm	x=160cm
815	1000.3	999.9	999.5
790	999.6	999.3	999.1
740	999.2	999	999.1
690	1000.1	999.4	999.1
640	1000.3	999.4	999.2
590	1000.2	1000.2	999.1
540	1000.1	1000	999.5
490	1000.4	999.8	999.2
440	1001.7	1000.2	999.2
390	1002.5	1000.6	1001.1
340	999.8	999.8	1013.3
290	-	-	1020.6
200	1020.4	1023.6	1024

B.2 Heavy Wall Jet Experimental Data

B.2.1 HWJ I

Table B.5: HWJ I - Velocity Measurements

Distance from flume bottom (mm)	Velocity (cm/sec)	
	x=30cm	x=280cm
160	0.00	4.61
140	7.06	2.00
120	8.28	5.83
100	9.50	7.67
80	10.60	5.83
60	13.90	7.06
40	18.25	8.00
20	19.33	11.15
5	24.75	11.70

Table B.6: HWJ I - Density Measurements (t=15min)

Distance from flume bottom (mm)	Density (kg/m^3)	
	x=30cm	x=280cm
820	998.7	998.3
740	1006	1002
640	1008.4	1005.1
540	1008.2	1006.2
440	1008.5	1006.7
340	1008.3	1007.7
240	1006.8	1008.7
140	1005.5	1009.5
0	1008.7	1009.6

Table B.7: HWJ I - Density Measurements (t=30min)

Distance from flume bottom (mm)	Density (kg/m^3)	
	x=30cm	x=280cm
820	998.6	998.6
740	1014.6	1010.9
640	1015.3	1013.7
540	1014.3	1014.1
440	1014.7	1014.8
340	1014.8	1015.6
240	1015.1	1014.4
140	1014	1016
0	1015.1	1015.6

Table B.8: HWJ I - Density Measurements (t=45min)

Distance from flume bottom (mm)	Density (kg/m^3)	
	x=30cm	x=280cm
820	998.4	998.9
740	1018	1015.6
640	1018.8	1017.4
540	1018.8	1018.1
440	1018.5	1018.8
340	1018.2	1019.2
240	1016.4	1019.1
140	1017.7	1018
0	1017.5	1018.7

B.2.2 HWJ II

Table B.9: HWJ II - Velocity Measurements

Distance from flume bottom (mm)	Velocity (cm/sec)	
	x=30cm	x=280cm
160	6.44	0.00
140	8.28	2.00
120	8.28	4.00
100	8.28	5.22
80	10.60	7.06
60	12.80	7.67
40	13.90	7.06
20	17.17	7.67
5	19.33	8.89

Table B.10: HWJ II - Density Measurements (t=15min)

Distance from flume bottom (mm)	Density (kg/m^3)	
	x=30cm	x=280cm
820	998.1	998.9
740	1006.3	1002.4
640	1007.6	1005.8
540	1008.0	1006.8
440	1006.0	1007.3
340	1005.8	1008.8
240	1005.6	1009.7
140	1005.8	1010.2
0	1009.7	1010.5

Table B.11: HWJ II - Density Measurements (t=30min)

Distance from flume bottom (mm)	Density (kg/m^3)	
	x=30cm	x=280cm
820	997.8	998.8
740	1013.8	1013.9
640	1014.9	1016.1
540	1016.1	1016.5
440	1016.1	1016.5
340	1016.2	1016.4
240	1013.8	1016.0
140	1015.0	1016.4
0	1016.8	1015.3

B.2.3 HWJ III

Table B.12: HWJ III - Density Measurements (t=15min)

Distance from flume bottom (mm)	Density (kg/m^3)	
	x=30cm	x=172.5 cm
815	999.1	999.0
740	998.9	999.0
640	998.9	999.1
540	999.3	999.7
440	999.9	999.2
340	1003.3	1004.8
240	1004.1	1006.0
140	1005.7	1007.1
40	1004.7	1007.6

Table B.13: HWJ III - Density Measurements (t=30min)

Distance from flume bottom (mm)	Density (kg/m^3)	
	x=30cm	x=172.5 cm
815	998.8	999.0
740	998.8	998.9
640	999.0	998.9
540	999.2	998.9
440	999.9	1000.0
340	1006.2	1012.7
240	1016.1	1016.0
140	1015.2	1015.6
40	1015.2	1017.4

Table B.14: HWJ III - Density Measurements (t=60min)

Distance from flume bottom (mm)	Density (kg/m^3)	
	x=30cm	x=172.5 cm
815	999.0	999.0
740	999.0	999.0
640	999.0	999.0
540	999.8	999.6
440	1000.0	999.8
340	1006.4	1011.7
240	1021.5	1020.1
140	1021.5	1019.6
40	1019.9	1020.7

B.2.4 HWJ IV

Table B.15: HWJ IV - Density Measurements (t=10min)

Distance from flume bottom (mm)	Density (kg/m^3)	
	x=30cm	x=172.5 cm
815	998.8	998.8
740	998.8	998.8
640	998.8	999.0
540	999.0	999.2
440	999.7	998.8
340	999.5	1001.5
240	1008.1	1005.4
140	1012.9	1006.6
40	1011.6	1007.4

Table B.16: HWJ IV - Density Measurements (t=20min)

Distance from flume bottom (mm)	Density (kg/m^3)	
	x=30cm	x=172.5 cm
815	998.8	998.8
740	998.8	998.8
640	999.0	999.0
540	999.5	998.6
440	999.6	999.5
340	1014.7	1014.4
240	1018.5	1014.4
140	1017.8	1016.5
40	1018.6	1016.8

Table B.17: HWJ IV - Density Measurements (t=40min)

Distance from flume bottom (mm)	Density (kg/m^3)	
	x=30cm	x=172.5 cm
815	998.8	998.8
740	998.8	998.8
640	999.0	999.0
540	999.1	999.2
440	999.2	999.9
340	1021.8	1020.1
240	1023.0	1022.3
140	1022.5	1022.0
40	1022.7	1020.2

Table B.18: HWJ IV - Density Measurements (t=60min)

Distance from flume bottom (mm)	Density (kg/m^3)	
	x=30cm	x=172.5 cm
815	998.8	998.8
740	998.8	998.8
640	999.0	999.0
540	999.1	999.1
440	999.7	1000.1
340	1020.3	1017.5
240	1022.4	1023.8
140	1024.0	1024.1
40	1021.2	1024.1

B.2.5 HWJ V

Table B.19: HWJ V - Density Measurements (t=6min)

Distance from flume bottom (mm)	Density (kg/m^3)			
	x=12cm	x=60cm	x=113cm	x=164cm
750	999.3	1000.9	1001.2	1001.3
550	999.8	1000.7	1002.0	1001.7
370	999.8	1001.6	1002.3	1002.6
150	1005.1	1006.9	1006.7	1005.5
0	1007.4	1008.0	1007.9	1008.1

Table B.20: HWJ V - Density Measurements (t=16min)

Distance from flume bottom (mm)	Density (kg/m^3)			
	x=12cm	x=60cm	x=113cm	x=164cm
750	999.4	999.8	1000.8	1000.4
550	999.4	1000.1	1000.4	1001.0
370	999.8	1000.5	1001.9	1001.1
150	1000.2	1001.8	1003.3	1004.7
0	1005.9	1008.0	1001.2	1008.8

B.2.6 HWJ VI

Table B.21: HWJ VI - Density Measurements (t=6min)

Distance from flume bottom (mm)	Density (kg/m^3)			
	x=12cm	x=60cm	x=113cm	x=164cm
750	1001.0	1000.6	1000.5	1000
550	1003.1	999.6	1001.5	1001
370	1004.1	1004.1	1004.2	1004
150	1004.2	1004.6	1005.0	1005
0	1004.5	1004.6	1005.0	1005

Table B.22: HWJ VI - Density Measurements (t=16min)

Distance from flume bottom (mm)	Density (kg/m^3)			
	x=12cm	x=60cm	x=113cm	x=164cm
750	1001.2	1000.5	999.8	1000
550	1002.2	1002.0	1000.8	1002
370	1003.4	1004.6	1004.5	1002
150	1005.0	1005.0	1004.6	1004
0	1004.8	1004.9	1004.7	1005

Appendix C BSJ II Photographs of the Interface Development

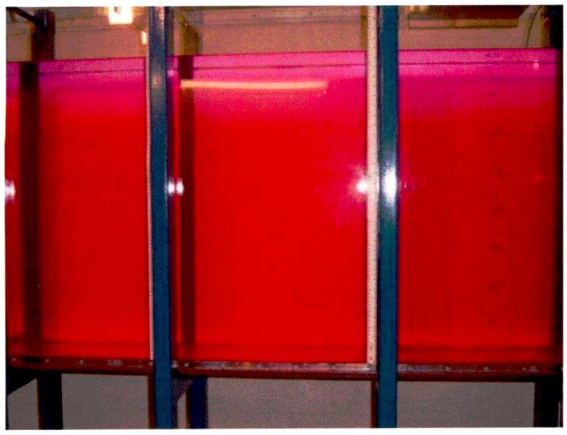

t=5min

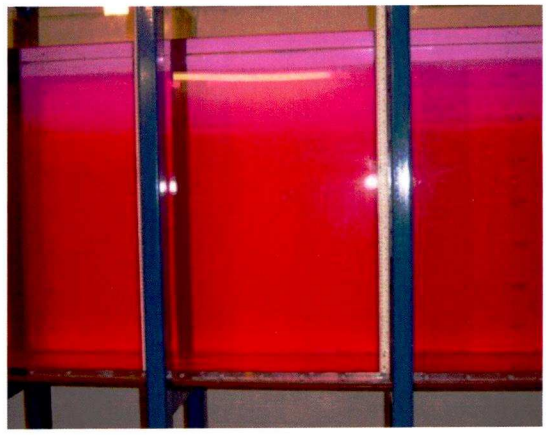

t=10min

t=15min

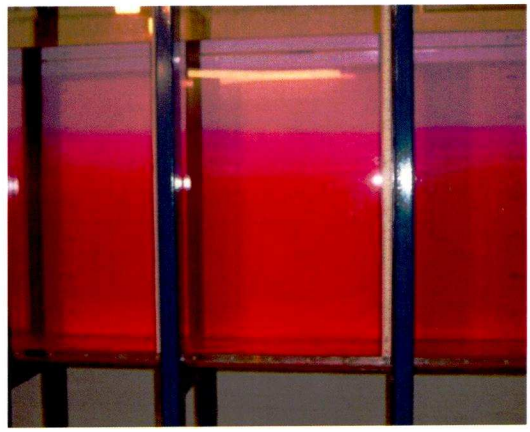

t=20min

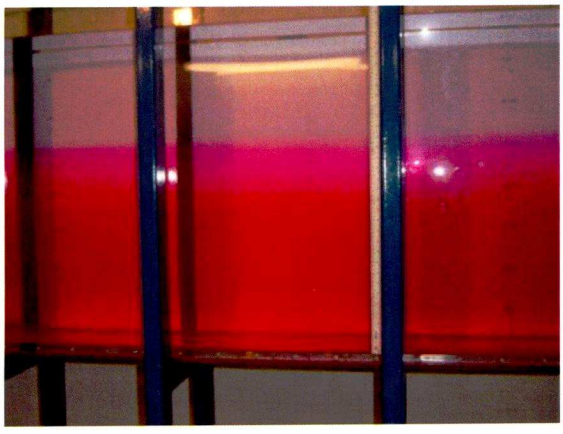

t=25min

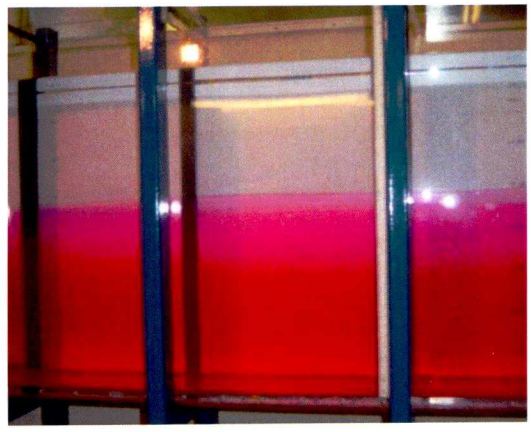

t=30min

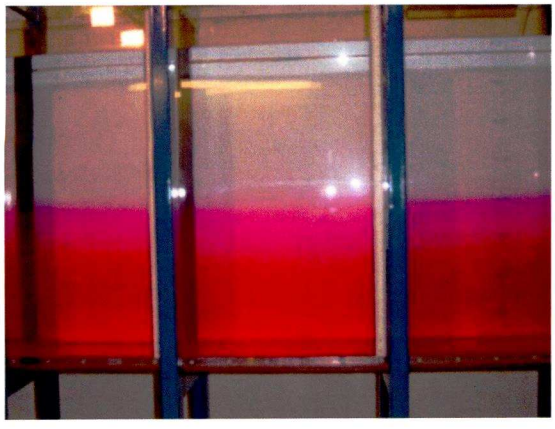

t=35min

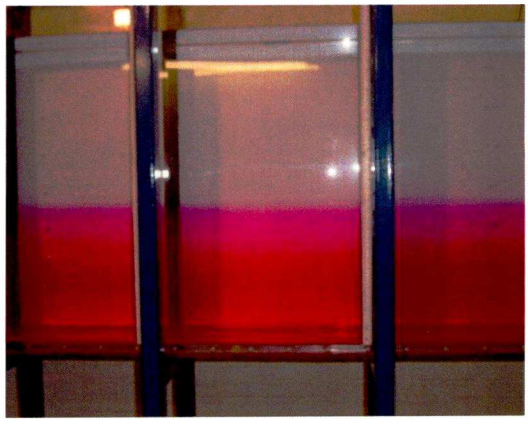

t=40min

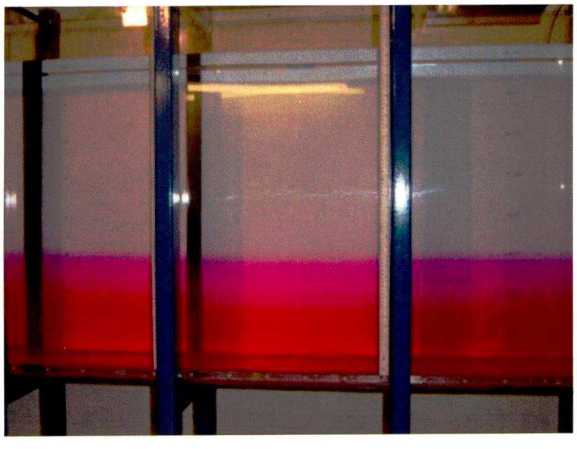

t=45min

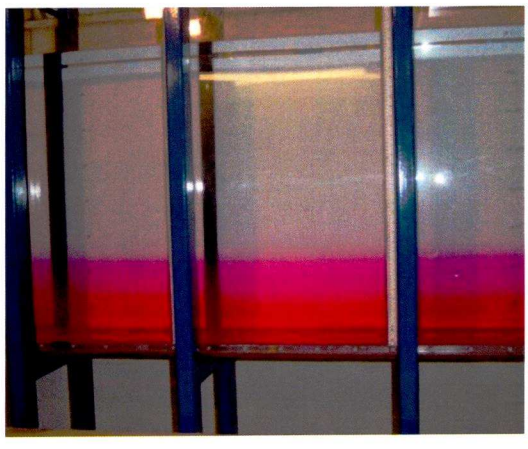

t=50min

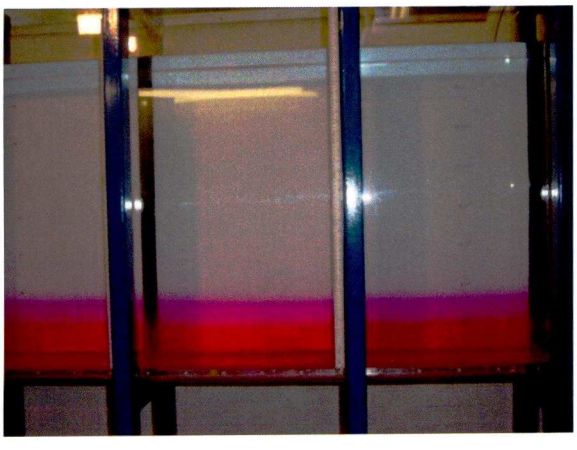

t=55min

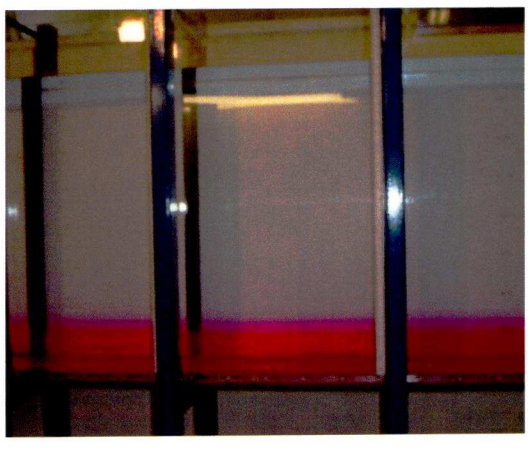

t=60min

Appendix D Grid Convergence Study Calculations

Table D.1: Grid Convergence Index Calculation

Distance from flume bottom (mm)	x - Axis Velocity magnitude (m/s)			GCI_{12}	GCI_{23}
	Coarse grid (h1)	Medium grid (h2)	Fine grid (h3)		
x = 20cm					
450	-0.0041	-0.0045	-0.0043	9.35%	4.14%
500	-0.0037	-0.0037	-0.0035	0.52%	2.36%
550	-0.0032	-0.0031	-0.0028	6.15%	10.28%
600	-0.0031	-0.0026	-0.0023	23.02%	12.03%
650	-0.0026	-0.0008	-0.0005	55.42%	15.35%
700	0.0015	0.0079	0.0083	6.90%	0.42%
750	0.0190	0.0270	0.0270	0.01%	0.00%
800	0.0497	0.0519	0.0510	3.64%	1.53%
840	0.0746	0.0702	0.0686	4.68%	1.81%
x = 40cm					
450	-0.0052	-0.0047	-0.0045	6.90%	2.46%
500	-0.0038	-0.0023	-0.0021	13.67%	2.28%
550	-0.0013	0.0005	0.0009	82.69%	8.55%
600	0.0004	0.0053	0.0057	12.39%	1.10%
650	0.0058	0.0136	0.0141	5.47%	0.37%
700	0.0172	0.0256	0.0258	1.20%	0.03%
750	0.0346	0.0393	0.0389	1.41%	0.12%
800	0.0524	0.0515	0.0504	2.20%	2.73%
840	0.0642	0.0589	0.0573	4.86%	1.51%
x = 60cm					
450	-0.0049	-0.0033	-0.0032	7.07%	0.80%
500	-0.0023	0.0007	0.0010	54.00%	3.50%
550	0.0027	0.0059	0.0063	10.04%	1.21%
600	0.0060	0.0129	0.0134	4.98%	0.33%
650	0.0140	0.0219	0.0222	1.75%	0.06%
700	0.0257	0.0319	0.0318	0.60%	0.01%
750	0.0390	0.0415	0.0408	2.95%	0.86%
800	0.0512	0.0492	0.0480	4.94%	3.22%
840	0.0587	0.0536	0.0520	5.35%	1.72%
x = 80cm					
450	-0.0039	-0.0015	-0.0013	20.43%	2.23%
500	-0.0002	0.0037	0.0040	10.15%	0.68%
550	0.0068	0.0099	0.0102	4.01%	0.36%
600	0.0109	0.0173	0.0175	1.29%	0.03%
650	0.0194	0.0254	0.0253	0.55%	0.01%
700	0.0296	0.0336	0.0331	2.27%	0.30%
750	0.0402	0.0410	0.0400	2.25%	3.14%
800	0.0493	0.0466	0.0451	7.45%	3.97%
840	0.0548	0.0496	0.0479	6.36%	2.17%
x = 100cm					
450	-0.0027	0.0002	0.0004	185.38%	6.83%
500	0.0018	0.0058	0.0059	4.20%	0.19%
550	0.0073	0.0120	0.0121	0.67%	0.01%
600	0.0140	0.0189	0.0188	1.08%	0.03%
650	0.0221	0.0261	0.0256	2.72%	0.34%

Distance from flume bottom (mm)	x - Axis Velocity magnitude (m/s)			GCI_{12}	GCI_{23}
	Coarse grid (h1)	Medium grid (h2)	Fine grid (h3)		
700	0.0311	0.0330	0.0321	6.62%	3.20%
750	0.0400	0.0390	0.0376	3.05%	4.57%
800	0.0474	0.0435	0.0417	9.19%	4.29%
840	0.0517	0.0458	0.0438	8.19%	2.89%
x = 120cm					
450	-0.0011	0.0017	0.0018	12.34%	0.63%
500	0.0039	0.0070	0.0070	0.36%	0.00%
550	0.0095	0.0128	0.0126	2.41%	0.17%
600	0.0161	0.0189	0.0184	3.96%	0.71%
650	0.0234	0.0250	0.0242	8.11%	4.14%
700	0.0311	0.0308	0.0296	0.39%	1.64%
750	0.0384	0.0357	0.0341	9.77%	5.75%
800	0.0445	0.0392	0.0374	9.33%	3.52%
840	0.0479	0.0411	0.0391	8.96%	2.86%
x = 150cm					
450	0.0007	0.0030	0.0031	4.69%	0.21%
500	0.0055	0.0075	0.0074	2.82%	0.23%
550	0.0109	0.0123	0.0118	6.57%	2.18%
600	0.0168	0.0171	0.0163	1.82%	4.38%
650	0.0230	0.0218	0.0207	6.93%	6.42%
700	0.0293	0.0261	0.0247	11.80%	5.42%
750	0.0351	0.0297	0.0280	10.37%	3.43%
800	0.0398	0.0323	0.0304	10.12%	2.78%
840	0.0425	0.0337	0.0316	10.10%	2.54%
x = 200cm					
450	0.0028	0.0041	0.0043	6.15%	0.81%
500	0.0066	0.0066	0.0068	0.05%	0.38%
550	0.0107	0.0092	0.0093	1.68%	0.13%
600	0.0149	0.0117	0.0118	0.78%	0.02%
650	0.0191	0.0141	0.0141	0.25%	0.00%
700	0.0232	0.0162	0.0162	0.11%	0.00%
750	0.0268	0.0180	0.0179	0.38%	0.00%
800	0.0296	0.0192	0.0191	0.57%	0.00%
840	0.0312	0.0199	0.0197	0.71%	0.01%
				10.27%	**2.26%**

Table D.2: Simulated and Extrapolated Velocities from GCI Study

Distance from flume bottom (mm)	FLUENT x- axis velocity (m/s)	Extrapolated x-axis velocity (m/s)	Error (%)
x = 20cm			
450	-0.0043	-0.0042	3.43%
500	-0.0035	-0.0034	1.92%
550	-0.0028	-0.0026	8.97%
600	-0.0023	-0.0021	10.65%
650	-0.0005	-0.0005	14.00%
700	0.0083	0.0083	0.33%
750	0.0270	0.0270	0.00%
800	0.0510	0.0503	1.24%
840	0.0686	0.0676	1.47%
x = 40cm			
450	-0.0045	-0.0044	2.01%
500	-0.0021	-0.0021	1.86%
550	0.0009	0.0009	6.40%
600	0.0057	0.0058	0.87%
650	0.0141	0.0142	0.30%
700	0.0258	0.0258	0.03%
750	0.0389	0.0388	0.10%
800	0.0504	0.0493	2.23%
840	0.0573	0.0566	1.22%
x = 60cm			
450	-0.0032	-0.0031	0.64%
500	0.0010	0.0010	2.73%
550	0.0063	0.0064	0.96%
600	0.0134	0.0134	0.27%
650	0.0222	0.0222	0.05%
700	0.0318	0.0317	0.01%
750	0.0408	0.0405	0.69%
800	0.0480	0.0467	2.64%
840	0.0520	0.0513	1.39%
x = 80cm			
450	-0.0013	-0.0013	1.82%
500	0.0040	0.0040	0.54%
550	0.0102	0.0102	0.29%
600	0.0175	0.0175	0.03%
650	0.0253	0.0253	0.01%
700	0.0331	0.0330	0.24%
750	0.0400	0.0390	2.58%
800	0.0451	0.0437	3.28%
840	0.0479	0.0471	1.76%
x = 100cm			
450	0.0004	0.0005	5.18%
500	0.0059	0.0060	0.15%
550	0.0121	0.0121	0.01%
600	0.0188	0.0188	0.03%
650	0.0256	0.0255	0.27%
700	0.0321	0.0313	2.63%
750	0.0376	0.0363	3.80%
800	0.0417	0.0403	3.55%
840	0.0438	0.0428	2.37%

Distance from flume bottom (mm)	FLUENT x- axis velocity (m/s)	Extrapolated x-axis velocity (m/s)	Error (%)
x = 120cm			
450	0.0018	0.0018	0.50%
500	0.0070	0.0070	0.00%
550	0.0126	0.0126	0.14%
600	0.0184	0.0183	0.57%
650	0.0242	0.0234	3.42%
700	0.0296	0.0292	1.33%
750	0.0341	0.0325	4.82%
800	0.0374	0.0363	2.90%
840	0.0391	0.0382	2.34%
x = 150cm			
450	0.0031	0.0031	0.17%
500	0.0074	0.0074	0.18%
550	0.0118	0.0116	1.78%
600	0.0163	0.0158	3.63%
650	0.0207	0.0196	5.42%
700	0.0247	0.0236	4.53%
750	0.0280	0.0272	2.82%
800	0.0304	0.0297	2.28%
840	0.0316	0.0310	2.08%
x = 200cm			
450	0.0043	0.0043	0.64%
500	0.0068	0.0068	0.30%
550	0.0093	0.0093	0.10%
600	0.0118	0.0118	0.01%
650	0.0141	0.0141	0.00%
700	0.0162	0.0162	0.00%
750	0.0179	0.0179	0.00%
800	0.0191	0.0191	0.00%
840	0.0197	0.0197	0.01%
			1.87%

REFERENCES

Abramovich, G.N., "The Theory of Turbulent Jets", The MIT Press, 1963

Arita, M., Jirka, G.H., Tamai, N., "Classification and Mixing of Two-Dimensional Buoyant Surface Discharges", Journal of Hydraulic Research, Vol.24, No.5, pp.333-345, 1986

Baddour, Chu, V.H., "Turbulent Gravity-Stratified Shear Flows", Technology Report, Department of Civil Engineering and Applied Mechanics, McGill University, Montreal, Canada, September 1978

Batchelor, G.K., "Introduction to Fluid Dynamics", Cambridge University Press, Chapter 1, 1967

Burrows, R., Ali, K.H.M., "Novel Boom/Skirt Systems for Improvement of Water Quality in Estuarial Impoundments Subject to Saline Influx", 1st World Water Congress of the Intarnational Water Association (IWA), Vol.2, pp.485-492, July 2000

Burrows, R., Ali, K.H.M., Crapper, M., "Entrainment from a Buoyant Surface Layer Created by an Under Baffle Wall-Jet", Recent Research Advances in the Fluid Mechanics of Turbulent Jets and Plumes, Kluwer Academic, pp. 785-795, 1994

Celik, I., Zhang, W.M., "Calculation of Numerical Uncertainty Using Richardson Extrapolation: Application to Some Simple Turbulent Flow Calculations", Journal of Fluids Engineering, Vol.117, No.3, pp.439-445, 1995

Chow, V.T., "Open Channel Hydraulics", International Edition, McGraw-Hill, 1973

Christodoulou, G.C., "Interfacial Mixing in Stratified Flows", Journal of Hydraulics Research, Vol.24, No.2, pp. 77-92, 1986

Chu, V.H. and Vanvari, M.R., "Experimental Study of Turbulent Stratified Shearing Flow", Journal of the Hydraulics Division, Vol.102, HY6, pp.691-707, June 1976

Coleman, H.W., Stern, F., "Uncertainties and CFD Code Validation", Journal of Fluids Engineering, Vol.119, pp.795-803, December 1997

Daily, J.W., Harleman, D.R.F., "Fluid Dynamics", Addison-Wesley Pub Co, 1966

D.E.F.R.A., "Water Quality: A Diffuse Pollution Review", Report, Department for Environment, Food and Rural Affairs, October 2004

De Souza, A.C., "How to Plan a CFD Analysis", NAFEMS Ltd, 2002

Ead, S., Rajaratnam, N., Plane Turbulent Wall Jets in Shallow Tailwater" Journal of Engineering Mechanics, ASCE, Vol. 128, No. 2, pp. 143-155, 2002

Engelund, F., "Hydraulics of Surface Buoyant Jet", Journal of the Hydraulics Division, Volume 102, No HY 9, pp.1315-1325, September 1976

Engelund, F., Pedersen, F.B., "Surface Jet at Small Richardson Numbers", Journal of the Hydraulics Division: Proceedings of the American Society of Civil Engineers, HY3, pp.405-416, March 1973

Fischer, H.B., List, E.J., Koh, R.C.Y., Imberger, J., Brooks, N.H., "Mixing in Inland and Coastal Waters", Academic Press, New York, 1979

Fluent 6.0 Manual

French, R.H., McCutcheon, S.C., Martin, J.L., "Environmental Hydraulics", Hydraulic Design Handbook, McGraw-Hill, New York, Chapter 5, 1999

Habashi, W.G., Dompierre, J., Bourgault, Y., "Certifiable Computational Fluid Dynamics through Mesh Optimization", AIAA Journal, Vol.36, No.5, pp.703-711, May 1998

Hardy, R.J., Lane, S.N., Ferguson, R.I., Parsons, D.R., "Assessing the Credibility of a Series of Computational Fluid Dynamic Simulations of Open Channel Flow", Hydrological Processes, March 2003

Harleman, D.R.F., "Withdrawal from two-layer Stratified Flows ", Journal of the Hydraulics Division, Volume 91, No HY 49, pp 43-58, July 1965

Harleman, D.R.F., Elder, R.A., "Withdrawal from Two-Layer Stratified Flows", Journal of the Hydraulics Division: Proceedings of the American Society of Civil Engineers, pp.43-58, July 1965

Heinz, S., Asce, A.M., "Dilution of Buoyant Two-Dimensional Surface Discharges", Journal of the Hydraulics Division: Proceedings of the American Society of Civil Engineers, pp.71-86, January 1972

Jameson, A., Martinelli, L., "Mesh Refinement and Modelling Errors in Flow Simulation", AIAA Journal, Vol.36, No.5, pp. 676-686, May 1998

Jirka, G.H., "Integral Model for Turbulent Buoyant Jets in Unbounded Stratified Flows", Environmental Fluid Mechanics, No.4, pp.1-56, 2004

Jirka, G.H., "Turbulent Buoyant Jets in Shallow Fluid Layers, in Turbulent Buoyant Jets and Plumes", Ed. By W. Rodi, Pergamon Press, pp.69-119, 1982

Jirka, G.H., Bleninger, T., Burrows, R., Larsen, T., "Environmental Quality Standards in the EC-Water Framework Directive: Consequences for Water Pollution Control from Point Sources", European Water Management Online

Koh, R.C.Y, "Two-Dimensional Surface Warm Jets", Journal of the Hydraulics Division: Proceedings of the American Society of Civil Engineers, Vol.97, HY6, pp. 819-836, June 1971

Lal, P.B.B., Rajaratnam, N., "An Experimental Study of Bluff Buoyant Turbulent Surface Jet", Journal of Hydraulic Research, Vol.15, No.3, pp.261-275, 1977

Launder, B.E., Rodi, W., "The Turbulent Wall Jet – Measurements and Modelling", Ann. Rev. of Fluid Mech., Vol.15, 1983

Launder, B. E. and Spalding, D. B., "The numerical computation of turbulent flows", Computer Methods in Applied Mechanics and Engineering, 3(2): 269-289, 1974

Mehta, U.B., "Credible Computational Fluid Dynamics Simulations", AIAA Journal, Vol. 36, No. 5, pp. 665-667, May 1998

Mehta, U.B., "Guide to Credible Computational Fluid Dynamics Simulations", AIAA Paper, 95-2229, 1995

Mehta, U.B., "Some Aspects of Uncertainty in Computational Fluids Dynamics Results", Journal of Fluids Engineering, Vol. 113, pp.538-543, December 1991

Oberkampf, W.L., Blottner, F.G., "Issues in Computational Fluid Dynamics Code Verification and Validation", AIAA Journal, Vol.36, No.5, pp.687-695, May 1998

Pande, B.B.,L., Rajaratnam, N., "An Experimental Study of Bluff Buoyant Surface Discharges", Journal of the Hydraulic Research, IAHR, Vol.15, No.3, pp.261-275, 1977

Pande, B.B.L., Rajaratnam, N., "Similarity Analysis of Buoyant Surface Jets into Quiescent Ambients", IAHR, 16th Congress, Brazil, Vol.3, C.8, pp.62-70, 1975

Rajaratnam, N., "An Experimental Study of Bluff Surface Discharges with Small Richardson Number", Journal of Hydraulic Research, Vol.23, No.1, pp.47-55, 1985

Rajaratnam, N., "Bluff Surfaces Discharges with Small Richardson Number", Journal of Hydraulic Research, Vol.23, No.1, pp.47-55, 1985

Rajaratnam, N., "Turbulent Jets", Elsevier, 1976

Rajaratnam, N., Humphries, J.A., "Turbulent Non-Buoyant Surface Jets", Journal of Hydraulic Research, IAHR, Vol.22, No.2, pp.103-115, 1984

Rajaratnam, N., Subramanya, S., "An Experimental Study of Plane Turbulent Buoyant Surface Jets and Jumps", University of Alberta, Rep. 83-3, 1983

Rajaratnam, N., Subramanya, S., "Plane Turbulent Buoyant Surface Jets and Jumps", Journal of Hydraulic Research, IAHR, Vol.23, No.2, pp.131-146, 1985

Rajaratnam, N., Subramanya, S., "Plane Turbulent Denser Wall Jets and Jumps", Journal of Hydraulic Research, IAHR, Vol.24, No.4, pp.281-296, 1986

Raudkivi, A.J., "Loose Boundary Hydraulics", 3rd Edition, Pergamon Press, 1990

Rizzi, A., Vos, J., "Toward Establishing Credibility in Computational Fluid Dynamics Simulations", Paper 96-2029 at the AIAA 27th Computational Fluid Dynamics Conference, May 1997

Roache, P.J., "A Method for Uniform Reporting of Grid Refinement Studies", Quantification of Uncertainty in Computational Fluid Dynamics, edited by I. Celik, C.J. Chen, P.J. Roache, and G. Scheurer, ASME FED, American Society of Mechanical Engineers, Vol.158, pp.109-120, 1993

Roache, P.J., "A Method for Uniform Reporting of Grid Refinement Studies", Proceedings of the AIAA 11th Computational Fluid Dynamics Conference, AIAA, Pt.2, pp.1057-1058, Washington D.C., 1993

Roache, P.J., "Need for Control of Numerical Accuracy", Journal of Spacecraft and Rockets, Vol.27, pp.98-102, 1990

Roache, P.J., "Perspective: A Method for Uniform Reporting of Grid Refinement Studies", Journal of Fluids Engineering, Vol. 116, No.3, pp. 405-413, September 1994

Roache, P.J., "Quantification of Uncertainty in Computational Fluid Dynamics", Report, Annual Review of Fluid Mechanics, pp.123-160, 1997

Roache, P.J., "Verification of Codes and Calculations", AIAA Journal, Vol. 36, No.5, pp.696-702, May 1998

Stolzenbach, K.D., Harleman, D.R.F., "An Analytical and Experimental Investigation of Surface Discharges of Heated Water", M.I.T. Parson's Laboratory Report, 1971

Streeter, V.L., "Handbook of Fluid Dynamics", 2nd ed., McGraw-Hill, pp. 26.2-26.10, 1982

Turner, J.S., "Buoyancy Effects in Fluid", Cambridge University Press, 1973

Vanvari, M.R., Chu, V.H, "Two Dimensional Turbulent Surface Jets of Low Richardson Number", McGill University, Department of Civil Engineering, Report 74-2, 1974

Versteeg, H.K., Malalasekera, W., "An Introduction to Computational Fluid Dynamics – The Finite Volume Method", Longman, 1995

Wilcox, D. C., "Turbulence Modelling for CFD", DCW Industries, 2nd Edition, 2002

Wiuff, R., "Experiments on Surface Buoyant Jets", Journal of the Hydraulics Division, pp.667-679, May 1978

Wood, I.R., Wilkinson, D.L., Barr, D.I.H., Silberman, E., "Surface Discharge of Horizontal Warm-Water Jet", Journal of the Power Division, Vol.92, No.2, pp.1-30, April 1966

Wu, S. and Rajaratnam, N., "Free jumps. Submerged jumps and wall jets" Journal of Hydraulic Research, Vol. 33, No.2, pp. 197-212. 1995